INTERNATIONL SCHOOL for ADVANCED STUDIES

HIGH ENERGY SECTOR
STATISTICAL PHYSICS CURRICULUM

QFT emerging models in condensed matter systems

Thesis submitted for the Degree of *Doctor Phylosophiae*

Advisor:
Prof. **Giuseppe Mussardo**

External Referee:
Prof. **German Sierra Rodero**

Co-advisor:
Dr. **Andrea Trombettoni**

Candidate
Luca Lepori

ACADEMIC YEAR 2009/2010

TO MY FATHER, WHEREVER HE IS

Ognuno sta solo sul cuor della terra,
trafitto da un raggio di sole:
ed e' subito sera.

Salvatore Quasimodo

Abstract

In this thesis we study some examples of quantum field theory (QFT) describing statistical mechanics and condensed matter systems near a second order phase transition or in the infrared limit (IR).
The work is divided in two parts. The first one concerns the study of some statistical models (Tricritical Ising model, 3-state Potts model) in the scaling regime, where an effective treatment by field theory methods holds. Mathematically, the QFTs involved are obtained by perturbations of a conformal field theory (CFT) describing the RG infrared fixed point related to a phase transition; moreover each perturbation is in one-to-one correspondence with the parameters driving the physical system out of criticality. For suitable perturbations the resulting QFTs are integrable; this allows to determine exactly (up to difficulties in the calculations) their spectrum and correlation functions. The analysis can be partly extended to non integrable multiple deformations, yielding an appreciable view about a considerable part of the entire space of parameters.
The second part deals with the simulation of relativistic fermionic theories using ultracold atoms. The study is motivated by the potential relevance of condensed matter simulations of QFTs for shading new light on elusive phenomena like chiral symmetry breaking and confinement, as well as in the behaviour of systems having a relativistic dispersion spectrum (graphene, fractionalizing systems, chiral superconductors, topological insulators). We discuss an ultracold atoms set-up able to simulate (3+1) Dirac fermions and some applications, relevant both in elementary particle and in condensed matter physics. We show in particular the possibility to add a tunable mass by using Bragg pulses, an effective external electromagnetic coupling and an internal interaction, also covariant. Finally we consider the 2D limit, describing the emergence of (2+1) Dirac fermions in presence of a strongly anisotropic lattice.

Contents

Chapter 1

INTRODUCTION

Although it was born in the framework of elementary particle physics, Quantum Field Theory (QFT) turned out to be an extremely powerful tool to analyze a wide range of physical systems, including Condensed Matter and Statistical Physics systems.
Motivated by the extreme relevance of the topic, the development of theoretical tools to investigate efficiently QFT in different energy regime has been a central issue in the physics research of the last fifty years. One of the main achievement obtained so far is represented by the perturbative diagrammatic expansion proposed by Feynman at the beginning of fifties and later largely. However, because of its perturbative nature, this approach turns out to be reliable only in low-coupling regime.
Far from this limit a full understanding of QFT still continues to be challenging and the presently available methods, like functional RG, solitons solutions, duality, SUSY solvable models and lattice simulations are only partly effective.
The situation is much more favorable in (1+1) *quantum* dimensions, where conformal (CFT) can be solved exactly and several paradigmatic examples of integrable field theory (IFT) are available. Notably, some integrable theories share peculiar properties with the (3+1) non abelian QFTs, like chiral symmetry breaking and dynamical mass gap creation or confinement and then they are studied as meaningful toy models.
CFT and ITF are deeply involved in one of the most spectacular application of QFT, the theory of critical phenomena. Indeed, in the critical regime close to a second order phase transition, characterized by to the diverging correlation length [1], a QFT treatment was argued to catch both the qualitative and the quantitative features of the dynamics. In particular, in a pioneering paper by Belavin, Polyakov and Zamolodchikov [67], systems exactly at the critical point were put in close relation with certain conformal field theories. Critical systems in arbitrary dimensionality, in fact, fall into universality classes which can be classified by CFT; in 2D the conformal invariance is powerful enough to solve exactly the critical dynamics through a systematic computation of correlators. The studied systems so far include, between the others, the Ising model in a magnetic field, the Tricritical Ising model (TIM), the q-state Potts model, percolation and self-avoiding walks.
Furthermore, dynamics in the vicinity of a critical point can be described by perturbations of CFTs,

[1] A continuos field theory analysis can be effective even for particular first order phase transitions, where the correlation length is large enough.

obtained by adding to the critical action some I.R. relevant operators which break the conformal symmetry and introduce a mass scale in the system; each perturbation is in one-to-one correspondence with the parameters that drag the physical system out of criticality. The most exciting aspect is that suitable choices of the perturbing operator make the off-critical massive field theory *integrable*, with consequent elasticity and factorization of the scattering. In two dimensions, this fact leads to the possibility of computing exactly the scattering amplitudes, which encode in their analytical structure the complete information about the spectrum. Moreover, the knowledge of the S-matrix permits to implement the so-called form factors approach, which makes possible the analysis of off–shell correlation functions. Within this program, during the the last years measurable universal quantities for many statistical models have computed. Notably, the analysis can be partly extended to non integrable multiple deformations, yielding an appreciable insight about a significant part of the parameters space describing the statistical model in the scaling regime.

Along these ideas, in the first part (Chapter 2) of the thesis, we studied parts of the scaling region of the TIM (Section 2) and of the 3-state Potts Model (Section 3) by analyzing the field theories obtained by certain perturbations (energy density and vacancy density for TIM, energy density and magnetic field for 3-Potts) of the corresponding RG infrared fixed points. We followed in particular the evolution of the mass spectra for varying couplings in the Landau-Ginzburg lagrangian (that means along the various RG trajectories), with particular attention to the interplay between local and topological degrees of freedom.
The analysis is carried on by numerical methods (TCSA) and by Form Factors perturbation theory for trajectories close to the integrable flows, where the spectrum is exactly known. Notably, even dealing with not integrable theories TCSA is able to give good estimations at least on the low-particle form factors; this allows, thanks to the fast convergence of the Lehman series in the massive case, to reproduce effectively the correlation functions for the various operators.

The point of view described above, i.e. considering QFT as a tool for investigation of condensed matter phenomena, can be someway reversed: statistical models can be used as simulators of QFTs, generally in not perturbative limit. This is the major link with what's described in the second part (Chapter 3) of the thesis.

In Chapter 3 we study the simulation of QFT using ultracold atoms. Last years saw an increasing interest for the simulation of strongly correlated systems by ultracold atoms. One of the main advantages of ultracold atoms devices is the possibility to control and tune various parameters of the hamiltonian and even to give them time and space dependence. Along the same line, they often allow a sufficient disentanglement of the studied phenomenon from the uninteresting background; this is generally not possible in experiments on real life systems.
The study is made feasible and more exciting by considering many available "ingredients", like optical lattices. Notably the last ones can be prepared in various geometries (and dimensions) and they can be filled both with bosons or fermions, even with mixtures of more species. Moreover, recent techniques allow to add disorder, tune short and long interactions (generally by Feshbach resonances) and to simulate static gauge fields. These unique features make ultracold atoms a central tool for investigations in condensed matter and quantum computation theory.

A further boost to the research on this field comes from last years proposals to simulate relativistic models, QFT and analogue gravity models. This program is expected to provide an efficient tool to test the present theories; in this regard we mention confirmations of Zitterbewegung or Klein paradox realized on graphene or single ion traps [109].
Interest for the quantum simulation of relativistic systems has different sources. Firstly, condensed matter systems hosting relativistic low energy excitations shows peculiarities in the phase diagram, transport features, surface effects. It is the case of graphene [95], of some type of topological insulators (having massive (3+1) Dirac-like excitation in the bulk and massless (2+1) at the boundary) [8] and notably of some unconvetional superconductors (like zero modes in p-wave superconductors). Furthermore, the physics of ultra-dense stars requires at the present point further information on condensed matter phenomena in relativistic regime, like diffusion, localization and superconductivity, especially in presence of many species of particles (quarks) [107].
These studies can give insights on the QCD behaviour in the unconfined phase and they motivate partly the interest by the high energy community for cold atoms. Indeed the major goal in this perspective is to investigate regions of the phase space of realistic interacting theories, like QCD; the most challenging obstacle appears to be at the present time the simulation of *dynamical* non abelian gauge fields.

Motivated by this perspective, in the second part of this thesis (Chapter 3), we discuss a cold-atoms set-up able to simulate (3+1) Dirac fermions and some applications, relevant both in elementary particle and in condensed matter physics. So far the discussion was mainly limited to (2+1) Dirac fermions (from graphene to Affleck-Marston model [129]), the present work being an attempt for the generalization to the higher dimensional case. We also show the possibility to add a tunable mass by using Bragg pulses, an effective external electromagnetic coupling and an internal interaction, also covariant. Finally we consider the 2D limit, describing the emergence of (2+1) Dirac fermions in presence of a strongly anisotropic lattice.

The thesis ends with a short overview on the possible future developments and applications.

Chapter 2

MASS SPECTRUM IN LOW DIMENSIONAL QFT

In this Chapter we describe the scaling regime of the TIM and of the 3-state Potts model (3-PM) by studying directly the low-dimensional QFT here realized. We analyze in particular the low-energy spectrum and the decay processes for a variety of RG trajectories, generally non integrable. In Section 1 we give a short overview on conformal field theories and on some integrability methods that we will use in the following two Sections. The material exposed is partly elaborated from [7]. For a wide review see [6]. In Section 2 we study the scaling limit of TIM, while Section 3 is devoted to 3-PM.

2.1 Quantum field theories in 2D and statistical physics

2.1.1 Critical systems and conformal field theories

A statistical mechanical system is said to be critical when its correlation length ξ, defined as the typical distance over which the order parameters are statistically correlated, increases infinitely ($\xi \to \infty$). Correspondingly, length scales lose their relevance, and scale invariance emerges. This is peculiar of the continuous (or second order) phase transitions. A remarkable property of these systems is that the fine details of their microscopic structure become unimportant, and the various possible critical behaviours are organized in universality classes, which depend only on the space dimensionality and on the underlying symmetry. This allows a description of the order parameter fluctuations in the language of a field theory, which is invariant under the global scale transformations

$$x^\mu \to x'^\mu = \lambda\, x^\mu \,,$$

provided that the fields transform as

$$\Phi(x) \to \Phi'(x') = \lambda^{-\Delta}\, \Phi(x) \,,$$

where Δ is called the scaling dimension of the field Φ.

The use of conformal invariance to describe statistical mechanical systems at criticality is motivated by a theorem, due to Polyakov, which states that local field theories which are scaling

invariant are also conformally invariant [9]. Therefore, every universality class of critical behaviour can be identified with a conformal field theory (CFT), i.e. a quantum field theory that is invariant under conformal symmetry. This way of studying critical systems started with a pioneering paper by Belavin, Polyakov and Zamolodchikov [67], and is systematically presented in many review articles and text books (see for instance [11, 12, 13]). We will now concisely summarize the main properties of CFT.

An infinitesimal coordinate transformation $x^\mu \to x^\mu + \xi^\mu(x)$ is called conformal if it leaves the metric tensor $g_{\mu\nu}$ invariant up to a local scale factor, i.e.

$$g_{\mu\nu}(x) \to \varrho(x) g_{\mu\nu}(x)\,.$$

These transformations, which include rotations, translations and dilatations, preserve the angle between two vectors and satisfy the condition

$$\partial_\mu \xi_\nu + \partial_\nu \xi_\mu = \frac{2}{d}\,\eta_{\mu\nu}(\partial\cdot\xi)\,, \tag{2.1}$$

where d is the dimension of space-time. In two dimensions, since the conformal group enlarges to an infinite set of transformations, it is possible to solve exactly the dynamics of a critical system, assuming conformal invariance and a short-distance operator product expansion (OPE) for the fluctuating fields. In fact, if we describe euclidean two-dimensional space-time with complex coordinates

$$z = x^0 + i x^1\,, \qquad\qquad \bar z = x^0 - i x^1\,,$$

eq.(2.1) specializes to the Cauchy-Riemann equations for holomorphic functions. Therefore the solutions are holomorphic or anti-holomorphic transformations, $z \to f(z)$ and $\bar z \to \bar f(\bar z)$, such that $\partial_{\bar z} f = \partial_z \bar f = 0$. These functions admit the Laurent expansion

$$f(z) = \sum_{n=-\infty}^{\infty} a_n\, z^{n+1}\,, \qquad\qquad \bar f(\bar z) = \sum_{n=-\infty}^{\infty} a'_n\, \bar z^{n+1}\,,$$

which has an infinite number of parameters. In this way, the conformal group enlarges to an infinite set of transformations.

Defining now a two–dimensional quantum field theory invariant under conformal transformations, we can associate to each field an holomorphic and an anti-holomorphic conformal dimensions h and $\bar h$, defined in terms of the scaling dimension Δ and of the spin s as

$$h = \frac{1}{2}(\Delta + s)\,, \qquad\qquad \bar h = \frac{1}{2}(\Delta - s)\,. \tag{2.2}$$

A field is called primary if it transforms under a local conformal transformation $z \to w = f(z)$ as

$$\phi'(w,\bar w) = \left(\frac{dw}{dz}\right)^{-h} \left(\frac{d\bar w}{d\bar z}\right)^{-\bar h} \phi(z,\bar z)\,. \tag{2.3}$$

Conformal invariance fixes the form of the correlators of two and three primary fields up to a multiplicative constant:

$$\langle \phi_1(z_1,\bar z_1)\,\phi_2(z_2,\bar z_2)\rangle \;=\; \begin{cases} \frac{C_{12}}{z_{12}^{2h}\,\bar z_{12}^{2h}} & \text{if } h_1 = h_2 = h \text{ and } \bar h_1 = \bar h_2 = \bar h \\ 0 & \text{otherwise} \end{cases}\,, \tag{2.4}$$

$$\langle \phi_1(z_1,\bar{z}_1)\,\phi_2(z_2,\bar{z}_2)\,\phi_3(z_3,\bar{z}_3)\rangle \;=\; C_{123}\frac{1}{z_{12}^{h_1+h_2-h_3}\,z_{23}^{h_2+h_3-h_1}\,z_{13}^{h_3+h_1-h_2}} \times\frac{1}{\bar{z}_{12}^{\bar{h}_1+\bar{h}_2-\bar{h}_3}\,\bar{z}_{23}^{\bar{h}_2+\bar{h}_3-\bar{h}_1}\,\bar{z}_{13}^{\bar{h}_3+\bar{h}_1-\bar{h}_2}}\,, \tag{2.5}$$

where $z_{ij}=z_i-z_j$ and $\bar{z}_{ij}=\bar{z}_i-\bar{z}_j$.

It is typical for correlation functions to have singularities when the positions of two or more fields coincide. The operator product expansion (OPE) is the representation of a product of operators (at positions x and y) by a sum of terms involving single operators multiplied by functions of x and y, possibly diverging as $x\to y$. This expansion has a weak sense, being valid for correlation functions, and leads to the construction of an algebra of scaling fields defined by

$$\phi_i(x)\phi_j(y)=\sum_k \hat{C}_{ij}^k(x,y)\phi_k(y)\,, \tag{2.6}$$

where $\hat{C}_{ij}^k(x,y)$ are the so-called structure constants. Translation and scaling invariance force these functions to have the following form:

$$\hat{C}_{ij}^k(x,y)=\frac{C_{ij}^j}{|x-y|^{\Delta_i+\Delta_j-\Delta_k}}\,,$$

where C_{ij}^j are exactly the undetermined multiplicative constants of the tree-point correlators (2.5).

A particularly important operator is the stress–energy tensor $T^{\mu\nu}$, which expresses the variation of the action under a transformation of coordinates $x^\mu\to x^\mu+\xi^\mu(x)$:

$$\delta S=-\frac{1}{2\pi}\int d^2x\,T^{\mu\nu}(x)\partial_\mu\xi_\nu\;.$$

Conformal invariance is equivalent to the vanishing of δS under the condition (2.1), and it is guaranteed by the fact that the stress-energy tensor is traceless. Together with translation and rotation invariance ($\partial_\mu T^{\mu\nu}=0$), the condition $T^\mu_\mu=0$ is expressed in complex coordinates as

$$\partial_{\bar{z}}T=0\qquad\text{and}\qquad\partial_z\bar{T}=0\,,$$

where $T(z)=T_{11}-T_{22}+2iT_{12}$ and $\bar{T}(\bar{z})=T_{11}-T_{22}-2iT_{12}$. Therefore the stress-energy tensor splits into a holomorphic and an anti-holomorphic part. In two dimensions, it is possible to deduce the following OPE for the stress-energy tensor and a primary field of dimension $(h,\bar{h})$:

$$T(z)\,\phi(w,\bar{w})=\frac{h}{(z-w)^2}\,\phi(w,\bar{w})+\frac{1}{z-w}\,\partial_w\phi(w,\bar{w})+\text{regular terms}\,, \tag{2.7}$$
$$\bar{T}(\bar{z})\,\phi(w,\bar{w})=\frac{\bar{h}}{(\bar{z}-\bar{w})^2}\,\phi(w,\bar{w})+\frac{1}{\bar{z}-\bar{w}}\,\partial_{\bar{w}}\phi(w,\bar{w})+\text{regular terms}\,.$$

Furthermore, it is possible to show that the OPE of the stress-energy tensor with itself has the form:

$$T(z)T(w)=\frac{c/2}{(z-w)^4}+\frac{2}{(z-w)^2}\,T(w)+\frac{1}{z-w}\,\partial T(w)+\text{regular terms}\,, \tag{2.8}$$

where the constant c, called central charge, depends on the specific model. A similar expression holds for the anti-holomorphic component. The holomorphic and anti-holomorphic components of the stress-energy tensor can be expanded in Laurent series respectively on modes L_n and $\bar{L}_n$, which are the quantum generators of the local conformal transformations

$$T(z) = \sum_{n=-\infty}^{\infty} \frac{L_n}{z^{n+2}} , \qquad \bar{T}(\bar{z}) = \sum_{n=-\infty}^{\infty} \frac{\bar{L}_n}{\bar{z}^{n+2}} , \tag{2.9}$$

and obey the Virasoro algebra

$$\begin{aligned} [L_n, L_m] &= (n-m)\, L_{n+m} + \frac{c}{12}\, n(n^2-1)\, \delta_{n+m,0} , \\ [\bar{L}_n, \bar{L}_m] &= (n-m)\, \bar{L}_{n+m} + \frac{c}{12}\, n(n^2-1)\, \delta_{n+m,0} , \\ [L_n, \bar{L}_m] &= 0 . \end{aligned} \tag{2.10}$$

In virtue of the decomposition of (2.10) in the direct sum of two algebras, one in the holomorphic and the other in the anti-holomorphic sector, the general properties of CFT have the same form in the two sectors, and from now on we will only restrict to the holomorphic part.

Comparing definition (2.9) with the OPE (2.7), we can deduce the action of some generators on a primary field:

$$\begin{aligned} (L_0\phi)(z) &= h\,\phi(z) \\ (L_{-1}\phi)(z) &= \partial\phi(z) \\ (L_n\phi)(z) &= 0 \quad \text{if} \quad n \geq 1 . \end{aligned} \tag{2.11}$$

The relation $[L_0, L_n] = -nL_n$ leads to the interpretation of generators L_n with $n > 0$ as destruction operators and with $n < 0$ as creation operators. Hence primary fields define highest weight representations of the Virasoro algebra, being annihilated by all destruction operators. The action of creation operators on these fields is encoded in the regular part of the OPE (2.7), and it defines the so-called descendant fields

$$\phi^{(n_1,n_2,\ldots,n_k)} = (L_{-n_1} L_{-n_2} \ldots L_{-n_k})\, \phi ,$$

which are again eigenvectors of L_0:

$$L_0 \left[\phi^{(n_1,n_2,\ldots,n_k)}\right] = \left(h + \sum_{i=1}^{k} n_i\right) \phi^{(n_1,n_2,\ldots,n_k)} .$$

The number $N = \sum_{i=1}^{k} n_i$ is called level of the descendant. As an example, the stress-energy tensor is a level two descendant of the identity ($T = L_{-2}\mathbb{I}$). The set $[\phi]$ constituted by all the descendant fields of a primary operator ϕ is called conformal family. It is possible to show that every correlation function involving descendant fields can be computed by applying a linear differential operator to the correlation function of the corresponding primary fields.

The Hilbert space of states of a CFT is built by acting on the vacuum with the operators evaluated at $z = 0$. Therefore, the primary states are given by

$$|\, h \,\rangle \equiv \phi(0)|\, 0 \,\rangle \ ,$$

and the descendent states can be obtained from them as $L_{-n_1} L_{-n_2} ... L_{-n_k} |\, h \,\rangle$.

In concluding this section, it is worth mentioning how the central charge c has the physical meaning of measuring the response of the system to the introduction of a macroscopic scale [14, 15, 16]. In fact, the complex plane can be conformally mapped to an infinite cylinder of circumference R by the transformation (see Fig. 2.1)

$$z \to w(z) = \frac{R}{2\pi} \ln z \ . \tag{2.12}$$

Implementing the above transformation on the stress–energy tensor one gets

$$T_{cyl.}(w) = \left(\frac{2\pi}{R}\right)^2 \left[T_{pl.}(z) z^2 - \frac{c}{24} \right] \ .$$

If we assume that the vacuum energy density $\langle T_{pl.} \rangle$ vanishes on the plane, we see that it is non–zero on the cylinder:

$$\langle T_{cyl.} \rangle = -\frac{c\pi^2}{6R^2} \ .$$

The central charge is then proportional to the Casimir energy, which naturally goes to zero as the macroscopic scale R goes to infinity. In particular, the hamiltonian and the momentum are expressed on the cylinder in terms of the Virasoro generators as

$$H = \frac{2\pi}{R} \left(L_0 + \bar{L}_0 - \frac{c}{12} \right) \qquad\qquad P = \frac{2\pi i}{R} \left(L_0 - \bar{L}_0 \right) \ . \tag{2.13}$$

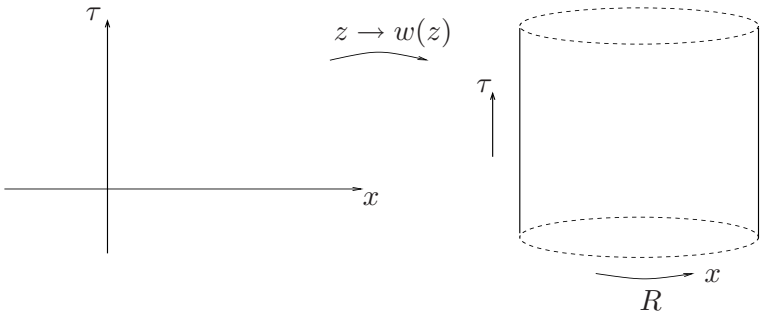

Figure 2.1: Conformal map (2.12) from plane to cylinder.

Examples: minimal models

We will now describe few examples of CFT, which will be further discussed in the thesis. We limit ourselves to the statement of the main results, whose proofs can be found in the literature [6].

Virasoro minimal models are particular CFT characterized by a finite set of conformal families, in virtue of a truncation of the operator algebra. These theories can be labelled as $\mathcal{M}(p,p')$ with two integers p and p', in terms of which the central charge and the conformal dimensions of primary fields are expressed as

$$c = 1 - 6\frac{(p-p')^2}{p\,p'} \,, \tag{2.14}$$

$$h_{r,s} = \frac{(p\,r - p'\,s)^2 - (p-p')^2}{4p\,p'} \,, \tag{2.15}$$

with

$$1 \le r < p' \qquad \text{and} \qquad 1 \le s < p \,.$$

The conformal dimensions are organized in a rectangle in the (r,s) plane, called Kac table. The number of distinct fields is $(p-1)(p'-1)/2$, since there is a symmetry $h_{r,s} = h_{p'-r,p-s}$ which makes half of the Kac rectangle redundant. It can be shown that minimal models are unitary only if $|p-p'| = 1$, and in this case they are usually labelled with $p' = m$ and $p = m+1$.

The simplest unitary minimal model is $\mathcal{M}(4,3)$, which has central charge $c = \frac{1}{2}$ and the Kac table shown in Fig. 2.2.

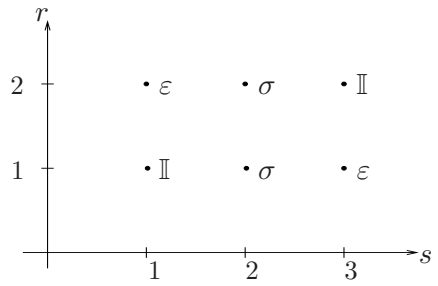

Figure 2.2: Kac table of the minimal model $\mathcal{M}(4,3)$.

This field theory is in the same universality class as the lattice Ising model [67], defined by the hamiltonian

$$E[\sigma] = -J\sum_{\langle i,j\rangle}\sigma_i\sigma_j - h\sum_i \sigma_i \,, \qquad \sigma_i \in \{-1,1\} \,.$$

Besides the identity operator $\phi_{1,1} = \mathbb{I}$, the theory contains the operator $\phi_{1,2} = \sigma$ with conformal dimension $h_\sigma = \frac{1}{16}$, which is the continuum version of the lattice spin σ_i, and $\phi_{1,3} = \varepsilon$, with $h_\varepsilon = \frac{1}{2}$,

which corresponds to the interaction energy $\sigma_i\sigma_{i+1}$. The algebra defined by the OPE (2.6) can be schematically represented in this model by the fusion rules

$$\begin{aligned}\sigma \times \sigma &\sim \mathbb{I} + \varepsilon \,, \\ \sigma \times \varepsilon &\sim \sigma \,, \\ \varepsilon \times \varepsilon &\sim \mathbb{I} \,.\end{aligned}$$

This notation means, for instance, that the OPE of σ with σ (or fields belonging to their families) may contain terms belonging only to the conformal families of $\mathbb{I}$ and ε.

The next unitary model, $\mathcal{M}(5,4)$., displays a richer structure. The Kac table of this model, which has central charge $c = \frac{7}{10}$, is shown in Fig. 2.3.

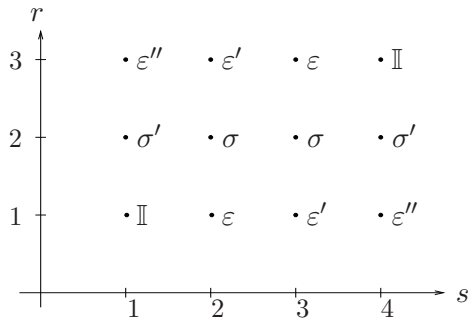

Figure 2.3: Kac table of the minimal model $\mathcal{M}(5,4)$

It was recognized in [17] that the lattice model associated with this conformal field theory is the dilute Ising model at its tricritical fixed point (TIM), defined by

$$E[\sigma,t] = -J\sum_{\langle i,j\rangle}\sigma_i\sigma_j t_i t_j - \mu\sum_i (t_i - 1) \,, \qquad \sigma_i \in \{-1,1\},\, t_i \in \{0,1\} \,,$$

where μ is the chemical potential and t_i is the vacancy variable. The corresponding phase diagrams is drawn in Figure 2.4, where I and II denote respectively a first and second order phase transition, and the point $(J_I, 0)$ represents the Ising model, with all lattice's site occupied.

The field $\phi_{1,2} = \varepsilon$, with $h_\varepsilon = \frac{1}{10}$, corresponds to the energy density, while $\phi_{1,3} = \varepsilon'$, with $h_{\varepsilon'} = \frac{6}{10}$, is the vacancy (or subleading energy) operator. The leading and subleading magnetization fields are respectively $\phi_{2,2} = \sigma$ and $\phi_{2,1} = \sigma'$, with $h_\sigma = \frac{3}{80}$ and $h_{\sigma'} = \frac{7}{16}$. The remaining field $\phi_{1,4} = \varepsilon''$ has conformal dimension $h_{\varepsilon''} = \frac{3}{2}$. Dividing the operators in even and odd with respect to the $\mathbb{Z}_2$ symmetry of the model under $\sigma_i \to -\sigma_i$, we can list the fusion rules in the following way:

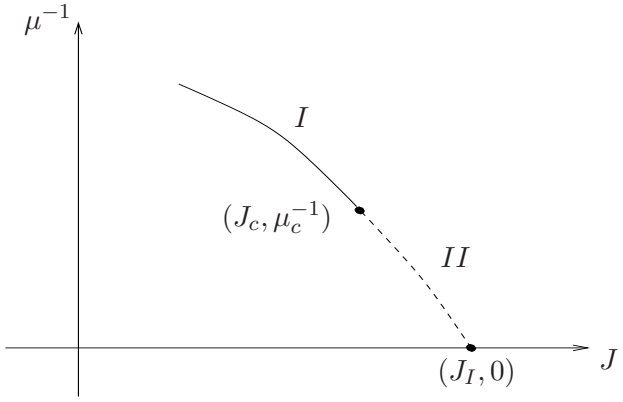

Figure 2.4: Phase diagram of the TIM.

even × even	even × odd	odd × odd
$\varepsilon \times \varepsilon = \mathbb{I} + \varepsilon'$	$\varepsilon \times \sigma = \sigma + \sigma'$	$\sigma \times \sigma = \mathbb{I} + \varepsilon + \varepsilon' + \varepsilon''$
$\varepsilon \times \varepsilon' = \varepsilon + \varepsilon''$	$\varepsilon \times \sigma' = \sigma$	$\sigma \times \sigma' = \varepsilon + \varepsilon'$
$\varepsilon \times \varepsilon'' = \varepsilon'$	$\varepsilon' \times \sigma = \sigma + \sigma'$	$\sigma' \times \sigma' = \mathbb{I} + \varepsilon''$
$\varepsilon' \times \varepsilon' = \mathbb{I} + \varepsilon'$	$\varepsilon' \times \sigma' = \sigma$	
$\varepsilon' \times \varepsilon'' = \varepsilon$	$\varepsilon'' \times \sigma = \sigma$	
$\varepsilon'' \times \varepsilon'' = \mathbb{I}$	$\varepsilon'' \times \sigma' = \sigma'$	

2.1.2 Integrable quantum field theories

The scaling region in the vicinity of second order phase transitions can be described by a given CFT perturbed by its relevant operators Φ_i (characterized by an anomalous dimension $\Delta_i < 2$), with the action

$$\mathcal{A} = \mathcal{A}_{CFT} + \sum_i \lambda_i \int d^2x \, \Phi_i(x) \, , \tag{2.1}$$

where the couplings have mass dimension $\lambda_i \sim [m]^{2-\Delta_i}$. The relevant operators, being super-renormalizable with respect to UV divergencies, do not affect the behaviour of the system at short distances, but they change it at large scales. Any combination of the relevant fields defines a Renormalization Group (RG) trajectory which starts from the given CFT and can reach another critical point (defined by a different CFT) or a non-critical fixed point, corresponding to a massive QFT. From now on, we will only consider this second case.

It was shown in [18] that, depending on the choice of the perturbing operator, the off-critical massive field theory can be integrable, with consequent elasticity and factorization of the scattering. In particular, every *single* perturbation of a conformal model by its relevant operators $\phi_{1,3}$, $\phi_{3,1}$, $\phi_{2,1}$ yields an integrable theory. Conversely, various arguments (see [6]) seem to indicate that multiple perturbations never retain integrability.

Obviously, this kind of theories covers only one particular class of the statistical systems of interest;

however this class includes many relevant physical problems. For instance, integrable QFT correspond to the Ising model with thermal or magnetic perturbation separately, described respectively by

$$\mathcal{A}_{\mathcal{M}(4,3)} + \lambda_\varepsilon \int d^2x\, \phi_{1,3}(x) + \lambda_\sigma \int d^2x\, \phi_{1,2}(x)\,, \tag{2.2}$$

or to the TIM perturbed by the leading energy operator

$$\mathcal{A}_{\mathcal{M}(5,4)} + \lambda_\varepsilon \int d^2x\, \phi_{1,2}(x)\,.$$

We will now present a brief overview of integrable massive quantum field theories, underlying their basic features (for an exhaustive review, see [19]). This will also give us the opportunity of introducing the most important kinematical quantities used in the following.
An integrable QFT is characterized by the presence of an infinite set of conserved charges, which make the corresponding scattering theory purely elastic and factorized [20]. This implies that an arbitrary n-particle collision process can be described by the product of $n(n-1)/2$ elastic pair collisions. Hence the determination of the complete S matrix reduces to that of the two-particle amplitudes, which are defined as

$$|A_i(p_1)\, A_j(p_2)\rangle_{in} = S_{ij}^{kl}\, |A_k(p_3)\, A_l(p_4)\rangle_{out}\,, \tag{2.3}$$

where $A_i(p_1)$ and $A_j(p_2)$ denote the incoming particles (with 2-momenta p_1^μ and p_2^μ), and $A_k(p_3)$ and $A_l(p_4)$ the outgoing states (see Fig. 2.5).

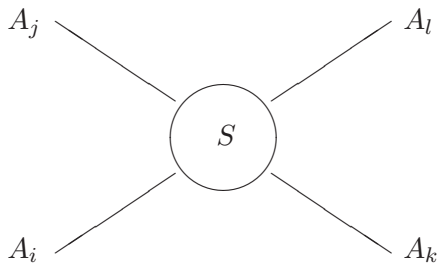

Figure 2.5: Two-particle S-matrix.

The Lorentz invariance fixes the two body S-matrix to be a function of the Mandelstam variables $s = (p_1 + p_2)^2$, $t = (p_1 - p_3)^2$ and $u = (p_1 - p_4)^2$, which satisfy the relation $s + t + u = \sum_{i=1}^4 m_i^2$. Since in (1+1) dimensions and for elastic scattering only one of these variables is independent, it is convenient to introduce a parameterization of the momenta in terms of the so-called rapidity variable θ:

$$p_i^0 = m_i \cosh\theta_i\,, \qquad\qquad p_i^1 = m_i \sinh\theta_i\,, \tag{2.4}$$

which corresponds to the following expression for the Mandelstam variable s:

$$s = (p_1 + p_2)_\mu\, (p_1 + p_2)^\mu = m_i^2 + m_j^2 + 2m_i m_j \cosh\theta_{ij}\,, \tag{2.5}$$

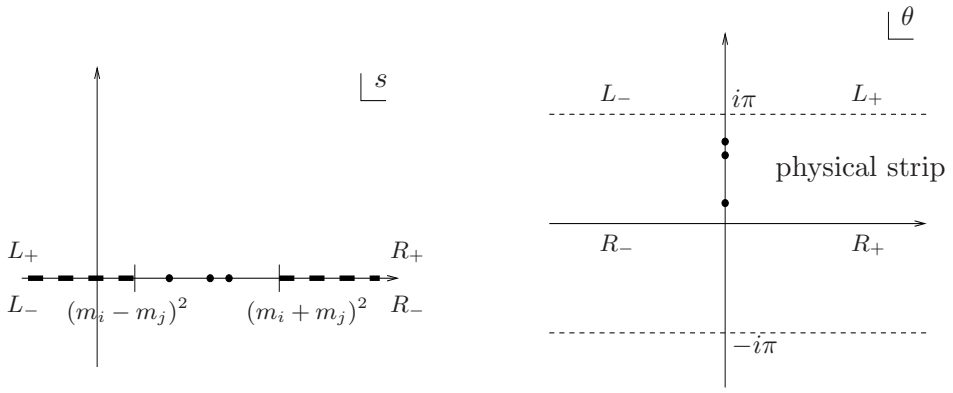

Figure 2.6: Analytic structure of the elastic S–matrix in the variables s and θ.

with $\theta_{ij} = \theta_i - \theta_j$. The functions S_{ij}^{kl} will then depend only on the rapidity difference of the involved particles:

$$|A_i(\theta_1)\, A_j(\theta_2)\rangle_{in} \;=\; S_{ij}^{kl}(\theta_{12})\; |A_k(\theta_2)\, A_l(\theta_1)\rangle_{out}\;,.$$

The elasticity of the scattering processes implies a drastic simplification in the analytic structure of the S–matrix, which can be extended to be an analytic function in the complex s–plane [21]. In fact, contrary to the generic case, where many branch cuts are present, in the elastic case the two–particle S-matrix only displays two square root branching points at the two–particle thresholds $(m_i - m_j)^2$ and $(m_i + m_j)^2$, and is real valued on the interval of the real axis between them. From (2.5) it follows that the functions $S_{ij}^{kl}(\theta)$ are meromorphic in θ, and real at $\mathrm{Re}(\theta) = 0$. The two cuts in the s variable, in fact, are unfolded by the transformation (2.5): for instance, the upper side of the cut along $[(m_i + m_j)^2, \infty]$ is mapped into the positive semiaxis $0 < \theta < \infty$, while the lower side is mapped into the negative semiaxis $-\infty < \theta < 0$. The physical sheet of the s–plane goes into the strip $0 \le \mathrm{Im}(\theta) \le \pi$, while the second Riemann sheet is mapped into $-\pi \le \mathrm{Im}(\theta) \le 0$. The structure in the θ plane repeats then with periodicity $2\pi i$. See Fig. 2.6 for a representation of the analytic structure of the S–matrix in the two variables s and θ.

The two-particle S-matrices satisfy the usual requirements of unitarity, expressed as

$$\sum_{n,m} S_{ij}^{nm}(\theta)\, S_{nm}^{kl}(-\theta) = \delta_i^k \delta_j^l\,, \tag{2.6}$$

and crossing symmetry, given by

$$S_{ik}^{lj}(\theta) = S_{ij}^{kl}(i\pi - \theta)\;, \tag{2.7}$$

since the analytic continuation $s \to t$ from the s-channel to the t-channel corresponds to the change of variable $\theta \to i\pi - \theta$. Furthermore, the amplitudes are restricted by the star-triangle (or Yang-Baxter) equations

$$S_{i_1 i_2}^{k_1 k_2}(\theta_{12})\, S_{k_1 k_3}^{j_1 j_3}(\theta_{13})\, S_{k_2 i_3}^{j_2 k_3}(\theta_{23}) = S_{i_1 i_3}^{k_1 k_3}(\theta_{13})\, S_{k_1 k_2}^{j_1 j_2}(\theta_{12})\, S_{i_2 k_3}^{k_2 j_3}(\theta_{23})\;, \tag{2.8}$$

where a sum over the intermediate indices is understood. The system of equations (2.6), (2.7) and (2.8) is in many cases sufficient to solve the kinematics of the problem, determining a consistent solution for the two-particle S-matrix, up to a so-called CDD ambiguity, which consists in multiplying the solution by factors that alone satisfy the same equations. Since the bound states of a theory correspond to singularities of the S-matrix, its analytic structure encodes the spectrum of the system. Stable bound states are usually associated to simple poles in the s variable located in the real interval $(m_i - m_j)^2 < s < (m_i + m_j)^2$. These are mapped by (2.5) onto the imaginary θ–axis of the physical strip (see Fig. 2.6). If a two–particle amplitude with initial states A_i and A_j has a simple pole in the s-channel at $\theta = iu_{ij}^n$ (A_n is the associated intermediate bound state), in the vicinity of this singularity we have

$$S_{ij}^{kl}(\theta) \sim \frac{iR_{ij}^n}{\left(\theta - iu_{ij}^n\right)} \qquad , \qquad R_{ij}^n \,=\, \Gamma_{ij}^n \Gamma_n^{kl} \tag{2.9}$$

where Γ_{ij}^n are the on-shell three–particle coupling constants of the underlying quantum field theory (see Fig. 2.7). Remembering that the corresponding singularity in the s variable is of the form $\left(s - m_n^2\right)^{-1}$ and using relation (2.5), we get the following expression for the mass of the bound state:

$$m_n^2 \,=\, m_i^2 + m_j^2 + 2\, m_i\, m_j\, \cos u_{ij}^n \,. \tag{2.10}$$

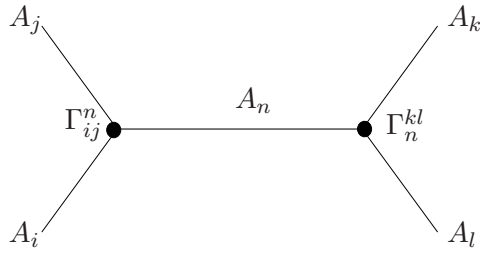

Figure 2.7: First-order pole in the S–matrix.

The dynamics of the system can be determined by implementing the so–called "bootstrap principle", which consists in identifying the bound states with some of the particles appearing as asymptotic states. This leads to further equations which permit to fix the CDD ambiguities mentioned above and to identify the particle content of the theory. Finally, it is worth recalling that unstable bound states (resonances) are associated to s–variable poles in the second Riemann sheet at $s = \left(m_k - i\frac{\Gamma_k}{2}\right)^2$, where Γ_k is the inverse life–time of the particle. These correspond to poles in θ located in the strip $-\pi \leq \mathrm{Im}(\theta) \leq 0$ at positions $\theta = -iu_{ij}^k + \alpha_{ij}^k$ satisfying

$$\begin{aligned} m_k^2 - \frac{\Gamma_k^2}{4} \,&=\, m_i^2 + m_j^2 + 2\, m_i\, m_j\, \cos u_{ij}^k\, \cosh \alpha_{ij}^k \,, \\ m_k\, \Gamma_k \,&=\, 2\, m_i\, m_j\, \sin u_{ij}^k\, \sinh \alpha_{ij}^k \,. \end{aligned} \tag{2.11}$$

The knowledge of the exact S-matrix further permits to extract non-perturbative information on the off-shell quantities of the theory, namely the correlation functions. The quite involved path towards this aim starts by expanding the spectral function $\rho^{(\Phi)}$

$$\langle\, 0 \,|\, \Phi(x)\Phi(0) |\, 0 \rangle \;\equiv \int \frac{d^2p}{(2\pi)^2}\, \rho^{(\Phi)}(p^2)\, e^{ip\cdot x} \;,$$

associated to a given operator Φ, as a sum over complete sets of particle states

$$\rho^{(\Phi)}(p^2) = 2\pi \sum_n \frac{1}{n!} \int \quad d\Omega_1 ... d\Omega_n \quad \delta(p^0 - p_1^0 ... - p_n^0)\, \delta(p^1 - p_1^1 ... - p_n^1) \;\times$$
$$\times \;\Big|\, F^{\Phi}_{a_1 ... a_n}(\theta_1, \ldots, \theta_n) \,\Big|^2 \;, \tag{2.12}$$

where $d\Omega \equiv \frac{dp}{2\pi\, 2E} = \frac{d\theta}{4\pi}$ and

$$F^{\Phi}_{a_1 ... a_n}(\theta_1, \ldots, \theta_n) = \langle\, 0 \,|\, \Phi(0) \,|\, A_{a_1}(\theta_1) \ldots A_{a_n}(\theta_n) \,\rangle \;. \tag{2.13}$$

The matrix elements (2.13), called "form factors" and pictorially depicted in Fig. 2.8, are subject to the Watson equations, which relate them to the scattering amplitudes. In the case of integrable theories these equations take a simplified form [22, 25, 24], allowing for the determination of form factors once the S-matrix is known. Furthermore, it has been shown in a series of works (see, for instance [25]) that the spectral representation for *massive* theories has a fast convergent behaviour, therefore accurate estimates of correlators can be obtained by just using few exact terms in the series (2.12). This feature greatly simplifies the problem.

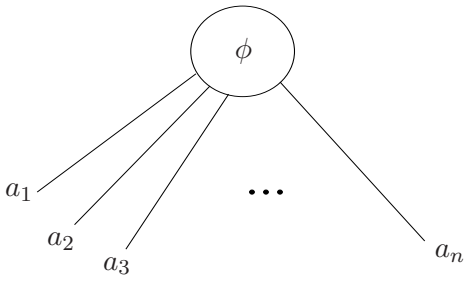

Figure 2.8: Form factor (2.13).

Here we limit ourselves to the description of the main equations ruling the simplest non–trivial form factors, i.e. the two–particle ones, that we will use and discuss in the following two Sections. The discontinuity of the matrix elements across the unitarity cut leads to the following relation with the two–particle scattering amplitudes:

$$F^{\Phi}_{ab}(\theta) \;=\; S^{cd}_{ab}(\theta) F^{\Phi}_{cd}(-\theta) \;, \tag{2.14}$$

where $\theta = \theta_1 - \theta_2$. The crossing symmetry of the form factor is expressed as

$$F^{\Phi}_{a\bar{a}}(\theta + 2i\pi) \;=\; e^{-2i\pi\gamma_{\Phi,a}} F^{\Phi}_{\bar{a}a}(-\theta) \;, \tag{2.15}$$

where the phase factor $e^{-2i\pi\gamma_{\Phi,a}}$ is inserted to take into account a possible semi-locality of the operator which interpolates the particle a (i.e. any operator φ_a such that $\langle 0|\varphi_a|a\rangle \neq 0$) with respect to the operator $\Phi(x)$. When $\gamma_{\Phi,a} = 0$, there is no crossing symmetric counterpart to the unitarity cut but when $\gamma_{\Phi,a} \neq 0$, there is a non-locality discontinuity in the plane of the Mandelstam variable s defined in (2.5), with $s = 0$ as branch point. In the rapidity parameterization there is however no cut because the different Riemann sheets of the s-plane are mapped onto different sections of the θ-plane; the branch point $s = 0$ is mapped onto the points $\theta = \pm i\pi$ which become therefore the locations of simple annihilation poles. The residues at these poles are given by

$$Res_{\theta=\pm i\pi} F^{\Phi}_{ab}(\theta) = i\delta_{\bar{a}b}(1 - e^{\mp 2i\pi\gamma_{\Phi,a}})\langle 0|\Phi|0\rangle \ . \tag{2.16}$$

Finally, the two–particle form factors inherit the s–channel bound state poles of the S–matrix, and the corresponding residua are given by

$$Res_{\theta=iu^c_{ab}} F^{\Phi}_{ab}(\theta) = i\Gamma^c_{ab} F^{\Phi}_c \ , \tag{2.17}$$

where the couplings Γ^c_{ab} coincide with the ones in (2.9). This last relation is pictorially represented in Fig. 2.9.

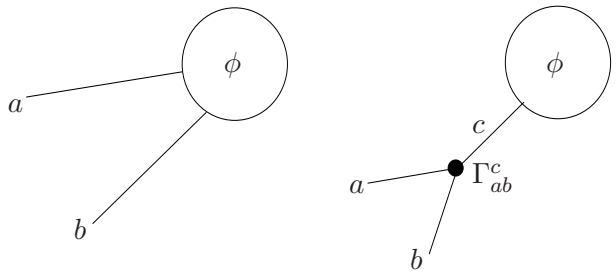

Figure 2.9: Dynamical pole (2.17) in the two–particle form factor $F^{\Phi}_{ab}(\theta)$.

2.1.3 Landau–Ginzburg theory

As we have seen in Sect. 2.1.1, statistical models at the critical point can be described by conformal field theories (CFT), and many systems of physical relevance have been identified with the Virasoro minimal models. The operators of these theories can be organized in a finite number of families, and this simplifies the dynamics allowing in principle for a complete solution. The only disadvantage of this kind of theories is that they have no Lagrangian formulation, therefore they cannot be studied by a path–integral approach and the underlying physics is not always transparent. However, for a class of minimal theories, the unitary ones $\mathcal{M}(m+1, m)$, there is a simple effective Lagrangian description, suggested in [26], which is realized by a self–interacting field ϕ subjected to a power–like potential. The field ϕ stands for the order parameter of the statistical system, and the potential $V(\phi)$, whose extrema correspond to the various critical phases of the system, is usually chosen to be invariant under the reflection $\phi \to -\phi$. For a potential of degree $2(m-1)$, this ensures the

existence of $m-1$ minima separated by $m-2$ maxima. Several critical phases of the system can coexist if the corresponding extrema coincide. The most critical potential is therefore a monomial of the form

$$V_m(\phi) \,=\, \phi^{\,2(m-1)} \,.$$

Starting from the field ϕ, one can construct composite fields $:\phi^k:$ by normal ordering its powers. These have been shown in [26] to display the same fusion properties as the operators present in the minimal model $\mathcal{M}(m+1,m)$, supporting in this way the correspondence. In particular, the field ϕ is always associated to the primary operator $\phi_{2,2}$.

One of the nicest features of the Landau–Ginzburg description is that it provides a very intuitive picture of the perturbation of CFT away from the critical points, since this simply corresponds to adding opportune powers of ϕ to V_m.

For instance, the universality class of the Ising model is described by $m=3$, the spin operator corresponds to $\sigma \sim \phi$ and the energy operator to $\varepsilon \sim :\phi^2:$. Therefore the thermal perturbation of the critical point is described by the Landau–Ginzburg theory

$$V(\phi) \,=\, A\,\phi^4 + B\,\phi^2 + C \,,$$

where the sign of B refers to high or low temperature, respectively (see Fig. 2.10).

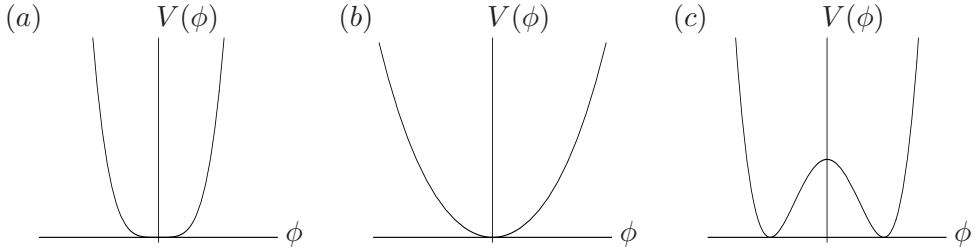

Figure 2.10: Landau–Ginzburg potential for the Ising model (a) at the critical point, (b) at high temperature, (c) at low temperature.

Another very interesting example is given by the case $m=4$, which corresponds to the TIM. The operator content of the theory is in this case identified as

$$\begin{cases} \sigma \sim \phi \\ \varepsilon \sim :\phi^2: \\ \sigma' \sim :\phi^3: \\ \varepsilon' \sim :\phi^4: \\ \varepsilon'' \sim :\phi^6: \end{cases}$$

Hence, for instance, the perturbation of the tricritical point by leading and subleading energy densities is described as

$$V(\phi) \,=\, A\,\phi^6 + B\,\phi^4 + C\,\phi^2 + D \,,$$

and some of the resulting potentials are shown in Fig. 2.11.

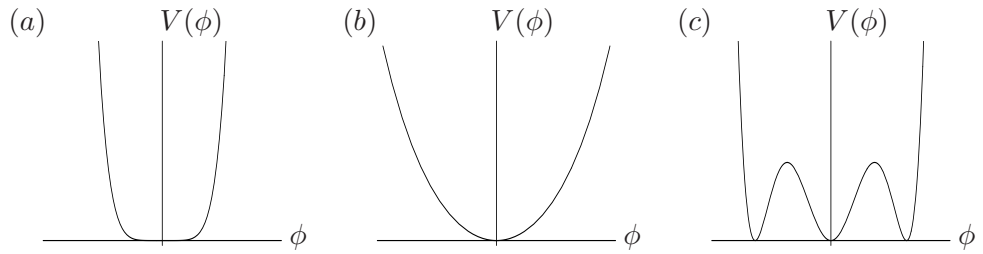

Figure 2.11: Landau–Ginzburg potential for the tricritical TIM (a) at the tricritical point, (b) with positive leading and subleading energy perturbations, (c) with positive leading and negative subleading energy perturbations.

In concluding this subsection it is worth to remark how the above mentioned correspondence between Lagrangians and minimal models is based on heuristic arguments which are not rigorously proven. Furthermore, quantum corrections can be very strong, hence a quantitative analysis of statistical system is generally not possible starting from the Lagrangian formulation. However, the qualitative picture offered by the Landau–Ginzburg theory, being essentially based on the symmetries of the model, remains valid also at quantum level. In particular, this description nicely illustrates the underlying physics in cases when the potential displays degenerate minima, since the classical solutions interpolating between the minima have a direct meaning of quantum particles, as we are going to show in the next sections.

2.1.4 Superconformal Models

We present here the main properties of conformal theories in which there is also a supersymmetry linking bosonic and fermionic fields. Here we focus our attention only on the two-dimensional super-symmetric theories. In two dimensions, the superconformal invariance is associated to two super-currents, $G(z)$ and $\bar{G}(\bar{z})$, purely analytic the latter and purely anti-analytic the former. They are both fermionic fields, with conformal weights $(\frac{3}{2}, 0)$ and $(0, \frac{3}{2})$ respectively. The algebra of these generators is defined by the singular terms of their OPE: for $G(z)$ we have

$$G(z_1)\, G(z_2) \;=\; \frac{2c}{3(z_1 - z_2)^3} + \frac{2}{z_1 - z_2} T(z_2) + \cdots \tag{2.1}$$

with an analogous expression for $\bar{G}$. The parameter c is the central charge. The field $G(z)$ (and $\bar{G}$) is itself a primary field, with operator product expansion

$$T(z_1) G(z_2) \;=\; \frac{3}{2(z_1 - z_2)^2} G(z_2) + \frac{1}{z_1 - z_2} \partial G(z_2) + \cdots \tag{2.2}$$

Let's define the generators L_n and G_n through the expansions

$$T(z) \;=\; \sum_{n=-\infty}^{\infty} \frac{L_n}{z^{2+n}} \qquad ; \qquad G(z) \;=\; \sum_{m=-\infty}^{\infty} \frac{G_m}{z^{3/2+m}} \tag{2.3}$$

which yields the explicit expressions:

$$L_n \,=\, \oint_C \frac{dz}{2\pi i} z^{n+1} T(z) \quad ; \quad G_m(z) \,=\, \oint_C \frac{dz}{2\pi i} z^{m+1/2} G(z) \ .$$

Note that in the expansion of the field $G(z)$ the indices can assume either integer or half-integer value. Indeed, $G(z)$ is a fermionic field and, analogously to the free fermion ψ of the thermal Ising model, is defined on the double covering of the plane, with a branch cut starting from the origin: making the analytic continuation $z \to e^{2\pi i}\, z$, we can have two possible boundary conditions

$$G(e^{2\pi i}\, z) \,=\, \pm G(z) \ . \tag{2.4}$$

In the periodic case (sign +), called Neveu-Schwarz (NS) sector, the indices m are half-integers, $m \in \mathbf{Z} + \frac{1}{2}$. In the anti-periodic case ($-$ sign), called Ramond (R) sector, the indices m are instead integer numbers, $m \in \mathbf{Z}$.

The OPE that involve $T(z)$ and $G(z)$ can be equivalently expressed as algebraic relations of their modes. Following the same steps in the derivation of the Virasoro algebra [6], we arrive indeed to the infinite-dimensional algebra [28] , [29]:

$$\begin{aligned} [L_n, L_m] &= (n-m) L_{n+m} + \frac{c}{12}\, n(n^2-1)\delta_{n+m,0} \\ [L_n, G_m] &= \frac{1}{2}\,(n-2m)\, G_{n+m} \\ \{G_n, G_m\} &= 2L_{n+m} + \frac{c}{3}\left(n^2 - \frac{1}{4}\right)\delta_{n+m,0}\,. \end{aligned} \tag{2.5}$$

Notice the presence of commutation and anti-commutation relations in the *graded* algebra.

As in the pure conformal case, the classification of superconformal theories reduces to finding all irreducible representations of the algebra (2.5) with the central charge c as a free parameter. The space $\mathcal{A}$ of these representations is given by the direct sum of the Neveu-Schwarz and Ramond subspaces:

$$\mathcal{A} = \mathcal{A}_{NS} \,\oplus\, \mathcal{A}_R \ .$$

Furthermore, each of the subspaces is decomposed into the direct sum of the *superconformal families*

$$\mathcal{A}_{NS} \,=\, \oplus_l [\Phi_l]_{NS} \quad ; \quad \mathcal{A}_R \,=\, \oplus_\lambda [\Phi_\lambda]_R \ , \tag{2.6}$$

where the *primary fields* Φ_l and Φ_λ of this algebra satisfy

$$\begin{aligned} &L_n \Phi_a \,=\, 0 && n > 0 \\ &L_0 \Phi_a \,=\, \Delta_a\, \Phi_a \\ &G_m \Phi_a \,=\, 0 && m > 0\,. \end{aligned} \tag{2.7}$$

As for the Virasoro algebra, the representations are built starting from the primary fields and applying to them the *creation operators* L_n and G_m, with $n, m < 0$. Each representation is uniquely identified by the conformal weights Δ_a of its primary field. The same considerations hold, as usual, for the anti-analytic sector.

The operators $T(z)$ and $G(z)$ can be used to define the generators of particular infinitesimal transformations

$$\delta_\epsilon \,=\, \oint_C \frac{dz}{2\pi i}\epsilon(z)\,T(z) \quad ; \quad \delta_\omega \,=\, \oint_C \frac{dz}{2\pi i}\omega(z)\,G(z) \tag{2.8}$$

on the coordinates $(Z,\bar{Z}) = (z,\theta;\bar{z},\bar{\theta})$ of a $2+2$ dimensional *super-space*. For the analytic part of this super-space, we have the following superconformal transformation

$$z \to z + \epsilon(z) - \omega(z)\theta \quad ; \quad \theta \to \theta + \frac{1}{2}\epsilon'(z) + \omega(z) \ . \tag{2.9}$$

It's clear that $\epsilon(z)$ and $\omega(z)$ are the bosonic and fermionic infinitesimal transformations respectively. The peculiar nature of (2.9) consists of being the conformal transformation of the 1-form $dz + \theta\, d\theta$; it is therefore convenient to consider $G(z)$ and $T(z)$ as the components of a *super-stress-energy tensor*

$$W(z,\theta) \,=\, G(z) + \theta\, T(z)\,. \tag{2.10}$$

Neveu-Schwarz sector. In the NS sector the representations are given in terms of the superfields

$$\Phi_l(Z,\bar{Z}) \,=\, \Phi_l(z,\bar{z}) + \theta\,\psi_l(z,\bar{z}) + \bar{\theta}\,\bar{\psi}_l(z,\bar{z}) + i\theta\,\bar{\theta}\,\tilde{\Phi}_l(z,\bar{z}) \tag{2.11}$$

where the primary fields Φ_l is the first component while $\psi_l = G_{-1/2}\Phi_l$, $\bar{\psi}_l = \bar{G}_{-1/2}\Phi_l$ and $\tilde{\Phi}_l = -iG_{-1/2}\bar{G}_{-1/2}\Phi_l$. In the next Section we will study an explicit example of SUSY theory in N-S sector, the TIM.

For a exhaustive description of the Ramond sector see [6] .

Irreducible representations and minimal models. The irreducible representations of the superconformal algebra are determined in the same way as those of the Virasoro algebra. In this case, the conformal weights read [28] [29]:

$$\Delta_{r,s} \,=\, \Delta_0 + \frac{1}{4}(r\beta_+ + s\beta_-)^2 + \frac{1}{32}[1-(-1)^{r+s}] \ , \tag{2.12}$$

where

$$\begin{aligned} &\Delta_0 = (\tilde{c}-1)/16 \\ &\beta_\pm \,=\, \frac{1}{4}\left(\sqrt{1-\tilde{c}} \pm \sqrt{9-\tilde{c}}\right) \quad ; \quad \beta_+\,\beta_- \,=\, -\frac{1}{2}\,. \end{aligned} \tag{2.13}$$

In this formula r and s are two natural numbers: for the NS fields, $r+s \in 2\mathbf{Z}$, whereas for the Ramond fields $r+s \in 2\mathbf{Z}+1$. When the parameter $\rho = -\beta_-/\beta_+$ becomes a rational number, the operator algebra closes within a *finite number* of superconformal families. Particularly interesting are the unitary superconformal series, here denoted by $\mathcal{SM}_p$ $(p = 3,4,5,\ldots)$, with

$$\rho \,=\, \frac{p}{p+2} \ .$$

In this case there are $[p^2/2]$ primary fields $\Phi_{r,s}$, where the indices r and s assume the values $r = 1,2,\ldots,(p-1); s = 1,2,\ldots(p+1)$ (where $[x]$ is the integer part of x). The central charge and

the conformal weights take the discrete values

$$c = \frac{3}{2}\left[1 - \frac{8}{p(p+2)}\right] \quad , \quad p = 3, 4, \ldots \tag{2.14}$$
$$\Delta_{r,s} = \frac{[(p+2)r - ps]^2 - 4}{8p(p+2)} + \frac{1}{32}[1 - (-1)^{r+s}] \, .$$

The Coulomb Gas method can be generalized to the superconformal model, both in the Neveu-Schwarz [30] and Ramond [31] sectors, and permits to determine the exact values of the structure constants of the operator algebra.

Landau-Ginzburg theory. It can be shown that the unitary superconformal models $\mathcal{S}M_p$ are associated to a supersymmetric Landau-Ginzburg theory [26]. The super-potential relative to the minimal models is given by $W(\Phi) = g\Phi^p$ and the action reads

$$\mathcal{A} = \int d^2x \, d^2\theta \, \left[-\frac{1}{2} D\Phi \, \bar{D}\Phi + W(\Phi)\right] , \tag{2.15}$$

where

$$D = \partial_\theta - \theta \, \partial_z \qquad \bar{D} = \partial_{\bar{z}} - \bar{\theta} \, \partial_{\bar{z}}$$

are the covariant derivatives, θ and $\bar{\theta}$ are Grassmann variables, while $\Phi(z, \bar{z}, \theta, \bar{\theta})$ is a superfield

$$\Phi(z, \bar{z}, \theta, \bar{\theta}) = \varphi + \theta \, \psi + \bar{\theta} \, \bar{\psi} + i \, \bar{\theta}\bar{\theta} \, \chi \ .$$

Identifying also in this case the NS superconformal primary field that sits in the position $(2, 2)$ of the Kac table with Φ, i.e. $\Phi_{2,2} \equiv \Phi$, and using the fusion rules of the superconformal minimal model, one can recursively define the composite operators $: \Phi^k :$ and show that their fusion rules lead to the operator identity

$$D \, \bar{D} \, \Phi \simeq \Phi^{p-1} \ . \tag{2.16}$$

This formula coincides with the equation of motion that can be derived by the supersymmetric action (2.15).

As for the minimal models of the Virasoro algebra, also for the superconformal minimal models we can determine the exact expression of the modular invariant partition functions on a torus [27].

The series of the superconformal minimal models has intersection with the Virasoro minimal models; the most studied example is the model $\mathcal{SM}_3$ that describes the TIM and coincides with the second minimal model of the Virasoro unitary series. The supersymmetry of this model provides a different interpretation of the primary fields and gives reason of the particular relationships that exist among the structure constants of the conformal model (see Table 2.2, $c_1 = c_2$).

2.2 Spectrum of the TIM with spin reversal symmetric perturbations

Based on the paper:
L. Lepori, G. Mussardo and G. Z. Toth,
"The particle spectrum of the Tricritical Ising Model with spin reversal symmetric perturbations",
J. Stat. Mech. **0809** (2008) P09004 [arXiv:0806.4715 [hep-th]].

2.2.1 Introduction

The two-dimensional TIM, which is the second in the unitary series of conformal minimal models after the critical Ising model [67], describes critical phenomena in a variety of systems with tricritical points. It also exhibits superconformal symmetry, being the first member of the series of superconformal minimal models [17], and it has interesting symmetries related to the coset constructions $su(2)_2 \otimes su(2)_1/su(2)_3$ and $e(7)_1 \otimes e(7)_1/e(7)_2$ [32, 33]. Due to these properties the TIM has attracted interest for many years.

In the present Section we study the particle spectrum of the TIM perturbed by those relevant scaling fields which are invariant under spin reversal. These fields are the energy density ε and the vacancy density t, with conformal weights given by $\Delta_2 = 1/10$ and $\Delta_4 = 3/5$ respectively[1]. The action of the perturbed model can formally be written as

$$\mathcal{S} = \mathcal{S}_0 + g_2 \int \varepsilon(z,\bar{z})\, \mathrm{d}^2 z + g_4 \int t(z,\bar{z})\, \mathrm{d}^2 z\,, \tag{2.17}$$

where $\mathcal{S}_0$ is the action of the TIM at its conformal point, whereas g_2 and g_4 are the two coupling constants of our theory. Their dimensions are fixed by the conformal weights of the conjugate fields, $g_i \sim \mathcal{M}^{2-2\Delta_i}$, where $\mathcal{M}$ is an arbitrary mass scale of the off-critical model. The ratios of the particle masses of the model (2.17), being universal quantities, depend only on a single dimensionless combination η of the two coupling constants g_2 and g_4, that we choose as

$$\eta = \frac{g_4}{|g_2|^{\frac{2-2\Delta_4}{2-2\Delta_2}}} = \frac{g_4}{|g_2|^{\frac{4}{9}}}\ . \tag{2.18}$$

In the following we write η_+ if $g_2 > 0$ and η_- if $g_2 < 0$.

The evolution of the particle spectrum by varying η is an important characteristic of the class of universality associated with the TIM. It is worth stressing that the action (2.17) provides the simplest example of a bosonic theory having kinks in its spectrum which do not get confined under continuous variations of the coupling constants. To appreciate this feature, one has to recall that, in a generic bosonic theory, the kinks are quite fragile objects: they get generally confined under a small perturbation of the parameters (see, for instance, refs. [35, 36]). The stability of the kinks can be guaranteed, for instance, by supersymmetry but in theories that have also fermions [38]. In purely bosonic theories, the robustness of the kink states may only come via a fine-tuning mechanism or special symmetry of the perturbing operators. In the model analyzed in this Section, the latter property is the spin reversal invariance of both perturbations. The study of the particle

[1] For further details on the model and its symmetry we refer the reader to the article [34].

spectrum of this model is, in any case, interesting in itself, since the action (2.17) is non-integrable if both g_2 and g_4 are non-zero.

2.2.2 The Tricritical Ising model

Let's discuss now the class of universality of the TIM, associated to the second unitary minimal model $\mathcal{M}_4$. One of its microscopic realization is provided by the Blume-Capel model [6]. Equivalently, this class of universality can be associated to a Landau-Ginzburg (LG) lagrangian based on a scalar field φ, a formulation having the advantage of an easy bookkeeping of the Z_2 symmetry property of each order parameter. The euclidean LG action is

$$\mathcal{S} = \int \mathrm{d}^2x \left[\frac{1}{2}(\partial_\mu \varphi)^2 + g_1\varphi + g_2\varphi^2 + g_3\varphi^3 + g_4\varphi^4 + \varphi^6 \right] \quad , \tag{2.19}$$

with the tricritical point identified by the condition $g_1 = g_2 = g_3 = g_4 = 0$. The statistical interpretation of the coupling constants reads as follows: g_1 plays the role of an external magnetic field h, g_2 measures the displacement of the temperature from its critical value, i.e. $g_2 \sim (T - T_c)$, g_3 may be regarded as a sub-leading magnetic field h' and, finally, g_4 may be interpreted as a chemical potential for the vacancies.

The model at the critical point is described by the second unitary minimal model $\mathcal{M}_4$: its central charge is $c = \frac{7}{10}$ and the exact values of its conformal weight are

$$\Delta_{l,k} = \frac{(5l - 4k)^2 - 1}{80} \quad , \quad \begin{matrix} 1 \le l \le 3 \\ 1 \le k \le 4 \end{matrix} \quad . \tag{2.20}$$

They are organized in the Kac table 2.1.

$\frac{3}{2}$	$\frac{6}{10}$	$\frac{1}{10}$	0
$\frac{7}{16}$	$\frac{3}{80}$	$\frac{3}{80}$	$\frac{7}{16}$
0	$\frac{1}{10}$	$\frac{6}{10}$	$\frac{3}{2}$

Table 2.1: Kac table of the unitary minimal model $\mathcal{M}_4$.

There are six scalar primary fields and, out of them, four are relevant operators: the operator product expansion algebra and the relative structure constants are reported in Table 2.2. The correlation functions of these fields can be computed straightforwardly using the Coulomb gas.
The six primary fields perfectly match the identification provided by the composite fields of the Landau-Ginzburg theory and by the symmetries of the model. There are two different Z_2 symmetries, one associated to the spin transformation, the other to the duality.

With respect to the Z_2 spin symmetry $\varphi \to -\varphi$ we have

even $*$ *even* $\epsilon * \epsilon = [1] + c_1\ [t]$ $t * t = [1] + c_2\ [t]$ $\epsilon * t = c_1\ [\epsilon] + c_3\ [\varepsilon'']$	$c_1 = \frac{2}{3}\sqrt{\frac{\Gamma(\frac{4}{5})\Gamma^3(\frac{2}{5})}{\Gamma(\frac{1}{5})\Gamma^3(\frac{3}{5})}}$ $c_2 = c_1$ $c_3 = \frac{3}{7}$ $c_4 = \frac{1}{2}$ $c_5 = \frac{3}{2}c_1$ $c_6 = \frac{3}{4}$ $c_7 = \frac{1}{4}c_1$ $c_8 = \frac{7}{8}$ $c_9 = \frac{1}{56}$
even $*$ *odd* $\epsilon * \sigma' = c_4\ [\sigma]$ $\epsilon * \sigma = c_4\ [\sigma'] + c_5\ [\sigma]$ $t * \sigma' = c_6\ [\sigma]$ $t * \sigma = c_6\ [\sigma'] + c_7\ [\sigma]$	
odd $*$ *odd* $\sigma' * \sigma' = [1] + c_8\ [\varepsilon'']$ $\sigma' * \sigma = c_4\ [\epsilon] + c_6\ [t]$ $\sigma * \sigma = [1] + c_5\ [\epsilon] + c_7\ [t] + c_9\ [\varepsilon'']$	

Table 2.2: Fusion rules for TIM operators.

1. two odd fields: the magnetization operator $\sigma = \phi_{\frac{3}{80},\frac{3}{80}} \equiv \varphi$ and the sub-leading magnetic operator $\sigma' = \phi_{\frac{7}{16},\frac{7}{16}} \equiv :\varphi^3:$

2. four even fields: the identity operator $1 = \phi_{0,0}$, the energy operator $\varepsilon = \phi_{\frac{1}{10},\frac{1}{10}} \equiv :\varphi^2:$, and the density operator $t = \phi_{\frac{6}{10},\frac{6}{10}} \equiv :\varphi^4:$, associated to the vacancies. Finally, there is also the irrelevant field $\varepsilon" = \phi_{\frac{3}{2},\frac{3}{2}}$. The operator product expansion of these fields gives rise to a sub-algebra of the fusion rules.

As for the Ising model, also for the TIM there is another Z_2 associated to the duality transformation, under which the fields change as

- the magnetization order parameters change into the disorder operators

$$\mu = D^{-1}\sigma D = \tilde{\phi}_{\frac{3}{80},\frac{3}{80}} \quad , \quad \mu' = D^{-1}\sigma' D = \tilde{\phi}_{\frac{7}{16},\frac{7}{16}} \ . \tag{2.21}$$

- the even fields transform instead in themselves

$$D^{-1}\varepsilon D = -\varepsilon \quad , \quad D^{-1}tD = t \quad , \quad D^{-1}\varepsilon" D = -\varepsilon" \, , \tag{2.22}$$

  ε and $\varepsilon"$ are odd fields while t is an even field under this transformation.

Supersymmetry

It is interesting to note that TIM provides an explicit realization of a supersymmetric field theory, being the first model of the minimal unitary superconformal series: the Z_2 even fields enter the definition of a super-field of the Neveu-Schwarz sector

$$\mathcal{N}(z,\bar{z},\theta,\bar{\theta}) = \varepsilon(z,\bar{z}) + \bar{\theta}\,\psi(z,\bar{z}) + \theta\,\bar{\psi}(z,\bar{z}) + i\,\theta\bar{\theta}\,t(z,\bar{z})\,, \tag{2.23}$$

while the Z_2 odd magnetization operators form two irreducible representations of the Ramond sector. The supersymmetric Landau-Ginzburg of the model can be written as

$$\mathcal{S} = \int d^2x\, d^2\theta \left[\frac{1}{2}\mathcal{D}\mathcal{N}\,\bar{\mathcal{D}}\mathcal{N} + \mathcal{N}^3\right] \ , \tag{2.24}$$

where $\mathcal{D}$ and $\bar{\mathcal{D}}$ are the covariant derivatives

$$\mathcal{D} = \frac{\partial}{\partial\theta} - \theta\frac{\partial}{\partial z} \quad , \quad \overline{\mathcal{D}} = \frac{\partial}{\partial\overline{\theta}} - \overline{\theta}\frac{\partial}{\partial\overline{z}} \ . \tag{2.25}$$

Note that the supersymmetry and the organization of its Z_2 even primary fields in a superfield are at the root of the relationships that link the various structure constants (see, for instance, the identity $c_2 = c_1$ in Table 2.2).

Exceptional algebra E_7

We mention that TIM can be also realized in terms of a coset on the exceptional algebra E_7

$$\mathcal{M}_4 \ = \ \frac{(E_7)_1 \otimes (E_7)_1}{(E_7)_2} \ . \tag{2.26}$$

For E_7, the dual Coxeter number is $\tilde{h} = 18$ and therefore the central charge of this coset theory is $c = \frac{7}{10}$. For details on the construction of the representations see [6].

2.2.3 A quick glimpse into the perturbed model

In the TIM, the parameter g_2 can be interpreted as the difference between the actual temperature and its critical value. The $g_2 = 0$ critical line divides the phase plane into the high temperature ($g_2 > 0$) and the low temperature ($g_2 < 0$) halves, which are mapped into each other by a duality transformation under which $(g_2, g_4) \leftrightarrow (-g_2, g_4)$. Along the critical line $g_2 = 0$, the model (2.17) is integrable and has also supersymmetry [39, 40, 41]: the $g_4 > 0$ half line consists of a massless renormalization group flow to the Ising critical point in which the supersymmetry is spontaneously broken, while the $g_4 < 0$ half line consists of first order phase transition points with unbroken supersymmetry. The meeting point of these half lines is the tricritical point. The model is also integrable along the $g_4 = 0$ line where its particle spectrum and S-matrix are related to the E_7 Lie-algebra [42, 43], therefore we shall refer to this line as the E_7-related line. In the subsection above we described the correspondence (at least at the tree level) between various term of the Landau-Ginzburg lagrangian and the relevant deformation of TIM. In our case this correspondence

allows one to associate the Landau-Ginzburg potentials with the various parts of the (g_2, g_4) phase plane, as shown in Figure 2.12.

The shape of the potentials in Figure 2.12 provides a useful guide to the nature of the excitations at the various points of the (g_2, g_4) plane. For instance, in the high temperature phase, where the spin reversal symmetry is unbroken, the potential has a unique vacuum and therefore the particles do not have topological charge in this phase. Moving up from the positive horizontal axis in the first quadrant, the curvature of the minimum decreases until it vanishes when we reach the positive vertical axis: the theory has a massless spectrum at this point. Instead, moving down from the positive horizontal axis in the forth quadrant, two metastable vacua start to appear and they become abruptly degenerate with the true vacuum once the negative vertical axis is reached. Right at this point the theory has kink excitations, i.e. topologically charged particles, that interpolate between the three vacua.

In the low temperature phase, i.e. in the second and third quadrants, the spin reversal symmetry is instead spontaneously broken and the ground state is doubly degenerate, hence in these regions we expect that the spectrum consists of kinks and possible bound states thereof. Moreover, it is sufficient to look at the evolution of the potential in these quadrants in order to conclude that the kinks of this model are always stable excitations (at least those with lowest mass), no matter how we vary the coupling constants. In more detail, starting from the negative horizontal axis and moving up in the third quadrant, the barrier between the two vacua decreases until it disappears when we reach the positive vertical axis. Hence, we expect the masses of the kinks and their possible bound states to decrease along this trajectory so that they adiabatically vanish once we arrive at the positive vertical axis. On the other hand, moving down from the negative horizontal axis in the third quadrant, a metastable vacuum starts to appear in the middle of the barrier: this state becomes abruptly degenerate with the two existing vacua just when we reach the negative vertical axis. At this point, the kink excitations between the two original vacua break down and give rise to two different sets of topological excitations relative to the new threefold vacuum structure.

In the following we are going to support the physical scenario described above by using a combination of analytic and numerical methods. The first method is the Form Factor Perturbation Theory (FFPT) [35] that allows us to get analytic information on the spectrum in the vicinity of the integrable lines. The second method is the Truncated Conformal Space Approach (TCSA) [23], which is one of the best suited numerical approaches for extracting the spectrum of perturbed conformal field theories. The spin reversal and the duality symmetries of the TIM play also an important role in the implementation of both methods. Let's finally mention that the two integrable cases $g_2 = 0$ and $g_4 = 0$ were studied by TCSA in [34]; the present work can thus be regarded as an extension of those studies to the non-integrable ($g_2 \neq 0$, $g_4 \neq 0$) domain.

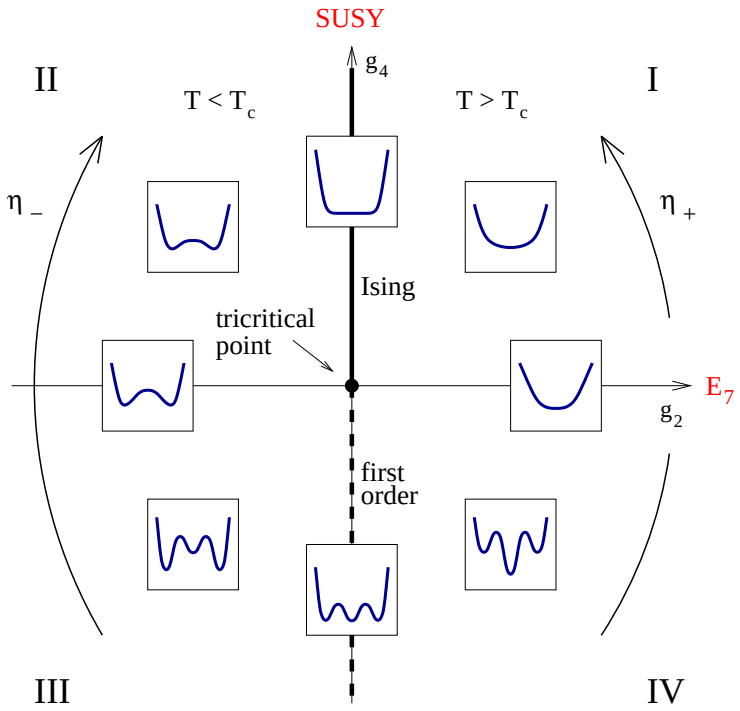

Figure 2.12: Landau-Ginzburg potentials associated with the various parts of the phase space.

2.2.4 The two methods

In this subsection we briefly discuss the two techniques that have been employed to study the evolution of the spectrum of our model.

Form Factor Perturbation Theory

The Form Factor Perturbation Theory permits to investigate the behaviour of a theory in the vicinity of an integrable direction, either if the integrable theory is massive [35, 36] or massless [37]. Let $\mathcal{A}_{\rm int}$ be the action of the integrable model and $\Upsilon(x)$ the field that moves the system away from integrability, so that nearby the action of the theory can be written as

$$\mathcal{A} = \mathcal{A}_{\rm int} + \lambda \int \mathrm{d}^2x \; \Upsilon(x) \; . \tag{2.27}$$

If the original integrable model has scalar excitations[2] $A_1(\theta), A_2(\theta), \ldots$, the first order correction in λ to their mass M_k is given by

$$\delta M_k^2 \simeq 2\,\lambda\, F_k^{\Upsilon}(\mathrm{i}\pi) \; , \tag{2.28}$$

[2]The rapidity variable θ expresses the dispersion relation of the excitations. If we consider a massive particle of mass m, its energy and momentum are given by $E = m\cosh\theta$, $p = m\sinh\theta$. If, instead, the particle is massless, it can be a right or a left mover excitation. The dispersion relations of a right mover are $E_R = p = M\mathrm{e}^{\theta}$, while those of a left mover $E_L = -p = M\mathrm{e}^{-\theta}$, where M is an arbitrary mass scale.

where

$$F_k^{\Upsilon}(\theta_{12}) \equiv \langle 0|\Upsilon(0)|A_k(\theta_1)\,A_k(\theta_2)\rangle \tag{2.29}$$

is the two-particle form factor of the operator $\Upsilon(x)$, with $\theta_{12}=\theta_1-\theta_2$. A similar formula also holds if the integrable model has massless excitations, with a proper interpretation of the rapidity variable θ [37]. If, instead, the integrable theory has topological kinks $|K_{ab}(\theta)\rangle$ interpolating between the vacuum states $|a\rangle$ and $|b\rangle$, the relevant formula is

$$\delta M_{ab}^2 \simeq 2\,\lambda\,F_{ab}^{\Upsilon}(\mathrm{i}\pi)\ , \tag{2.30}$$

where

$$F_{ab}^{\Upsilon}(\theta_{12}) \equiv {}_k\langle 0|\Upsilon(0)|K_{ab}(\theta_1)\,K_{ba}(\theta_2)\rangle\ . \tag{2.31}$$

In integrable field theories the form factors of a generic scalar operator $\Upsilon(x)$ can be computed exactly [22, 24] and therefore we can study the evolution of the spectrum near to the integrable lines. However, one has to be careful when applying the formulas (2.29) and (2.31) since the two-particle form factor can be singular at $\theta_{12}=\mathrm{i}\pi$. This happens if the perturbing operator $\Upsilon(x)$ has a semi-local index γ with respect to the particle excitations (this is usually the case of the topological kinks, for instance). In this case the point $\theta_{12}=\pm\mathrm{i}\pi$ is the location of a simple pole of the two-particle form factor, whose residue is given by [36, 24]

$$-\,\mathrm{i}\,\mathrm{Res}_{\theta_{12}=\pm\mathrm{i}\pi}\,F_{ab}^{\Upsilon}(\theta_{12}) = (1-\mathrm{e}^{\mp 2\mathrm{i}\pi\gamma})\ {}_k\langle 0|\Upsilon|0\rangle_k\ . \tag{2.32}$$

The result of the brief analysis given above can be summarized as follows. If $F_l^{\Upsilon}(\mathrm{i}\pi)$ is finite, the corresponding particle or kink excitation survives the perturbation and its mass is adiabatically shifted from the original value. Vice versa, if $F_l^{\Upsilon}(\mathrm{i}\pi)$ is divergent, the corresponding excitation no longer survives as asymptotic particle of the perturbed theory, i.e. it gets confined.

The truncation method

The Truncated Conformal Space Approach (TCSA) [23] can be used to study perturbed conformal field theories. It consists in a finite size analysis of the spectrum of a theory on a cylinder of circumference R. This is realized by truncating the conformal basis at a certain level n in the Verma modules of the irreducible representations of the primary fields and solving the eigenvalue and eigenvector problem of the truncated Hamiltonian operator numerically.

To extract a quantity F relative to the $R\to\infty$ limiting model, one calculates $F(R,n)$ (i.e. F at a cylinder circumference R and truncation level n) for several values of R, and possibly also for several values of n. Usually there is a range $R_{F,\min}<R<R_{F,\max}(n)$ such that in this range $F(R,n)$ is an approximately constant function of R, and its value can be regarded as a good approximation of the infinite-volume value of F. This range is called the *physical window* for F. Both $R_{F,\min}$ and $R_{F,\max}(n)$ depend on F, and $R_{F,\max}(n)$ also depends on n and is expected to tend to infinity as n is increased. Hence, the approximation to F usually improves if n is increased. For $R>R_{F,\max}(n)$ the truncation effects spoil the approximation to F and give rise to an unphysical window of values for this quantity.

We determine the masses of the particles from the energy differences

$$\Delta E_i(R,n)\equiv(E_i(R,n)-E_0(R,n))\ , \tag{2.33}$$

where $E_0(R,n)$ is the lowest energy line. In our case, the individual energy levels $E_i(R,n)$ diverge as $n \to \infty$ if $g_4 \neq 0$, since the conformal weight of the perturbation t is greater than $1/2$, the energy differences $E_i(R,n) - E_0(R,n)$ are however convergent [45]. We also use the TCSA to calculate form factors and vacuum expectation values. This can be done by computing numerically the eigenvectors belonging to the various energy eigenvalues.

The Hamiltonian operator of the model (2.17) on a cylinder of circumference R is

$$\begin{aligned} H &= \tfrac{2\pi}{R}\left(L_0 + \bar{L}_0 - \tfrac{c}{12}\right) + \\ &+ 2\pi g_2 \lambda_2 R^{-2\Delta_2} \int_0^R \varepsilon(x,0)\,\mathrm{d}x + 2\pi g_4 \lambda_4 R^{-2\Delta_4} \int_0^R t(x,0)\,\mathrm{d}x\,, \end{aligned} \tag{2.34}$$

where $c = 7/10$ is the central charge of the TIM, whereas L_0 and $\bar{L}_0$ are the zero index generators of the chiral Virasoro algebras. For convenience, we have chosen to introduce the quantities

$$\lambda_2 = (2\pi)^{2\Delta_2 - 1} \times 0.0928344\ , \qquad \lambda_4 = (2\pi)^{2\Delta_4 - 1} \times 0.1486960\ . \tag{2.35}$$

These are precisely the values of the coupling constants that ensure a mass gap $M = 1$ when we specialize the above Hamiltonian to the integrable massive cases ($g_2 = \pm 1, g_4 = 0$) and ($g_2 = 0, g_4 = -1$) [46]. Further data which are necessary to implement the TCSA for the TIM can be found in [34].

To study the mass spectrum it is sufficient to consider the zero momentum subspace only. Moreover, one can also treat the parts of the Hamiltonian which are even or odd with respect to spin reversal separately[3]. In our calculation we used periodic boundary conditions, which selects the sector of zero topological charge in the Hilbert space of the multi-particle states. As we will show below, there may be other phenomena related to the boundary conditions and to the finite size of the system that have to be properly taken into account in order to interpret the spectrum correctly.

In our numerical calculations we varied the coupling constants g_2 and g_4 along the square with corners $(\pm 1, \pm 1)$ shown in Figure 2.13. The truncation level that we used is $n = 8$, that corresponds to a Hamiltonian truncated to 1624 conformal states. The finite volume spectra shown in Figures 2.15, 2.19, 2.20 and 2.21 are always plotted as functions of mR, where m is the mass gap, whose value depends however on the region of the coupling constants which each figure refers to.

[3] In addition to the two spin reversal even fields ε and t, the TIM possesses other two even fields, the identity operator I and the supersymmetry generator G, with conformal weights 0 and 3/2 respectively. The spin reversal odd sector is generated by the magnetization operator σ and the sub-leading magnetization σ', with $\Delta_\sigma = 3/80$ and $\Delta_{\sigma'} = 7/16$.

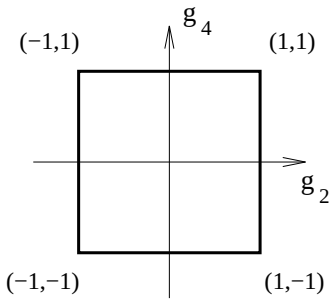

Figure 2.13: The square in the (g_2, g_4) plane along which the TCSA calculations were done.

2.2.5 The spectrum in the high temperature phase

In this subsection we describe our results on the particle spectrum of the model (2.17) in the high temperature phase, made up of the first and the fourth quadrant of the (g_2, g_4) plane. This phase is described by the variable $\eta_+ \in (-\infty, +\infty)$: the value $\eta_+ = -\infty$ corresponds to the negative vertical axis, $\eta_+ = 0$ to the positive horizontal axis, and $\eta_+ = +\infty$ to the positive vertical axis.

In this phase the $\mathbb{Z}_2$ spin reversal symmetry is exact and there is a unique vacuum of the theory (although in the fourth quadrant there are also two false vacua). Hence here the excitations are ordinary scalar particles. In order to follow the evolution of the spectrum it is convenient to start our analysis from the vicinity of the negative vertical axis, i.e. from the fourth quadrant.

The fourth quadrant

Precisely at $\eta_+ = -\infty$, the model has a first order phase transition. This means that along the negative vertical axis the theory has three degenerate ground states $|0\rangle$, $|+\rangle$ and $|-\rangle$: the vacuum $|0\rangle$ is even under the spin reversal symmetry Q, while $|+\rangle$ and $|-\rangle$ are mapped into each other: $|-\rangle = Q|+\rangle$ (see Figure 2.14.a). Right at $\eta_+ = -\infty$, the theory presents also an exact supersymmetry: the particle spectrum consists of four kinks $|K_{-0}\rangle$, $|K_{0-}\rangle$, $|K_{0+}\rangle$ and $|K_{+0}\rangle$ of equal mass. These kinks, that do not have bound states, provide an irreducible representation of supersymmetry and their exact S-matrix was obtained in [40]. The action of the spin reversal symmetry Q on the kinks is given by $Q|K_{-0}\rangle = |K_{+0}\rangle$, $Q|K_{0-}\rangle = |K_{0+}\rangle$.

On a cylinder of circumference R, the three degenerate vacua give rise to three exponentially split energy lines, for the phenomenon of tunneling that occurs at a finite volume. With periodic boundary conditions, there are however no energy lines corresponding to the one-particle states of the kinks. Above the three exponentially degenerate lines of the ground states, one finds instead doublets of lines corresponding to the neutral kink-antikink configurations (see Figure 2.15). The proper counting of the states appearing in the finite volume with periodic boundary conditions is explained in Figure 2.14.b.

It is now important to understand what happens if we deform the theory away from this integrable situation, moving into the fourth quadrant by means of the perturbation $g_2 \int \varepsilon(x) \mathrm{d}x$ $(g_2 > 0)$. The drastic effect of this perturbation is to lift the degeneracy of the three vacua: in the perturbed theory, the central vacuum $|0\rangle$ becomes the true ground state of the theory, whereas the

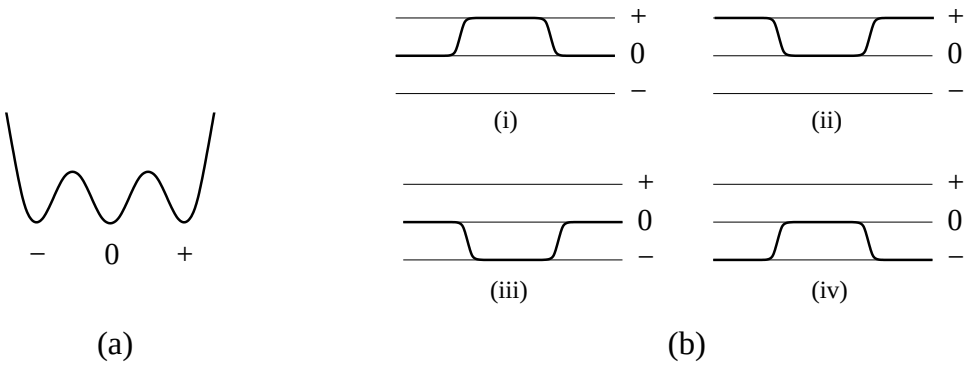

Figure 2.14: (a) The three vacua in the first-order transition point. (b) Unbound kink-antikink pairs. On the cylinder with periodic boundary the configurations (i) and (ii) represent the same state, and so do (iii) and (iv).

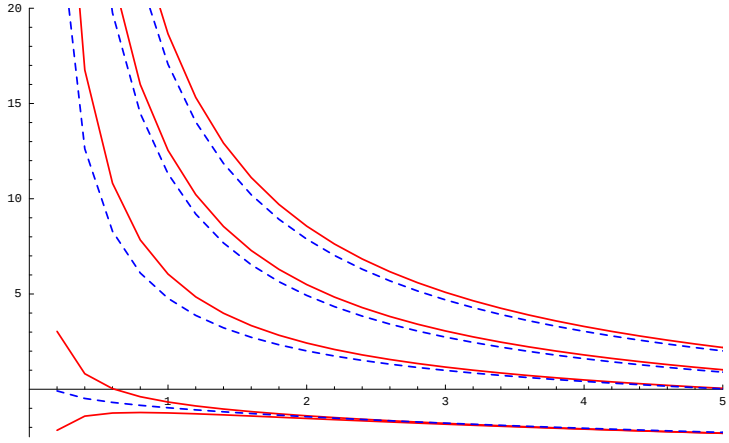

Figure 2.15: The lowest nine energy levels E_i, $i = 0...8$ in the first-order transition point as functions of mR, obtained by TCSA. Red lines are even, blue (dashed) lines are odd under spin reversal. m denotes the mass gap.

other two vacua $|\pm\rangle$ become metastable ground states, separated from $|0\rangle$ by a gap

$$\Delta E \sim g_2(\langle\Omega|\epsilon|\Omega\rangle - \langle 0|\epsilon|0\rangle) \ , \tag{2.36}$$

where $|\Omega\rangle = |\pm\rangle$. As a consequence, we expect that the kinks of the unperturbed system will get confined as soon as we move away from $\eta_+ = -\infty$ by switching on the coupling g_2 of the energy operator ϵ. This can be directly seen by the FFPT, reported in Appendix 3: the two-particle form factors on the kink states of the ϵ operator have in fact a pole at $\theta = \mathrm{i}\pi$ [49]. The linear confining potential between the constituents of the two pairs of neutral kink-antikink states $|K_{0-}K_{-0}\rangle$ and $|K_{0+}K_{+0}\rangle$ gives rise then to a dense sequence of bound states, with the number of bound states going to infinity as $g_2 \to 0$ [36] (see Figure 2.16).

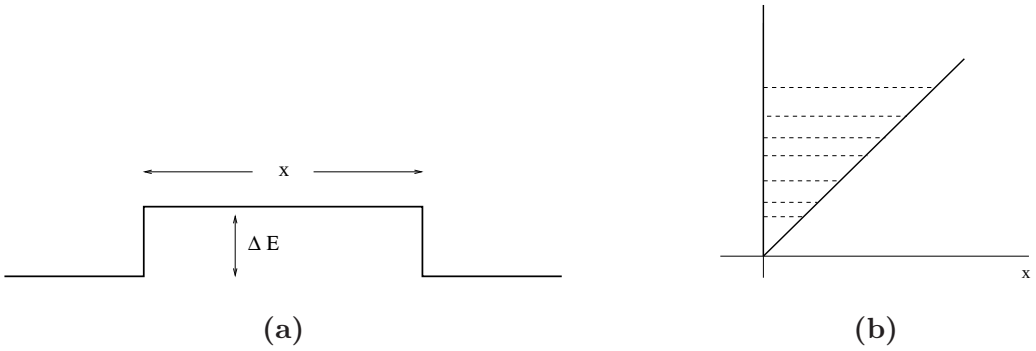

Figure 2.16: (a) Kink-antikink state at distance x, where ΔE is the gap of the unbalanced vacua. The kink and the antikink are subject to a linear confining potential (b), with slope given by ΔE, and they give rise to an infinite sequence of bound states.

This analytic result is indeed confirmed by our numerical calculations. In particular, Figure 2.17 shows that the number of particles below the stability threshold increases to infinity as the first order transition line is approached (i.e. $\eta_+ \to -\infty$). This scenario is similar to the one observed in the scaling region of the critical Ising model near the thermal axis once it is perturbed by a magnetic field [35] and it realizes the so-called McCoy-Wu scenario [48]. An important difference from the Ising model, however, is the $\mathbb{Z}_2$ symmetry of our model. At $\eta_+ = -\infty$, the two-kink states $|K_{0-}K_{-0}\rangle$ and $|K_{0+}K_{+0}\rangle$ (the rapidities of the kinks are suppressed) are mapped into each other by spin reversal, so they form degenerate pairs (although in finite volume this degeneracy is lifted). The two-kink states $|K_{-0}K_{0-}\rangle$ and $|K_{+0}K_{0+}\rangle$ also form similar degenerate pairs, and so do the two-kink states $|K_{-0}K_{0+}\rangle$ and $|K_{+0}K_{0-}\rangle$. The degeneracy is lifted as soon as the perturbation is switched on; the arising bound states are singlets with definite parity. As the kinks do not have bound states at $\eta_+ = -\infty$, all the bound states in the neighbourhood $g_2 > 0$ of the transition point arise from the free two-kink configurations mentioned above. Since the $|\pm\rangle$ vacua are lifted, the original two-particle states $|K_{-0}K_{0-}\rangle$, $|K_{+0}K_{0+}\rangle$, $|K_{-0}K_{0+}\rangle$, and $|K_{+0}K_{0-}\rangle$ of the continuum disappear entirely from the spectrum. In their place, there is a sequence of bound states $|B_n^{\pm}\rangle$, which arises from the even and odd superpositions of the $|K_{0-}K_{-0}\rangle$ and $|K_{0+}K_{+0}\rangle$ states:

$$|B_n^{\pm}\rangle \sim \frac{|K_{0-}K_{-0}\rangle \pm |K_{0+}K_{+0}\rangle}{\sqrt{2}} \ . \tag{2.37}$$

The superscript in $|B_n^{\pm}\rangle$ denotes parity, the subscript numbers the elements of the tower of bound states. As we mentioned, $|B_n^+\rangle$ and $|B_n^-\rangle$ are not degenerate. Due to the exactness of the $\mathbb{Z}_2$ symmetry the vacuum is expected to be even, and then the first state above it, i.e. the lowest one-particle state, is expected to be odd, and generally the parity is expected to alternate in the sequence of one-particle states.

The numerical data that we obtained by varying η_+ indeed confirm that in the high temperature phase the spin reversal symmetry is unbroken, there is a unique vacuum and the excitations are singlet scalar particles with alternating parity. The disappearance of the two-kink states $|K_{-0}K_{0-}\rangle$, $|K_{+0}K_{0+}\rangle$, $|K_{-0}K_{0+}\rangle$ and $|K_{+0}K_{0-}\rangle$ does not have a drastic effect on the numerical spectrum on the cylinder with periodic boundary conditions, since the $|K_{-0}K_{0+}\rangle$, and $|K_{+0}K_{0-}\rangle$ are filtered out and $|K_{-0}K_{0-}\rangle$ and $|K_{+0}K_{0+}\rangle$ are identified with $|K_{0-}K_{-0}\rangle$ and $|K_{0+}K_{+0}\rangle$ under these boundary conditions: what happens is that, energy lines that were previously asymptotic degenerate, now become separated by tiny gaps.

The doubly degenerate false vacuum can be seen in the $\eta_+ < 0$ domain in the TCSA spectra in the form of a linearly rising double line-like pattern (see Figure 2.20.a). The slope of the pattern, which equals to the gap ΔE between the false and true vacua, increases from 0 as η_+ is increased, and finally the pattern disappears from the finite volume spectrum as η_+ approaches 0. ΔE can be calculated by FFPT around the first order phase transition line. At $g_4 = -1$ the exact result to first order in perturbation theory is

$$\frac{\Delta E}{g_2} = 0.3076... = 2\Lambda_2 \times (2\pi)^{\frac{1-\Delta_2-\Delta_4}{1-\Delta_4}} \lambda_4^{\frac{\Delta_2}{1-\Delta_4}} \lambda_2 \ , \tag{2.38}$$

where

$$\Lambda_2 = 2.668319... \tag{2.39}$$

is the exact value of the vacuum expectation values of ε given in [51, 52], and the factor next to $2\Lambda_2$ arises from various normalization factors used in the present paper and in [51, 52] (see Appendix 2 for more details on the calculation of ΔE). On the other hand, by TCSA we obtain

$$\frac{\Delta E}{g_2} = 0.29 \, , \tag{2.40}$$

which is in reasonable agreement with the exact value.

Figure 2.17 shows the numerically calculated mass ratios m_i/m_1 (m_1 being the mass of the lightest particle) as functions of η_+. Truncation errors tend to increase for large absolute values of η_+, therefore the figure shows only a limited range around $\eta_+ = 0$. The masses m_1 and m_2 of the two lightest particles are also shown in Figure 2.18. The stability threshold, taking into account spin reversal symmetry, is $2m_1$ for even particles and $m_1 + m_2$ for odd particles (if there are no even particles, then the threshold is $3m_1$).

Hence, increasing η_+, the number of stable excitations decreases. Around $\eta_+ = 0$, i.e. near to the positive horizontal axis, there are four stable excitations. However, precisely at $\eta_+ = 0$, the theory acquires three more stable particles, all of them above threshold. In order to understand the nature of the spectrum near to $\eta_+ = 0$, it is obviously more convenient to switch to the integrable formulation of the theory along the positive horizontal axis.

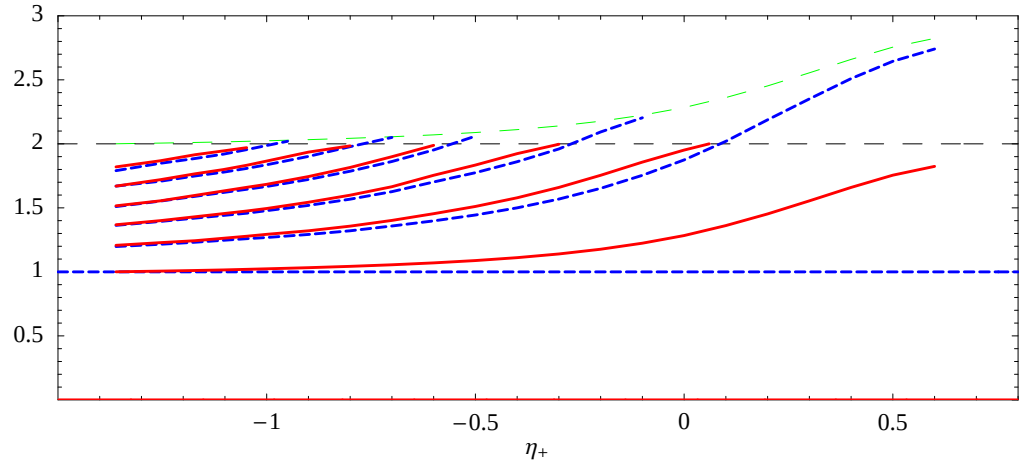

Figure 2.17: The particle mass ratios m_i/m_1 as functions of η_+ in the high temperature phase in the range $-1.361 \leq \eta_+ \leq 0.6$, obtained by TCSA. Even states are shown in red, odd states in blue and with dashed line. The thresholds $2m_1$ and $m_1 + m_2$ for even and odd particles are drawn with dashed thin black and green lines.

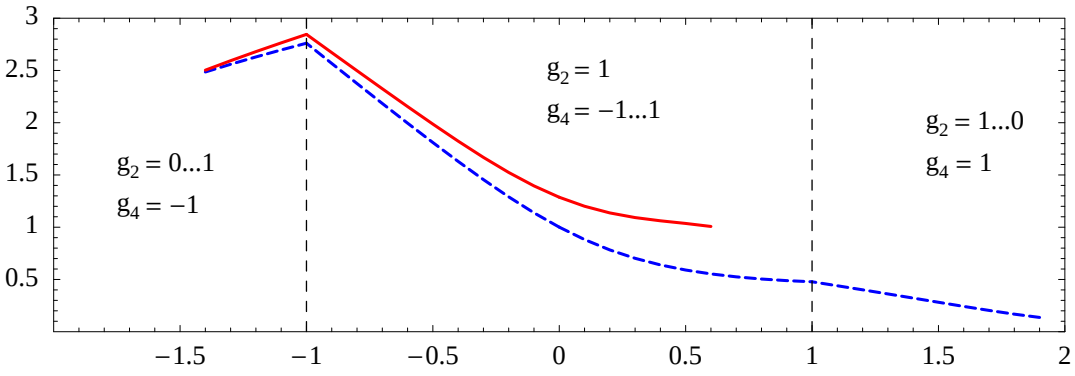

Figure 2.18: The particle masses m_1 (in red) and m_2 (in blue and with dashed line) obtained by TCSA along the square shown in Figure 2.13. The section $0 < g_2 < 0.6$, $g_4 = -1$ is not shown.

Table 2.3: Masses and spin reversal parities of the particles on the E_7-related axis in the high temperature phase.

mass	m_i/m_1	$\mathbb{Z}_2$ parity
m_1	1	$-$
$m_2 = 2m_1 \cos(5\pi/18)$	1.28557	$+$
$m_3 = 2m_1 \cos(2\pi/18)$	1.87938	$-$
$m_4 = 2m_1 \cos(\pi/18)$	1.96961	$+$
$m_5 = 4m_1 \cos(\pi/18)\cos(5\pi/18)$	2.53208	$+$
$m_6 = 4m_1 \cos(4\pi/18)\cos(2\pi/18)$	2.87938	$-$
$m_7 = 4m_1 \cos(\pi/18)\cos(2\pi/18)$	3.70166	$+$

The E_7-related line and FFPT

As we mentioned in the introduction, the $\eta = 0$ line corresponds to an integrable model related to the Toda field theory based on the exceptional Lie algebra E_7. In the high temperature phase, this integrable model has a spectrum composed of seven scalar particles A_i, $i = 1 \dots 7$. Their masses m_i, $i = 1 \dots 7$ (see Table 2.3) and S-matrix amplitudes are known exactly [42, 43].

Note that A_1, A_3 and A_6 are odd under spin reversal symmetry while the other particles are even. Only the first four particles have a mass below the stability thresholds $2m_1$ and $m_1 + m_2$. The higher three particles are nevertheless stable along this axis due to the integrability of the theory.

Decay processes

Moving away from the axis $\eta_+ = 0$, the expectation is that there exists a range of values of η_+ where the four lowest particles are still stable, whereas the higher three particles decay in all possible channels compatible with the symmetry of the perturbation. The perturbation that breaks the integrability of the theory at $\eta_+ = 0$ and plays the role of the operator $\Upsilon(x)$ in eqn. (2.27) is the field t, which is even under the $\mathbb{Z}_2$ spin reversal symmetry. This implies certain selection rules in the decay processes. So, for instance, the particle A_5 can only decay in the channel

$$A_5 \to A_1\, A_1\,, \tag{2.41}$$

even though the decay process $A_5 \to A_1\, A_2$ would be permitted by kinematics. Similarly, it is easy to check that the other possible decay processes compatible with the selection rule are

$$\begin{aligned} A_6 &\to A_1\, A_2 \\ A_7 &\to A_1\, A_1 \\ A_7 &\to A_2\, A_2 \\ A_7 &\to A_1\, A_3 \\ A_7 &\to A_2\, A_4 \\ A_7 &\to A_1\, A_1\, A_2\,. \end{aligned} \tag{2.42}$$

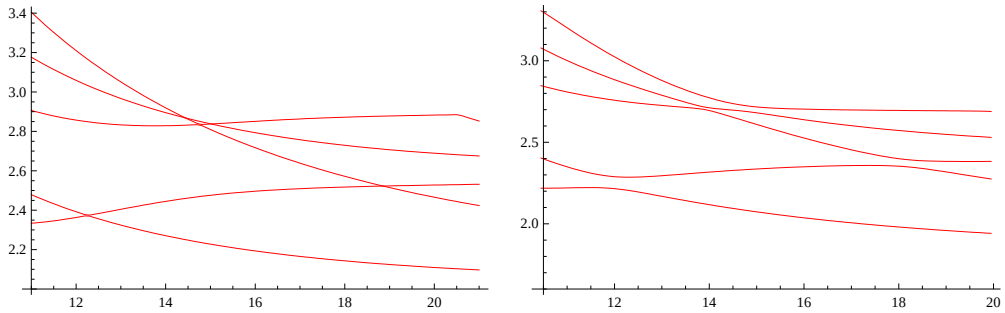

(a) (b)

Figure 2.19: Signature of the appearance of a resonance out of the integrability in the finite volume spectrum. (a) Integrable point. (b) Perturbation switched on. These are the plots of the energy levels versus mR, where m is the mass gap.

The decay processes have a fingerprint in the finite volume spectra, namely the repulsion of the energy lines [35]. Observe, for instance, Figure 2.19.a: this refers to the lowest energy difference lines above the two-particle threshold (in the even sector only) on the integrable E_7 axis. One can see that there are several level crossings; in particular there is one around $mR \sim 12$ between the first and the second lines. The first line corresponds to the threshold state $|A_1 A_1\rangle$, whereas the second line corresponds to the particle $|A_5\rangle$. When we switch on the g_4 perturbation, the crossing disappears, as it can clearly be seen in Figure 2.19.b. In particular, the repulsion of the first and second lines at $mR \sim 12$ corresponds to the decay $A_5 \to A_1 A_1$.

In principle, the widths Γ_{ij}^k of the decays $A_k \to A_i A_j$ can be determined from the repulsion of energy lines by a method proposed in [54]. In this approach, which was called Breit-Wigner method in [54], Γ is related to the two-particle phase shifts of the various two-particle levels $|A_i A_j\rangle$. In more detail, in order to measure Γ one can use the formula

$$\Delta\delta = \min \delta_1(E) - \max \delta_2(E) = 4\sqrt{-\beta\Gamma} \,, \tag{2.43}$$

where

$$\beta = \left. \frac{\mathrm{d}\delta_0}{\mathrm{d}E} \right|_{E=E_k} \tag{2.44}$$

should be negative, E_k is the center of the resonance and $\delta_0(E)$ is defined by the integrable S-matrix as

$$\delta_0(E) = -\mathrm{i} \ln S(E) \,. \tag{2.45}$$

For the sake of clarity, we have suppressed the labels i, j, k relative to the particles. The symbols $\delta_1(E)$, $\delta_2(E)$ in (2.43) refer to the phase shifts of two neighbouring two-particle levels $|A_i A_j\rangle$ and are given by

$$\delta_a(E) \;=\; -R(E)\, p_a(E) \qquad , \qquad a = 1, 2 \,, \tag{2.46}$$

where R is the circumference of the cylinder and $p_a(E)$ is the momentum, defined by the equation

$$E \;=\; \sqrt{p_a^2 + m_i^2} + \sqrt{p_a^2 + m_j^2} \,. \tag{2.47}$$

Hence, from the numerical determination of the energy levels we can measure $E(R)$ as a function of R; from this measurement, using (2.46), we can extract $\delta_1(E)$ and $\delta_2(E)$, and then (2.43) provides Γ.

Using the above consideration we have studied the decay processes

$$A_5 \to A_1 A_1$$
$$A_6 \to A_1 A_2$$

at $g_2 = 1$ and small g_4, finding the following numerical values for the decay rates

$$\Gamma^5_{11} \sim 2 \cdot g_4^2 \ , \qquad \Gamma^6_{12} \sim 0.2 \cdot g_4^2 \ , \tag{2.48}$$

and therefore the universal ratio

$$\frac{\Gamma^6_{12}}{\Gamma^5_{11}} \ \sim \ 0.1 \ . \tag{2.49}$$

This result shows that the decay of A_6 is considerably slower than the decay of A_5. Although the kinematical phase space factor $\Phi^M_{m_i,m_j}$ generally tends to suppress the decay of heavier particles in $1+1$ dimensions [55], in the present case this effect is not sufficient, however, to justify the result above: in fact, the phase space estimate of the universal ratio (2.49) gives in this case

$$\frac{\Gamma^6_{12}}{\Gamma^5_{11}} \sim \frac{\Phi^6_{12}}{\Phi^5_{11}} \ = \ \sqrt{\frac{m_5^2(m_5^2-4m_1^2)}{(m_6^2-(m_1-m_2)^2)(m_6^2-(m_1+m_2)^2)}} = 0.783... \ . \tag{2.50}$$

Therefore the longer lifetime of A_6 has to be attributed to the dynamics of the model. We plan to analyze this aspect in a future publication.

Mass corrections

Coming back to the stable particles of the spectrum, it is relatively easy to compute the correction to the masses of the two lowest particles once we move away from the E_7 integrable axis. This can be done by combining the FFPT and the TCSA, together with a cross-checking between the two methods. The first order mass correction of the particle A_i moving away from the $\eta_+ = 0$ axis is given by

$$\delta m_i = \frac{g_4}{m_i} 2\pi\lambda_4 F^t_{ii}(\mathrm{i}\pi) \, , \tag{2.51}$$

where $F^t_{ii}(\theta_1 - \theta_2) = \langle 0|t(0)|A_i(\theta_1)A_i(\theta_2)\rangle$ is the two-particle form factor of t. As a matter of fact, $F^t_{11}(\mathrm{i}\pi)$, $F^t_{22}(\mathrm{i}\pi)$, $F^t_{33}(\mathrm{i}\pi)$ and $F^t_{44}(\mathrm{i}\pi)$ can be directly extracted by TCSA (see Appendix 2 and [50, 52]). At $g_2 = 1$ we obtained

$$F^t_{11}(\mathrm{i}\pi) \ = -\tfrac{1.28}{2\pi\lambda_4} \, , \qquad F^t_{22}(\mathrm{i}\pi) \ = -\frac{1.25}{2\pi\lambda_4} \, , \tag{2.52}$$

$$F^t_{33}(\mathrm{i}\pi) \ = -\tfrac{2.03}{2\pi\lambda_4} \ , \qquad F^t_{44}(\mathrm{i}\pi) \ = -\frac{3.41}{2\pi\lambda_4} \ . \tag{2.53}$$

Similarly, from TCSA we can also compute the absolute value of the one-particle form factors $F_2^t = \langle 0|t(0)|A_2(\theta)\rangle$ and $F_4^t = \langle 0|t(0)|A_4(\theta)\rangle$. The result is

$$|F_2^t| \,=\, \frac{0.35}{2\pi\lambda_4}\,, \qquad |F_4^t| \,=\, \frac{0.26}{2\pi\lambda_4}\,. \tag{2.54}$$

As shown in the Appendix 1, there is an exact relation between the two-particle form factors $F_{11}^t(i\pi)$ and $F_{22}^t(i\pi)$ and the one-particle form factors F_2^t and F_4^t, expressed by

$$F_{11}^t(\mathrm{i}\pi) \quad = 11.397\cdot F_2^t + 10.3632\cdot F_4^t\,, \tag{2.55}$$
$$F_{22}^t(\mathrm{i}\pi) \quad = 23.1056\cdot F_2^t + 26.2404\cdot F_4^t\,. \tag{2.56}$$

If we assume that $F_2^t < 0$ and $F_4^t > 0$, then (2.54), (2.55) and (2.56) yield

$$F_{11}^t(\mathrm{i}\pi) \,=\, \frac{-1.29}{2\pi\lambda_4}\,, \qquad F_{22}^t(\mathrm{i}\pi) \,=\, \frac{-1.26}{2\pi\lambda_4}\,, \tag{2.57}$$

which is in satisfactory agreement with (2.52).

With the above values, we can extract the universal ratios

$$\begin{aligned} \delta m_2/\delta m_1 &= 0.76\,, \\ \delta m_3/\delta m_1 &= 0.84\,, \\ \delta m_4/\delta m_1 &= 1.35\,. \end{aligned} \tag{2.58}$$

In order to get another universal ratio, let us look at the first order correction to the vacuum energy density ϵ_{vac}. By TCSA (see Appendix 2) we obtain

$$\frac{\delta\epsilon_{vac}}{g_4} = 0.11\,. \tag{2.59}$$

On the other hand, the exact value of this quantity is

$$\frac{\delta\epsilon_{vac}}{g_4} = 0.1130... = \Lambda_4\times(2\pi)^{\frac{1-\Delta_2-\Delta_4}{1-\Delta_2}}\lambda_2^{\frac{\Delta_4}{1-\Delta_2}}\lambda_4\,, \tag{2.60}$$

which is in good agreement with the above numerical result. $\Lambda_4 = 3.70708...$ is the vacuum expectation value of t calculated in [51, 52] (the factor next to Λ_4 arises from various normalization factors used in the present paper and in [51, 52]). This allows us also to extract the universal ratio

$$\frac{\delta\epsilon_{vac}}{m_1\delta m_1} = -0.086\,. \tag{2.61}$$

The first quadrant

After the analysis in the previous subsection we can now proceed to investigate the evolution of the spectrum in the first quadrant. First of all, note that the corrections to the two lowest masses have the same sign, which depends on the sign of g_4. We can use the above results for δm_1 and δm_2 to estimate the value of $\eta_+^{(2)}$ where the mass $m_2(\eta_+)$ of the second particle reaches the threshold

$2m_1(\eta_+)$ of the lowest particle. This happens for a value of $\eta_+ > 0$ of the first quadrant, given by $\eta_+^{(2)} \simeq 1$: although this is higher than the value $\eta_+^{(2)} \simeq 0.7$ extracted from the numerical data shown in Figure 2.17, it is nevertheless a reasonable estimation of this quantity since the theoretical result was based on just first-order perturbation theory.

Besides the three higher particles A_5, A_6, A_7 that were stable only at $\eta_+ = 0$ and decay as soon as we move away from the horizontal axis, the TCSA analysis shows that the same pattern as was seen in the fourth quadrant also persists in the first quadrant: namely, increasing the value of η_+, the number of stable particles continues to decrease. The first particle that disappears into the threshold $2m_1(\eta_+)$ is A_4 at the critical value $\eta_+^{(4)}$, which can be estimated from first-order perturbation theory to be $\eta_+^{(4)} \simeq 0.04$. This is followed by A_3 that disappears into its lowest threshold, given by $(m_1(\eta_+) + m_2(\eta_+))$, at the critical value $\eta_+^{(3)}$, for which perturbation theory gives $\eta_+^{(3)} \simeq 0.62$. These theoretical results for $\eta_+^{(3)}$ and $\eta_+^{(4)}$ are in reasonably good agreement with the numerical data (Figure 2.17). An example of the finite volume spectra calculated numerically is shown in Figure 2.21.a at $\eta_+ = 0.3$, where the theory contains 3 stable particles.

As just described, moving toward the positive vertical axis, there is a depletion of the number of stable particles, until there remains only one in the neighbourhood of $\eta_+ = +\infty$. At the same time, notice that increasing η_+, the value of this lowest mass becomes also smaller[4]. The mass gap of the theory finally vanishes when $\eta_+ = +\infty$, i.e. when we have reached the vertical axis.

During this evolution, however, there has also been a qualitative change of the spectrum: in fact, reaching the positive vertical axis the lowest excitation has turned into a fermion. This becomes evident by looking directly at the nature of the theory at $\eta_+ = +\infty$ (notice that the positive vertical axis also corresponds to $\eta_- = +\infty$).

2.2.6 The spontaneously SUSY breaking axis

The analytic control of the theory in the vicinity of $\eta_\pm = +\infty$ is provided by the integrability of the model along the vertical axis, where the system is also supersymmetric. Along the positive vertical axis the supersymmetry is however spontaneously broken: the low-energy excitations are given in this case by the massless right and left mover Majorana fermions, which play the role of goldstino [39, 40, 41]. The factorized scattering theory was proposed in [40] and the basic form factors were calculated in [47]. The massless Majorana fermions are nothing else than those of the Ising model, connected to the TIM by the massless renormalization group flow that occurs along this line.

Breaking the integrability of the $\eta_\pm = \infty$ model by means of the operator $\Upsilon = \varepsilon$, the left and right moving excitations become adiabatically massive, as it can be directly observed in the TCSA data (see Figure 2.18). To compute the mass m of the fermion generated by the perturbation, we need to employ in this case the massless FFPT [37]: at the lowest order, we have

$$m \simeq g_2 \lim_{\theta_{RL} \to -\infty} F_{RL}^{\varepsilon}(\mathrm{i}\pi + \theta_{RL}) \ , \tag{2.62}$$

[4]This behavior is in agreement with the first-order correction (2.51) to m_1, that is negative for $g_4 > 0$.

where the two-particle (right-left) form factor of the ε operator is given by [47]

$$F^{\varepsilon}_{RL}(\theta) \,=\, \exp\left(\frac{\theta}{4} - \int_0^{\infty} \frac{\mathrm{d}t}{t} \frac{\sin^2\left(\frac{(\mathrm{i}\pi-\theta)t}{2\pi}\right)}{\sinh t \cosh\frac{t}{2}}\right) \,. \tag{2.63}$$

Using (2.62) and (2.63), one can easily check that m is a *finite* quantity, positive for $g_2 > 0$ and negative for $g_2 < 0$. Note that, for a Majorana fermion, a negative value of the mass signals that we are in a low temperature phase, i.e. that the theory has two degenerate vacua. This is the topic of the next subsection.

2.2.7 The spectrum in the low temperature phase

The low temperature phase is composed of the second and the third quadrants. This phase is described by the variable $\eta_- \in (-\infty, +\infty)$: $\eta_- = \infty$ corresponds to the positive vertical axis, $\eta_- = 0$ to the negative horizontal axis and $\eta_- = -\infty$ to the negative vertical axis.

In this phase the model presents generically two degenerate ground states $|-\rangle$ and $|+\rangle$, which are mapped into each other by the spin reversal symmetry operation Q: $|+\rangle = Q|-\rangle$. An important feature that is worth stressing is the following: no matter how we vary the coupling constants in this parameter region, the two vacua $|-\rangle$ and $|+\rangle$ always remain degenerate, the only changes being in the shape and the height of the barrier between them. Hence, in this model the kink states that interpolate between the two vacua are always stable excitations. As we will comment below, this can be explicitly checked and confirmed by a FFPT computation at $\eta_- = 0$, where the theory has the E_7 structure.

The only points where one has to be careful are the two limiting cases $\eta_- = \infty$ and $\eta_- = -\infty$. In the former case, the barrier between the two vacua disappears and, as we saw at the end of subsection 2.2.5, the kinks become massless. In the latter case, the two vacua $|-\rangle$ and $|+\rangle$ and the false vacuum $|0\rangle$ that emerges between them in the region $\eta_- < 0$ become degenerate precisely at $\eta_- = -\infty$. Hence, at this point, the original kinks break into a new set of smaller kinks, i.e. those relative to the three vacua of the first order phase transition of the TIM.

To obtain the spectrum of the theory in the low temperature phase we can take advantage of the duality of the model. At a formal level, note that the masses at a given point (g_2, g_4) in the low temperature phase are the same as the masses in the dual point $(-g_2, g_4)$ in the high temperature phase. This result can be obtained as follows: since ε is odd and t is even under the duality transformation D:

$$\begin{aligned} D^{-1}\varepsilon D &= -\varepsilon \,, \\ D^{-1} t D &= t \,, \end{aligned}$$

for the Hamiltonian we have

$$D^{-1} H(g_2, g_4)\, D \,=\, H(-g_2, g_4) \,. \tag{2.64}$$

However, to interpret correctly the TCSA data, one needs to take into account the existence of kink states and the periodic boundary conditions imposed to the system.

Note that D maps the even sector of the Hilbert space onto itself, so in the even sector $H(g_2, g_4)$ has the same spectrum as $H(-g_2, g_4)$. Concerning the odd sector of the spectrum, the particles

with odd parity in the high temperature phase become instead kinks in the low temperature phase, i.e. topologically charged states that interpolate between the two vacua. However, the periodic boundary conditions that we have imposed on the TCSA filter only topologically neutral states. Hence, by switching $g_2 \to -g_2$, we expect that the net result in the numerical outcomes will be the disappearing of the energy levels corresponding to the odd particles in the high temperature phase: in the low temperature phase these lines should become exponentially degenerate with the energy lines of the even levels. In other words, in the low temperature phase the TCSA data should show doubly degenerate lines and each doublet should have an even and odd member. This is indeed the case, as clearly shown in Figures 2.20 and 2.21, where we present the spectrum of the theory at given values (g_2, g_4) and $(-g_2, g_4)$. This feature is nothing but a finite volume manifestation of the spontaneous breaking of the $\mathbb{Z}_2$ spin reversal symmetry: the two vacua (and all the excitations above them) have in fact an exponential splitting of their energy for the tunneling phenomenon that occurs at finite volume.

Summarizing the considerations above, in the low temperature phase and at infinite volume the model has two ground states $|+\rangle$, $|-\rangle$, each ground state has a sequence $|C_n\rangle_\pm$ of topologically neutral particles above it, and there is also a sequence of kinks and antikinks $|\mathcal{D}^m_{+-}\rangle$, $|\mathcal{D}^m_{-+}\rangle$ which interpolate between the vacua[5]. Under spin reversal symmetry the ground states, particles and kinks have the following property:

$$
\begin{aligned}
|\pm\rangle &= Q|\mp\rangle \ ; \\
|C_n\rangle_\pm &= Q|C_n\rangle_\mp \ ; \\
|\mathcal{D}^n_{+-}\rangle &= Q\,|\mathcal{D}^n_{-+}\rangle \ .
\end{aligned}
$$

The masses of the neutral states at a given point of the plane of the coupling constants are the same as the masses of the even particles in the high temperature phase at the dual point, whereas the masses of the kinks are the same as the masses of the odd particles in the high temperature phase. In finite volume with periodic boundary conditions, however, we do not see individual kinks or other topologically charged configurations. We do see the vacua, the neutral particles and only neutral configurations of two or other even number of free kinks, which, moreover, get mixed in finite volume into even and odd eigenstates of the spin reversal operator and acquire an exponential splitting due to tunneling effects. With periodic boundary conditions there are also identifications between certain configurations, similarly as in the first order transition point (see Figure 2.14).

After the discussion above we can proceed to describe the spectrum in the second and third quadrants in detail.

The third quadrant

At $\eta_- = -\infty$ the model is at the first order phase transition point, which was described in subsection 2.2.5. As we move into the third quadrant by switching on the perturbation $g_2 \int \varepsilon(x)\mathrm{d}x$ $(g_2 < 0)$, the degeneracy of the three vacua is lifted. In contrast with the fourth quadrant, the central vacuum $|0\rangle$ now becomes a metastable ground state, and the two other vacua $|\pm\rangle$ remain true ground states. The gap ΔE separating $|0\rangle$ from $|\pm\rangle$ at a given point is equal to the gap at the dual point in the

[5]The indices n and m number the members of the sequences, while $+$ and $-$ refer to the vacua between which the kinks interpolate or which support the neutral states.

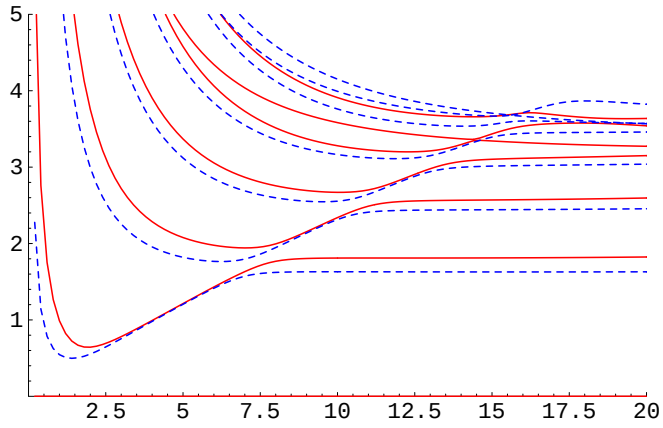

(a) $g_2 = 1$, $g_4 = -0.4$

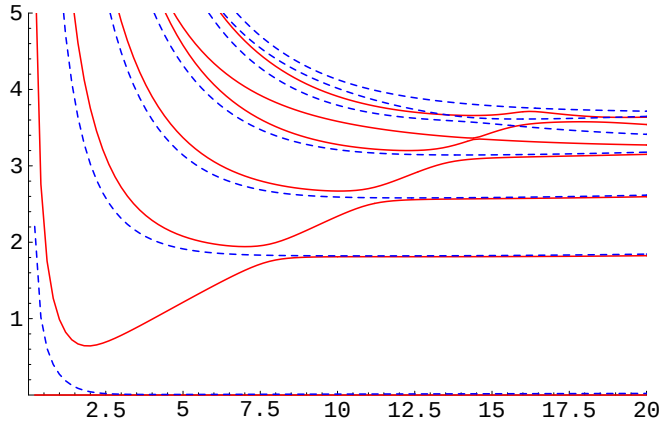

(b) $g_2 = -1$, $g_4 = -0.4$

Figure 2.20: The first 14 energy level differences $E_i - E_0$, $i = 0...13$, as functions of mR in the (a) 4th and (b) 3rd quadrants at the dual values of the couplings constants. Even levels are in red, odd levels are in blue with dashed line. m denotes the mass gap.

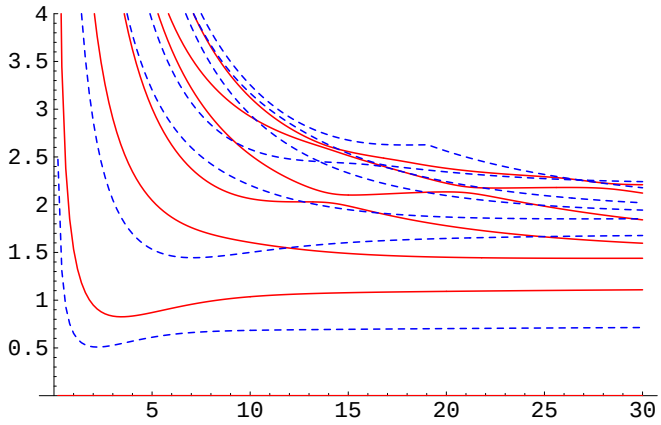

(a) $g_2 = 1$, $g_4 = 0.3$

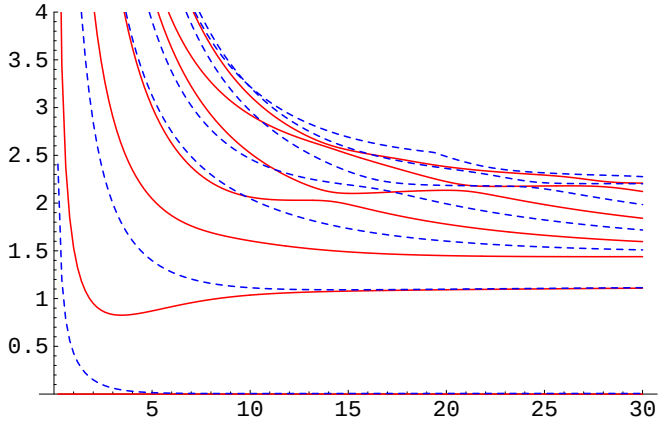

(b) $g_2 = -1$, $g_4 = 0.3$

Figure 2.21: The first 14 energy level differences $E_i - E_0$, $i = 0...13$, as functions of mR in the (a) 1st and (b) 2nd quadrants at the dual values of the coupling constants. Even levels are in red, odd levels are in blue with dashed line. m denotes the mass gap.

fourth quadrant. The expected consequence of the lifting of the degeneracy of the vacua is again the confinement of the kinks of the unperturbed system, which is confirmed by the same FFPT argument as for the fourth quadrant. The linear confining potential between the kinks gives rise to a dense sequence of bound states. As in the fourth quadrant, the number of these bound states goes to infinity as $g_2 \to 0$. In the third quadrant, however, the two-kink states $|K_{0-}K_{-0}\rangle$ and $|K_{0+}K_{+0}\rangle$ are those which disappear from the spectrum, and the bound states arise from the other two-kink states $|K_{-0}K_{0+}\rangle$, $|K_{+0}K_{0-}\rangle$, $|K_{-0}K_{0-}\rangle$ and $|K_{+0}K_{0+}\rangle$. Some of the bound states above are topologically charged, i.e. they are kinks, while others are neutral. The neutral particles arise from the neutral two-kink configurations:

$$|C^n\rangle_+ \sim |K_{+0}K_{0+}\rangle\,, \qquad |C^n\rangle_- \sim |K_{-0}K_{0-}\rangle\,. \tag{2.65}$$

It is important to note that $|C^n\rangle_+$ and $|C^n\rangle_-$ are degenerate for any given n, due to the spontaneously broken $\mathbb{Z}_2$ symmetry, although their degeneracy is exponentially lifted in finite volume. The topologically charged particles arise from topologically charged two-kink states:

$$|\mathcal{D}^n_{-+}\rangle \sim |K_{-0}K_{0+}\rangle\,, \qquad |\mathcal{D}^n_{-+}\rangle \sim |K_{-0}K_{0+}\rangle\,, \tag{2.66}$$

where the subscripts $-+$ and $+-$ in $|\mathcal{D}^n_{-+}\rangle$ and $|\mathcal{D}^n_{+-}\rangle$ denote the vacua between which these kink configurations interpolate. $|\mathcal{D}^n_{-+}\rangle$ and $|\mathcal{D}^n_{+-}\rangle$ are mapped into each other by the spin reversal: $Q|\mathcal{D}^n_{-+}\rangle = |\mathcal{D}^n_{+-}\rangle$, therefore they have equal mass.

As we mentioned, under duality an even particle $|B^+_n\rangle$ in the high temperature phase corresponds to the neutral particles $|C^n\rangle_\pm$ of the same mass in the low temperature phase, and an odd particle $|B^-_n\rangle$ corresponds to a kink-antikink pair $|\mathcal{D}^n_{+-}\rangle$, $|\mathcal{D}^n_{-+}\rangle$ of the same mass.

The neutral particles $|C^n\rangle_\pm$ (more precisely, their even and odd superpositions) can indeed be seen in the TCSA spectra, whereas the kinks $|\mathcal{D}^n_{+-}\rangle$ and $|\mathcal{D}^n_{-+}\rangle$ are filtered out by the periodic boundary conditions. The neutral two-kink states constituted by $|\mathcal{D}^n_{+-}\rangle$ and $|\mathcal{D}^n_{-+}\rangle$ can nevertheless be observed in the numerical data. The disappearance of the original two-kink states $|K_{0-}K_{-0}\rangle$ and $|K_{0+}K_{+0}\rangle$ does not have drastic effect on the spectra with periodic boundary conditions for similar reasons as for the third quadrant.

The false vacuum with even parity can also be seen in the $\eta_- < 0$ domain in the TCSA spectra in the form of a linearly rising line-like pattern (see Figure 2.20.b). The duality relates this metastable vacuum to the metastable vacua in the first quadrant.

The E_7-related line

The number of stable particles at any given point in the low temperature phase is equal to the number of particles in the dual point in the high temperature phase, and this number decreases as η_- is increased. The number of stable particles around $\eta_- = 0$ is 4, however at $\eta_- = 0$, i.e. on the negative horizontal axis, 3 more particles become stable above threshold. These particles are related by duality to the three highest particles existing at $\eta_+ = 0$. In particular, there are two neutral particles $|C^5\rangle_\pm$, $|C^7\rangle_\pm$ of masses m_5 and m_7 (see Table 2.3) which correspond to the even particles $|A_5\rangle$, $|A_7\rangle$, and there is one kink-antikink pair $|\mathcal{D}^6_{+-}\rangle$, $|\mathcal{D}^n_{-+}\rangle$ of mass m_6 corresponding to the odd particle $|A_6\rangle$.

It was stressed in the introduction that an important property of the model is the presence of kinks in the low temperature phase which do not get confined under perturbations. At $\eta_- = 0$ this non-confinement can be explicitly verified by FFPT. For this, one has to show that the form factors giving the first-order corrections to the masses of $|\mathcal{D}^i_{+-}\rangle$ and $|\mathcal{D}^i_{-+}\rangle$ are finite. This is indeed the case, since these form factors

$$\langle -|t(0)|\mathcal{D}^i_{-+}(\mathrm{i}\pi)\,\mathcal{D}^i_{+-}(0)\rangle \ ,$$
$$\langle +|t(0)|\mathcal{D}^i_{+-}(\mathrm{i}\pi)\,\mathcal{D}^i_{-+}(0)\rangle \ ,$$

(where $i = 1, 3$) are equal by duality to the form factors $\langle 0|t(0)|A_i(\mathrm{i}\pi)A_i(0)\rangle$, and the latter are finite since t does not have non-trivial semi-local index with respect to the $|A_i\rangle$ particles, which are local excitations.

The particles $|C^5\rangle_\pm$, $|C^7\rangle_\pm$, $|\mathcal{D}^6_{+-}\rangle$, $|\mathcal{D}^6_{-+}\rangle$ are unstable near the $\eta_- = 0$ axis, the allowed decay processes can be obtained from (2.41) and (2.42) by replacing A_i by the appropriate dual particles. For example, (2.41) corresponds to

$$C^5_+ \ \to \ \mathcal{D}^1_{+-}\mathcal{D}^1_{-+} \ , \qquad C^5_- \ \to \ \mathcal{D}^1_{-+}\mathcal{D}^1_{+-} \ . \tag{2.67}$$

The second quadrant

Similarly to the third quadrant, the particle spectrum in the second quadrant is related by duality to the spectrum in the first quadrant. Even particles in the first quadrant correspond to neutral particles, odd particles correspond to kinks. The number of particles decreases from 4 to 1 as η_- increases from 0 to ∞, the critical values where the particles and kinks cross the threshold are the same as in the first quadrant, i.e. $\eta_+^{(4)}$, $\eta_+^{(3)}$, $\eta_+^{(2)}$. For $\eta_- > \eta_+^{(2)}$ there is only one kink-antikink pair in the spectrum. Similarly to the first quadrant, metastable vacua are not present. As η_- goes to infinity, the potential barrier between the two vacua $|\pm\rangle$ and the mass of the kink-antikink pair decrease until they finally vanish at the second-order transition point $\eta_- = \infty$. An example of the finite volume spectra calculated numerically is shown in Figure 2.21.b at $\eta_- = 0.3$, which is dual to the point $\eta_+ = 0.3$ that the example Figure 2.21.a for the first quadrant shows.

2.2.8 Conclusions

In this Section we have studied the particle spectrum of the TIM with spin reversal symmetric perturbations. This is the simplest bosonic non-integrable field theory where kink excitations do not get confined by changing the coupling constants over a wide range of values. By varying the couplings, the model interpolates between a SUSY theory (either in its exact or in its spontaneously broken phase) and a theory ruled by the exceptional algebra E_7, with a spectrum given by purely scalar particles (in the high temperature phase) and kinks and bound states thereof (in the low temperature phase).

Our results, obtained both by the FFPT and TCSA methods, are also in agreement with the Landau-Ginzburg picture of the TIM. We have found that the particle masses are the same at dual points in the high and low temperature phases, whereas the spin reversal symmetry properties and the topological charges of the particles are different in the two phases: even particles in the high temperature phase correspond to topologically neutral particles in the low temperature phase, odd

particles correspond to (topologically charged) kink states. The number of stable particles tends to infinity in the vicinity of the first-order transition line, which is similar to the accumulation of particles found in the low temperature Ising model perturbed by a magnetic field [48]. However, in contrast with the Ising model, in TIM the parity is a good quantum number and the corresponding particles emerging from the kink-antikink threshold carry even or odd parity eigenvalues.

We have also computed the first-order corrections to the lowest four masses and the vacuum energy density at the E_7-related line, as well as the corrections to the energy densities of the three degenerate vacua at the first-order phase transition line. All these analytic results are in good agreement with the numerical estimates extracted by means of the TCSA.

Finally, we would like to mention that the three-frequency sine-Gordon model also has a tricritical point, the neighbourhood of which was studied by the TCSA in [56, 57]. In the light of the results of this paper, it would be interesting to investigate more thoroughly the first order transition in the three-frequency sine-Gordon model and, in particular, to study the evolution of the particle spectrum of this model. Moreover, the strategy adopted in the present Section can be also used to study the spectrum of higher multi-critical theories, described by higher minimal models of conformal field theories perturbed by several operators.

2.3 Particle spectrum of the 3-state Potts field theory: A Numerical study

Based on the paper:
L. Lepori, G. Z. Toth and G.Delfino,
"Particle spectrum of the 3-state Potts field theory: a numerical study",
J. Stat. Mech. **0911** (2009) P11007 [arXiv:0909.2192 [hep-th]].

2.3.1 Introduction

The q-state Potts field theory describes the universality class associated with the spontaneous breaking of the permutation symmetry of q colors. In two space-time dimensions the theory is defined for $q \leq 4$. The transition between the disordered (symmetric) phase and the ordered (broken symmetry) phase occurs as the temperature is varied. If an external magnetic field is allowed to be switched on, then the theory provides a model of confinement with several interesting features [60]. Below critical temperature and in absence of the field, the particle spectrum contains kinks, which interpolate between the q degenerate vacua. The magnetic field breaks (at least partially) the degeneracy of the vacua and those kinks which start or end on vacua that become false get removed from the spectrum. Those multikink configurations which consist of such kinks but start and end on vacua that remain true can give rise to new particles, which will be bound states of the confined kinks. The role of the kinks is analogous to that of quarks in chromodynamics, and the arising kink bound states play a role analogous to that of mesons and baryons, therefore the kinks and the bound states are sometimes referred to as quarks, mesons and baryons.

The mechanism of confinement through the breaking of the degeneracy of discrete vacua is quite general in two dimensions. The Ising case (corresponding to $q = 2$) provides the simplest example and was first studied in [61] (see [62] for more references). In this as in other cases [63, 2, 64] the single-component order parameter leads to bound states made by a kink and an anti-kink, i.e. only mesonic particles are present. The $q = 3$ Potts model provides the simplest example allowing also for baryonic particles (made of three kinks), as well as for an extended phase in the parameter space in which some kinks are deconfined. Moreover, in this case the renormalization group trajectories originate from a non-trivial fixed point.

A qualitative characterization of the evolution of the mass spectrum in the three- and four-state Potts models for generic values of the temperature and of a magnetic field chosen to act on a single color was given in [60]. Our aim in the present Section is to verify that picture in the $q = 3$ case by numerical calculations. We use the method called truncated conformal space approach (TCSA) [23], which is suitable for studying mass spectra. Its application requires that the theory is formulated as a perturbation of a conformal field theory. In the $q = 3$ case this is the D_4 minimal conformal model, and the fact that this is a "non-diagonal" minimal model makes the situation technically somewhat more complicated compared to the usual applications of the TCSA. Interestingly enough, our investigation of the off-critical region allows us to fix also some previously unknown data concerning the conformal point.

The Section is organized as follows. In subsection 2.3.2 we introduce the model and discuss the implementation of the TCSA, before presenting the results of the numerical study in subsection 2.3.3. Subsection 2.3.4 is devoted to the comparison with analytic results that can be obtained

in the case of weak magnetic field, while subsection 2.3.5 contains a few final remarks. The results concerning the conformal point are given in the Appendix 6.

2.3.2 Model and numerical method

The three-state Potts model on the lattice [65, 66] is a generalization of the Ising model in which each site variable $s(x)$ can take three different values (colors) $1, 2, 3$. At temperature T and in the presence of an external magnetic field H acting only on the sites with one specific color, say 3, the reduced Hamiltonian reads as

$$\mathcal{H} = -\frac{1}{T}\sum_{(x,y)} \delta_{s(x),s(y)} - H\sum_{x} \delta_{s(x),3} \ , \tag{2.68}$$

where the first sum is over nearest neighbours. At zero magnetic field this Hamiltonian is invariant under the group S_3 of permutations of the three colors. If the magnetic field is nonzero, then $\mathcal{H}$ is invariant only under the group $S_2 = \mathbb{Z}_2$ of permutations of the first two colors.

The system described by the model has two phases, an ordered one and a disordered one. While the disordered phase is characterized by a unique ground state which is invariant under the $\mathbb{Z}_2$ symmetry, in the ordered phase the system has two possible ground states, which are interchanged by the $\mathbb{Z}_2$ transformation. The phase boundary separating the two phases in the (T, H) plane has a first order and a second order part. The second order part runs through the half-plane with negative magnetic field and relates the $q = 3$ Potts critical point at $H = 0$ to the $q = 2$ (Ising) critical point at $H = -\infty$, where the third color is unaccessible. The first order transition takes place below the critical temperature T_c at zero magnetic field, where three ground states, which are permuted by the S_3 symmetry, coexist; along the first order transition the system also exhibits spontaneous magnetization (the variables $\sigma_\alpha(x) = \delta_{s(x),\alpha} - \frac{1}{3}$, $\alpha = 1, 2, 3$ have non-zero expectation value).

The field theoretical description of the scaling limit of the model (2.68) begins with the observation that the S_3-invariant critical point at $(T, H) = (T_c, 0)$, where the first and second order transitions meet, belongs to the universality class described by the D_4 minimal model of two-dimensional conformal field theory [67, 68, 69]. The corresponding value $c = 4/5$ of the central charge is the lowest one for which two different modular invariant partition functions can be obtained on a torus with periodic boundary condition [69]. The first realization, known as A_5, contains, with multiplicity one, all the primary operators ϕ whose conformal weight Δ_ϕ appears in the Kac's table 2.4, and describes the tetracritical point of the Ising model. The second realization, known as D_4, contains only a subset of the primaries in table 2.4, some of them with multiplicity two, as expected for the 3-state Potts model, which has a two-component order parameter ($\sum_{\alpha=1}^{3} \sigma_\alpha = 0$). The primaries entering the description of the 3-state Potts model are listed in table 2.5 together with their transformation properties under the group S_3, which is the semidirect product of $\mathbb{Z}_2$ and $\mathbb{Z}_3$; contrary to what happens in the A_5 case, some operators in table 2.5 have a non-zero spin $s = \Delta - \bar{\Delta}$.

The 3-state Potts field theory describing the scaling limit of (2.68) is obtained perturbing the D_4 conformal theory by the leading thermal operator ϵ and the leading $\mathbb{Z}_2$-even magnetic operator $\sigma_+ = (\sigma_1 + \sigma_2)/\sqrt{2}$. This leads to the Euclidean action

$$\mathcal{A} = \mathcal{A}_{D_4} + \tau \int d^2x\, \epsilon(x) - h \int d^2x\, \sigma_+(x) \, , \tag{2.69}$$

Table 2.4: Kac table for $c = 4/5$.

0	1/8	2/3	13/8	3
2/5	1/40	1/15	21/40	7/5
7/5	21/40	1/15	1/40	2/5
3	13/8	2/3	1/8	0

Table 2.5: Primary fields of D_4 and their transformation properties.

ϕ	$(\Delta_\phi, \bar{\Delta}_\phi)$	$\mathbb{Z}_3$	$\mathbb{Z}_2$
I	$(0,0)$	1	1
ϵ	$(2/5, 2/5)$	1	1
X	$(7/5, 7/5)$	1	1
Y	$(3,3)$	1	1
σ_1	$(1/15, 1/15)$	$\exp(2\pi\mathrm{i}/3)$	σ_2
σ_2	$(1/15, 1/15)$	$\exp(4\pi\mathrm{i}/3)$	σ_1
Ω_1	$(2/3, 2/3)$	$\exp(2\pi\mathrm{i}/3)$	Ω_2
Ω_2	$(2/3, 2/3)$	$\exp(4\pi\mathrm{i}/3)$	Ω_1
J	$(7/5, 2/5)$	1	-1
$\bar{J}$	$(2/5, 7/5)$	1	-1
W	$(3,0)$	1	-1
$\bar{W}$	$(0,3)$	1	-1

where $\mathcal{A}_{D_4}$ is the conformal part, $\tau \sim \text{mass}^{2-2\Delta_\epsilon}$ is related to the deviation of the temperature from its critical value and $h \sim \text{mass}^{2-2\Delta_{\sigma_+}}$ is proportional to the magnetic field. The field theory (2.69) describes a family of renormalization group trajectories flowing out of the origin in the (τ, h) plane. They are conveniently parameterized by the dimensionless combinations

$$\eta_\pm = \frac{\tau}{(\pm h)^{(2-2\Delta_\epsilon)/(2-2\Delta_{\sigma_+})}} = \frac{\tau}{(\pm h)^{9/14}}\,, \tag{2.70}$$

where the positive (negative) sign applies when h is positive (negative).

As a (1+1)-dimensional theory, (2.69) describes relativistic particles whose mass spectrum, measured in units of the lightest mass, is a function of $\eta_\pm$ only. In order to study numerically the evolution of this spectrum we resort to the method known as truncated conformal space approach (TCSA) [23]. This involves first of all considering the theory on a cylinder of circumference R, in such a way that the Hamiltonian operator takes the form

$$H = \frac{2\pi}{R}\left(L_0 + \bar{L}_0 - \frac{c}{12}\right) + \tau \int_0^R \epsilon(x,0)\,dx - h\int_0^R \sigma_+(x,0)\,dx\ , \tag{2.71}$$

where the conformal part is expressed in terms of the zero index generators L_0 and $\bar{L}_0$ of the chiral Virasoro algebras with central charge $c = 4/5$. At the conformal point the eigenvalues of $L_0 + \bar{L}_0$ are simply the scaling dimensions $\Delta + \bar{\Delta}$ of the operators, so that the conformal space of states coincides with the operator space. Also the matrix elements of the perturbing operators ϵ and σ_+ on this space of states can be computed exactly, since they are related to the structure constants C_{ijk} of the conformal operator product expansion as

$$\langle \phi_i | \phi_j(0,0) | \phi_k \rangle = (2\pi/R)^{2\Delta_{\phi_j}} \, C_{ijk} \, . \tag{2.72}$$

In this way the eigenvalues of (2.71) can be determined by numerical diagonalization of the Hamiltonian matrix on a finite-dimensional subspace of the conformal space. Obviously, the truncation of the space of states puts upper bounds on the number of levels and on the values of R which are numerically accessible. Nevertheless, with a number of states which is very reasonable from the point of view of computer time, it is normally possible to obtain a sufficiently accurate description of many energy levels in the lower part of the spectrum, up to values of R for which the asymptotic regime relevant for the theory on the plane is already visible.

After its appearance [23], the TCSA has been widely used, including for the study of multiple perturbations [35], non-minimal models [70] and theories with boundaries [71] (see e.g. [57] for additional references). Its use for the case at hand would not present special difficulties were not for the following point. Although minimal (i.e. containing a finite number of operator families), the conformal theory we start from does not belong to the series of minimal models (known as A-series) for which the structure constants appearing in (2.72) are known completely from the work of Dotsenko and Fateev [72]. The 3-state Potts conformal point, as already said, belongs to the D-series of minimal models, and for this series not all the structure constants are completely known; more precisely, some of them are known only up to signs [73, 74]. Of course, these signs are themselves essential for the determination of the energy spectra through the TCSA. As a matter of fact, we managed to determine them (at least those needed for our purposes) requiring that the output of the TCSA is physically meaningful. The results are given in the Appendix 6.

2.3.3 Evolution of the particle spectrum

We used the TCSA to follow the evolution of the lower part of the spectrum of the Hamiltonian operator (2.71) in the whole range of the parameters $\eta_\pm$. More precisely, we numerically determined the spectrum at 80 points along the curve $\tau^{14} + |h|^9 = \text{constant}$ shown in figure 2.22: each renormalization group trajectory flowing out of the origin in the (τ, h) plane and corresponding to a specific value of η_+ or η_- intercepts such a closed curve at a specific point, in such a way that making a round trip along the curve amounts to spanning all the trajectories. Since *mass ratios* are fixed along a given trajectory, it is sufficient to determine them at a single point.

For the study of the mass spectrum it is sufficient to consider the subspace of states with vanishing total momentum on the cylinder, namely the operators with zero spin[1]. Moreover, one can treat the parts of the Hamiltonian which are even and odd under the $\mathbb{Z}_2$ symmetry separately. We included in our numerical calculations conformal states up to level 8 of descendance within the

[1]Notice that also the primaries with non-zero spin in table 2.5 contribute scalar descendants.

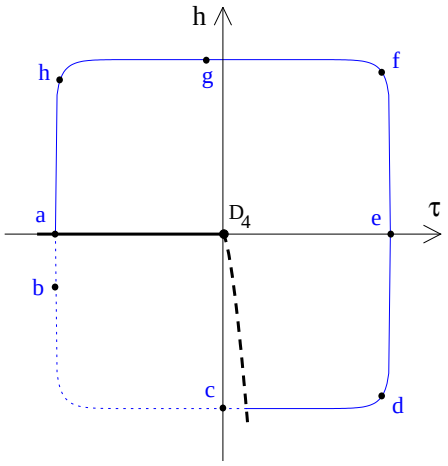

Figure 2.22: Phase diagram of the field theory (2.69). The thick lines correspond to the first order (continuous line) and second order (dashed line) phase transitions. Dots on the closed path $\tau^{14} + |h|^9 =$ constant mark the points corresponding to the spectra shown in figures 2.23a–h. The ordered phase corresponds to the dotted part of the path.

conformal family associated to each primary operator. This corresponds to 2426 states in the even sector and 1829 states in the odd sector.

Examples of the results we obtained for the spectrum at different values of $\eta_\pm$ are given in figures 2.23a–h. They show, as a function of the cylinder circumference R, the energy differences $E_i - E_0$, where E_i is the energy of the i-th level, with the ground state corresponding to $i = 0$. As a consequence, in these figures the ground state coincides with the horizontal axis. Due to the absence of phase transitions on the cylinder, the ground state is always unique at finite R. When other levels are seen to approach the horizontal axis as R increases, the spectrum refers to values of τ and h corresponding to the ordered phase (with degenerate ground states) on the plane $(R = \infty)$.s

The energy levels behave as $1/R$ in the conformal limit $R \to 0$ (see (2.71)) and approach constant values as $R \to \infty$. These asymptotic constants determine the particle spectrum of the theory on the plane, the one we are interested in in this paper. The lowest non-zero asymptotic value determines the mass of the lightest particle (or multi-particle) state with quantum numbers compatible with the boundary conditions chosen on the cylinder geometry. In this paper we always work with periodic boundary conditions, which select states with zero topological charge, and determine the mass of the kinks (which are topologically charged) in the ordered phase from that of the kink-antikink states.

If m_1 is the mass of the lightest particle, the continuous part of the spectrum on the plane starts at $2m_1$. On the cylinder, the continuum breaks into infinitely many discrete levels which become dense when $R \to \infty$: the lowest one (the threshold) corresponds to a pair of particles at rest, the others to a pair with momenta p and $-p$. Of course, in our truncated numerical approach, only a finite number of these "momentum lines" are visible. In general, the theory on the plane possesses

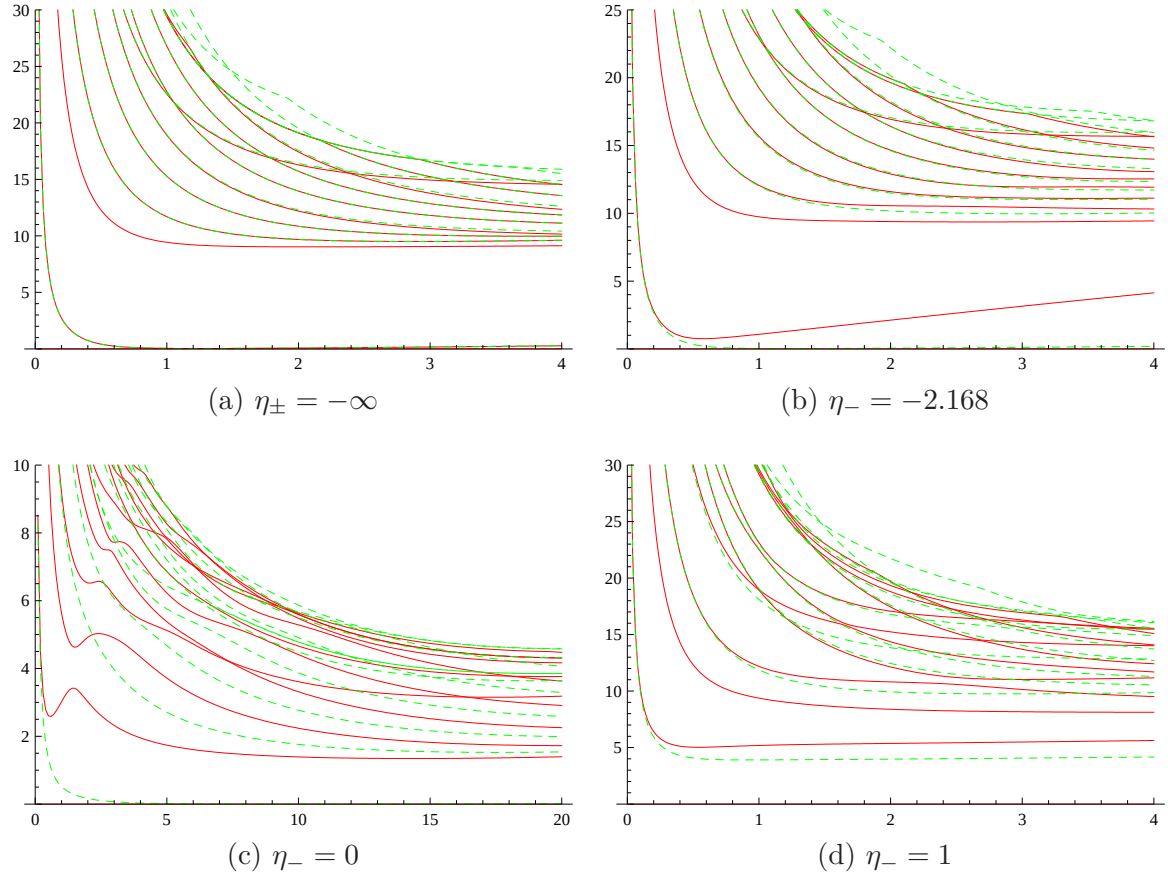

(a) $\eta_{\pm} = -\infty$ (b) $\eta_{-} = -2.168$

(c) $\eta_{-} = 0$ (d) $\eta_{-} = 1$

several stable particles with masses m_i, and the total spectrum is made of all the states resulting from the combination of these particles.

With these remarks in mind, it is not difficult to see that the numerical results indeed confirm the evolution of the particle spectrum predicted in [60]. Referring the reader to that paper for the detailed arguments at the origin of the prediction, we recall here the main features and how they appear in the TCSA.

Ordered phase

We start our discussion at low temperature ($\tau < 0$) and zero magnetic field, where the model is on the first order phase transition line. Here the system on the plane exhibits a spontaneous breaking of the S_3 symmetry and has three degenerate ground states $|0_\alpha\rangle$, $\alpha = 1, 2, 3$. The spectrum of elementary excitations is known [75] to contain only the kinks $K_{\alpha\beta}$, $\alpha \neq \beta$, of equal mass m, which interpolate between the ground states α and β. The finite volume spectrum calculated by the TCSA is shown in figure 2.23a. Two superimposed levels are clearly seen to approach the horizontal axis to produce the asymptotic triple ground state degeneracy. The splitting of the vacua is due to tunneling effects and, up to truncation errors, decreases exponentially at large R. The unique finite volume ground state belongs to the $\mathbb{Z}_2$-even sector; it becomes $|0_3\rangle$ asymptotically, while the other

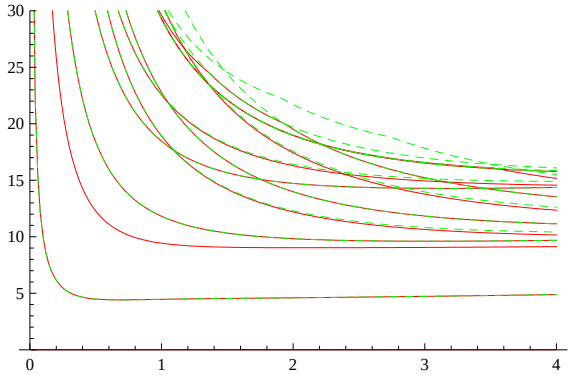

(e) $\eta_{\pm} = +\infty$

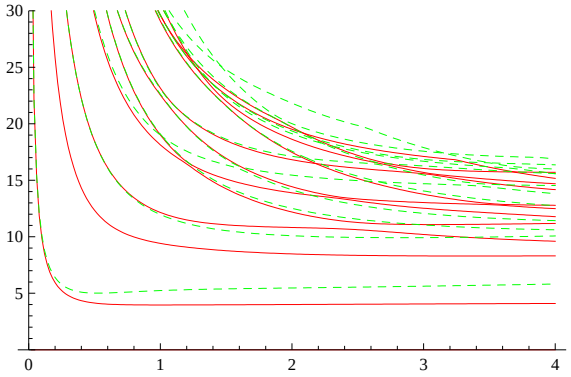

(f) $\eta_{+} = 1$

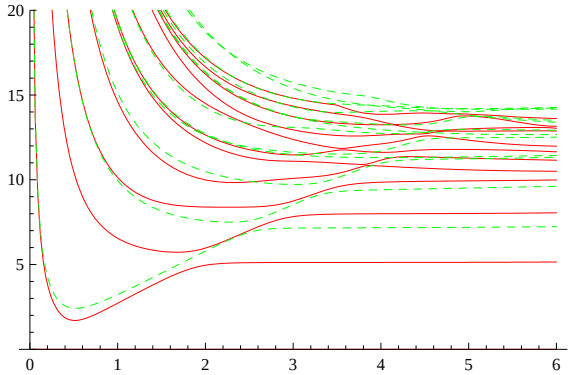

(g) $\eta_{+} = -0.1$

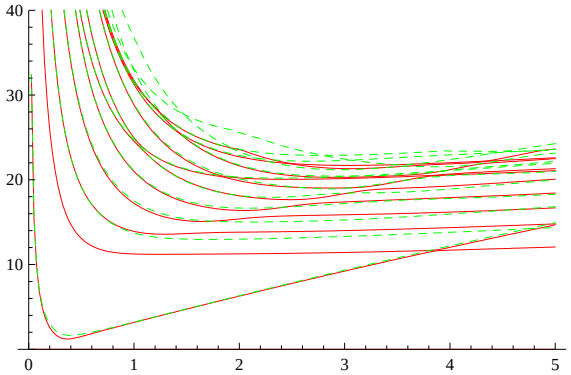

(h) $\eta_{+} = -1.07$

Figure 2.23: The low lying energy differences $E_i - E_0$ as functions of R at the points a–h along the closed path of figure 2.22. Even levels are in red, odd levels are in green with dashed lines. Units refer to a fixed mass scale.

two levels go into $|0_1\rangle \pm |0_2\rangle$. The single-kink states do not appear due to the periodic boundary conditions, but two-kink states $K_{\alpha\beta}K_{\beta\alpha}$ as well as three-kink states $K_{\alpha\beta}K_{\beta\gamma}K_{\gamma\alpha}$ are clearly visible.

When, starting from this situation, a magnetic field of the form specified in (2.69) is switched on, the vacuum $|0_3\rangle$ is no longer degenerate with the other two: in particular, for $h < 0$ its energy is higher and it becomes a false vacuum. In the finite volume this translates into an energy level linearly increasing with R, a feature perfectly visible in figure 2.23b. Since finite-energy excitations cannot start from or end on a false vacuum, the kinks K_{13}, K_{23} and their antikinks get removed from the spectrum, while K_{12} and K_{21} survive. The multi-kink states in which $\gamma = 3$ enters only as an internal index preserve a finite energy in the negative field. This is the case, in particular, of the state $K_{13}K_{32}$, which however cannot remain a two-kink excitation at $h < 0$, since the false nature of the intermediate vacuum prevents the two kinks from moving arbitrarily far apart. They are instead confined into the topologically charged "mesons" $\pi_{12}^{(n)}$, with n a positive integer indexing mesons of increasing mass. While the mesonic spectrum becomes dense above $2m$ as $h \to 0^-$, the number of stable mesons is expected to decrease as one moves away from the first order transition line. Indeed, since the mass splittings increase in the process, more and more mesons become unstable crossing the decay threshold $3m$, above which the decay channel $\pi_{12}^{(n)} \to K_{12}K_{21}K_{12}$ opens.

The pattern of the levels visible in figure 2.23b is consistent with these expectations. Because of the periodic boundary conditions the topologically charged particles K_{12} and $\pi_{12}^{(n)}$ and their antiparticles appear only through neutral combinations[1]. So the mass gap corresponds to the $K_{12}K_{21}$ threshold and the levels converging at $3m$ to the $\pi_{12}^{(1)}K_{21}$ threshold. Figure 2.23c shows that at $\eta_- = 0$ the theory still is in the ordered phase (the single-particle excitations do not appear, so they are kinks). The absence of lines converging at three times the mass of the kinks now indicates that no stable topologically charged meson is left so far away from the first order transition. The non-monotonic behaviour of the lowest lines in the even sector is a residual manifestation of the false vacuum visible in figure 2.23b, which is now very unstable.

Second order phase transition

The reduction of the mass gap from figure 2.23b to figure 2.23c is consistent with the expectation that the ordered phase ends at a critical value η_-^c where the kink mass vanishes and a second order transition of Ising type takes place. The value η_-^c had been naively set to 0 in [60]. There is, however, no symmetry (like duality in the TIM) which selects this value and it was observed in [77] that, since the Potts Curie temperature is larger at $q = 2$ than at $q = 3$, η_-^c is more likely positive. This latter expectation is indeed confirmed by the TCSA, which neatly shows a phase transition at $\eta_-^c \simeq 0.14$ and confirms that it corresponds to a crossover from $q = 3$ to $q = 2$ criticality.

To see this point notice that the signature of a crossover to Ising criticality in the finite volume spectrum is that for sufficiently large values of R the energy levels behave again as $1/R$, more precisely as

$$E_i - E_0 \sim \frac{2\pi}{R}(\Delta_i + \bar{\Delta}_i)\,, \tag{2.73}$$

where $\Delta_i + \bar{\Delta}_i$ are scaling dimensions of Ising operators. Since we are considering the zero mo-

[1]The topologically charged mesons, whose stability is specific of the Potts model with $q = 3$, were not mentioned in [60]. They have been recently discussed in [76].

	0	1	2	3	4	5	⋯
$(0,0)$	1	0	1	1	4	4	⋯
$(1/2,1/2)$	1	1	1	1	4	4	⋯
$(1/16,1/16)$	1	1	1	4	4	9	⋯

Table 2.6: Multiplicities of low lying states of zero spin in the representations of the conformal algebra entering the Ising model; n is displayed in the top row.

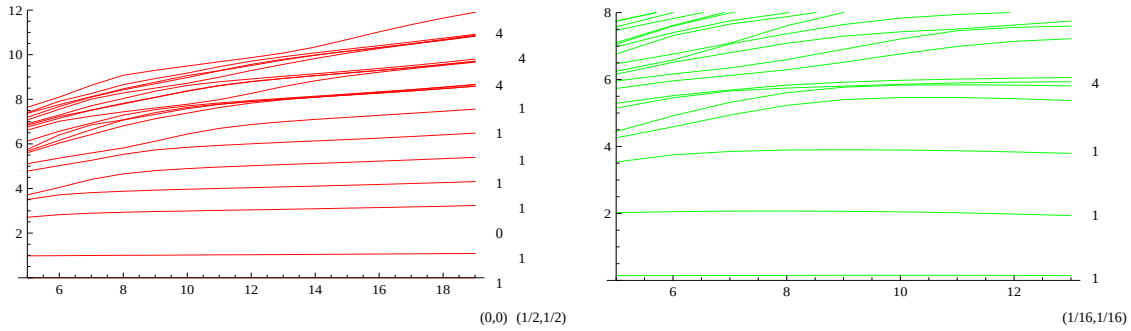

(a) even sector (b) odd sector

Figure 2.24: $\frac{R}{2\pi}(E_i - E_0)$ as functions of R for the lowest values of i in the (a) even and (b) odd sectors at the second order phase transition point. Degeneracies predicted by the critical Ising model (Table 2.6) are shown on the right hand side.

mentum sector, and on the cylinder the momentum coincides with the spin, only those states with $\Delta = \bar{\Delta}$ have to be taken into account. The Ising model with periodic boundary conditions contains three representations of the conformal algebra with highest weights $\Delta = 0, 1/2, 1/16$. The scaling dimensions entering (2.73) are then $2(\Delta + n)$, where $n = 0, 1, 2, \ldots$ labels the conformal levels. The multiplicities of the states with these dimensions are shown in table 2.6.

Figure 2.24 shows $\frac{R}{2\pi}(E_i - E_0)$ as functions of R in the even and odd sectors at the point $\eta_- = 0.14$ (the same absolute ground state energy is subtracted in both sectors). According to (2.73) these functions should be approximately constant for sufficiently large values of R. The data are in good agreement with this expectation and also the location and the multiplicities of the lines agree well with the data of the critical Ising model. For the lowest energy difference in each sector the accuracy of the data can be appreciated in figure 2.25.

Similar studies of second order phase transitions by means of the TCSA were done in [78, 56]. A second order phase transition was also observed in the TIM [2], however its type (which is known to be Ising) could not be established numerically because of large truncation errors.

Disordered phase

When, starting from the first order transition line, the magnetic field is switched on with a *positive* sign, $|0_3\rangle$ remains as the unique true vacuum of the theory. We thus enter the disordered phase in

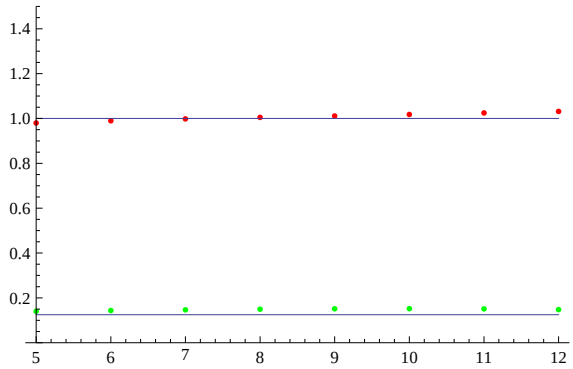

Figure 2.25: The lowest energy difference $\frac{R}{2\pi}(E_i - E_0)$ in the two sectors as a function of R at the second order phase transition point. Data are shown with dots, the constants 2Δ equal $1/8$ and 1 predicted by the critical Ising model are shown with continuous lines.

which all kinks are confined inside topologically neutral mesons originating from $K_{31}K_{13} \pm K_{32}K_{23}$, and baryons originating from $K_{31}K_{12}K_{23} \pm K_{32}K_{21}K_{13}$, where we have taken linear combinations with definite $\mathbb{Z}_2$-parity. We keep the notation of [60] and denote $\pi_0^{(n)}$ and $\pi_1^{(n)}$ the even and odd mesons, respectively, and $p_\pm^{(n)}$ the baryons with parity ± 1. In all cases the positive integer n indexes particles with increasing mass, and again the spectra of these particles become dense (above $2m$ for the mesons and above $3m$ for the baryons) in the limit $h \to 0$; as we move away from the first order transition line more and more particles should cross the two-meson decay thresholds and become unstable.

These expectations are fully consistent with the numerical spectrum shown in figure 2.23h, which exhibits a large number of lines corresponding to single-meson states and a doubly degenerate linearly rising line corresponding to the two false vacua. A linearly rising line-like feature with the same slope can also be seen somewhat upper, which is the signature of some topologically neutral configuration unstable because supported by the false ground states[2]. A line corresponding to the baryon $p_+^{(1)}$ is also present, although it is not very clearly seen because of truncation errors and the presence of many other lines in its vicinity.

At $\eta_+ = +\infty$ the theory is integrable and is known [79, 80] to possess a doublet of massive particles as the only single-particle excitations. By duality[3] their mass coincides with the mass of the kinks at $\eta_\pm = -\infty$. It is expected that the two lightest mesons $\pi_0^{(1)}$ and $\pi_1^{(1)}$ are the only products of kink confinement which do not decay as η_+ increases, and that they become the above mentioned doublet at $\eta_+ = +\infty$. This prediction is confirmed by the numerical calculations. The reduction in the number of stable single-particle states as η_+ increases can be appreciated in figures 2.23g and 2.23f. In the latter only the two lightest mesons are left below threshold; their mass difference vanish at $\eta_+ = +\infty$ (figure 2.23e) and changes sign with the magnetic field (figure 2.23d).

[2]See [55] for a discussion of (possibly stable) particles above threshold.
[3]See [60] for the relation between the scattering theories at $\tau > 0$ and $\tau < 0$ in zero field.

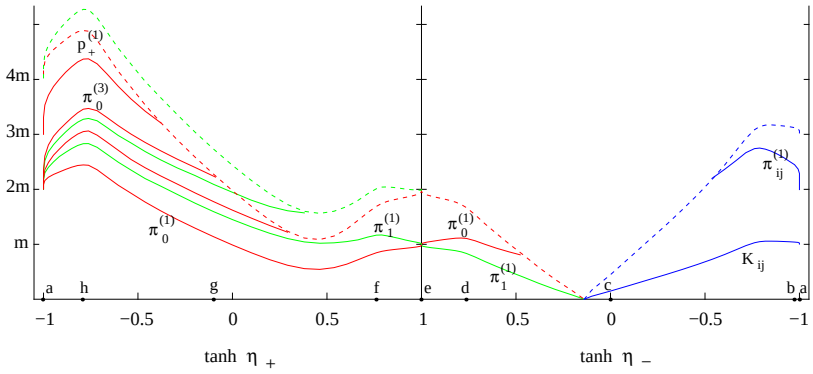

Figure 2.26: Masses of the lightest mesons $\pi_0^{(1)}$, $\pi_1^{(1)}$, $\pi_0^{(2)}$, $\pi_1^{(2)}$, $\pi_0^{(3)}$, the lightest baryon $p_+^{(1)}$, the elementary kinks K_{ij} and the lightest mesonic kinks $\pi_{ij}^{(1)}$, along the closed path of figure 2.22. Even particles are shown in red, odd particles in green and the kinks in blue. Dashed lines show the stability thresholds for even particles (twice the mass of the lightest particle), odd particles (mass of the lightest even particle plus that of the lightest odd particle) and mesonic kinks (mass of K_{ij} plus that of $\pi_{ij}^{(1)}$) in red, green and blue, respectively. The points a-h, having a correspondence in figures 2.22 and 2.23, are also marked.

Complete evolution

The systematic collection and analysis of the TCSA spectra at regular small intervals along the closed path of figure 2.22 allows us to follow the evolution of the lightest particles of the theory in the whole range of the parameters $\eta_\pm$. The result is shown in figure 3.40 and shows a remarkable agreement with the qualitative prediction given in figure 8 of [60]. The data show how the confinement of kinks at $h > 0$ produces both mesons and baryons, and how all the mesons, excluding the two lightest, and all the baryons reach the decay thresholds as η_+ increases. The mesons $\pi_0^{(1)}$ and $\pi_1^{(1)}$ are the only stable particles of the theory in a sufficiently wide range around $\eta_\pm = +\infty$, the point of enhanced (S_3) symmetry where their mass trajectories cross. At $h < 0$ the even meson $\pi_0^{(1)}$ is no longer the lightest particle of the theory, and decays before the second order transition point, where the mass of $\pi_1^{(1)}$ vanishes, is reached. In the ordered phase the spectrum of stable particles contains the deconfined elementary kinks K_{12}, K_{21} and, close enough to the first order transition point $\eta_\pm = -\infty$, the mesonic kinks $\pi_{12}^{(n)}$, $\pi_{21}^{(n)}$.

Of course, more and more particles emerge from the thresholds and become stable as $\eta_\pm \to -\infty$. Figure 3.40 includes only the five lightest topologically neutral mesons, the lightest baryon and the lightest mesonic kink. The behaviour of the curves at $h = 0$ follows from the discussion in the next subsection.

2.3.4 Weak magnetic field

A number of analytic results can be obtained at $h = 0$, where the theory is integrable, and for small h, using perturbation theory around the integrable case. In this subsection we compare some of these results with the numerical ones that we obtain by the TCSA.

At $h = 0$ and, by duality, for both signs of τ, the vacuum energy density and the mass of the elementary excitations can be written as

$$\epsilon_0 = a\,\tau^{10/6}, \qquad m = b\,\tau^{5/6}, \tag{2.74}$$

with a and b dimensionless constants whose exact values are known to be[4] [46]

$$a = -5.856..\,, \qquad b = 4.504..\,. \tag{2.75}$$

The measure of the slope of E_0 and of the mass gap at large R in the TCSA gives $a \approx -5$ and $b \simeq 4.5$. We are able to determine a only with a low accuracy, a circumstance that is not unexpected: as a general experience absolute energies are given less precisely by the TCSA than mass gaps (energy differences).

Consider now the high temperature phase, $\tau > 0$. The first order correction to ϵ_0 is proportional to the spontaneous magnetization, which is zero. The second order correction reads

$$\delta\epsilon_0 = -\frac{h^2}{2}\int d^2x \langle\sigma_+(x)\sigma_+(0)\rangle = d\,h^2\tau^{-13/9}\,. \tag{2.76}$$

The susceptibility was computed in [81] (see also [82], Appendix 2) within the two-particle approximation in the form factor approach, with the result $d \simeq -0.135$, which compares very well with the result $d \simeq -0.133$ we obtain using the TCSA.

Let us denote

$$\delta m_i^{(1)} = e_i\,h + f_i\,h^2 + .. \tag{2.77}$$

the correction to the mass of the meson $\pi_i^{(1)}$, $i = 0, 1$. At first order one has [35, 60]

$$e_i = -\frac{1}{m}\langle\pi_i^{(1)}(0)|\sigma_+(0)|\pi_i^{(1)}(0)\rangle\ . \tag{2.78}$$

These matrix elements are known (see [82] and references therein) in a basis $A, \bar{A}$ in which $\pi_i^{(1)} = (A + (-1)^i\bar{A})/\sqrt{2}$, and read

$$e_0 = -e_1 = -0.7036..\,\tau^{-13/18}\,. \tag{2.79}$$

Our TCSA determination $e_0 = -e_1 \simeq -0.71..\,\tau^{-13/18}$ is in reasonable agreement with this exact result. Concerning the second order mass corrections, we obtain the numerical results $f_0 \approx 0.09\,\tau^{-41/18}$ and $f_1 \approx 0.12\,\tau^{-41/18}$. These numbers probably have considerable errors, nevertheless it will be interesting to compare them with analytic results when these will be available.

Turning to the low temperature phase, the confinement of kinks at leading order in the magnetic field can be described within the non-relativistic framework [60]. The detailed analysis has been recently performed in [76] for the mesonic spectrum, both at low energy and in the semiclassical

[4] Throughout the paper we use the normalization of the operators in which $\langle\phi(x)\phi(0)\rangle \to |x|^{-4\Delta_\phi}$ as $|x| \to 0$.

limit, as a generalization of the Ising case. Concerning the low energy part of the spectrum at $h > 0$, the linear confining potential in one dimension produces mesons with masses $m_i^{(n)}$ which deviate from twice the kink mass by a term $c_i^{(n)} h^{2/3}$; the constants $c_i^{(n)}$ are proportional to the zeros of the Airy function for the odd mesons ($i = 1$), and to the zeros of the derivative of the Airy function for the even mesons ($i = 0$) [76].

A precise quantitative investigation of this region of the phase diagram in which the mesonic spectrum tends to a continuum requires a numerical accuracy higher than that of our TCSA data. Nevertheless, we found that for moderately large values of the magnetic field ($\eta_+ \leq -1$) the data for the masses of the five lightest mesons are described relatively well by the $h^{2/3}$ power law; the exponent that we could extract by fitting a power function to the data is approximately 0.7. Concerning the pre-factors, we obtain very approximately $c_1^{(1)}/c_0^{(1)} \approx 2$, to be compared with the value close to 2.3 corresponding to the analytic prediction.

2.3.5 Conclusions

In this Section we studied the scaling limit of the two-dimensional three-state Potts model as a function of temperature and magnetic field. This has been done directly in the continuum limit, considering the perturbation of the D_4 minimal model of conformal field theory by its leading thermal and magnetic operators. The magnetic perturbation was chosen to be coupled to one color only, in such a way to leave a residual permutation symmetry in the first two colors. We studied the particle spectrum of the theory in the whole plane of the coupling constants using the numerical method called truncated conformal space approach, with the aim of verifying the qualitative predictions made in [60].

Our results confirm these predictions, clearly showing that kink confinement produces both mesonic and baryonic particles and that deconfined kinks survive within an extended ordered phase whose boundary contains a first order and a second order part. In particular, we determined numerically the location of the second order transition, which is not fixed by symmetry. The evolution of the masses of the first few lightest mesonic and baryonic states has been followed through the whole parameter range of the theory, exhibiting the decay pattern and confirming that the two particles of the disordered phase in zero field are the two lightest mesons produced when breaking the ordered phase by a positive field.

The implementation of the numerical method required the knowledge of the structure constants of the thermal and magnetic operators in the D_4 conformal field theory. We determined the signs of the structure constants which were left undetermined in [73, 74]. The integrability of the model at zero magnetic field makes it possible to obtain analytic results for the particle masses and for the vacuum energy density at zero and small magnetic fields. We compared our numerical results with such analytic results at high temperature finding a good agreement. We also presented numerical results for the second order corrections of the meson masses, which could be useful for comparison with future analytic results. We could partially confirm recent results of [76] for the meson masses at low temperature and small magnetic field. This region of the phase diagram is numerically more demanding because the mesonic spectrum becomes dense as the magnetic field approaches zero, so that a complete verification requires a numerical accuracy larger than that of the present study. Normally this can be achieved by increasing the truncation level.

Following the appearance of the source article as a preprint, G. Takacs informed us that complete results for the structure constants of the D-series minimal models were obtained in [83]. We checked that, once the different conventions and normalizations are suitably taken into account, the structure constants of [83] for the D_4 case exactly coincide with those we give in the Appendix 6.

2.4 Appendices

2.4.1 Appendix 1: Form Factor Bootstrap

In this Appendix we explain the derivation of the relations (2.55) and (2.56) by the form factor approach. The two-particle form factor $F_{ii}^t(\theta)$ can be written as [36]

$$F_{ii}^t(\theta) = Q_{ii}^t(\theta)\frac{F_{ii}^{min}(\theta)}{D_{ii}(\theta)}, \tag{2.80}$$

where $F_{ii}^{min}(\theta)$ and $D_{ii}(\theta)$ can be obtained by specializing the general formulas [36] to the present case:

$$\begin{aligned} D_{11}(\theta) &= P_{10}(\theta)P_2(\theta) \\ D_{22}(\theta) &= P_{12}(\theta)P_8(\theta)P_2(\theta) \\ F_{11}^{min}(\theta) &= -\mathrm{i}\sinh\tfrac{\theta}{2}\, g_{10}(\theta)g_2(\theta) \\ F_{22}^{min}(\theta) &= -\mathrm{i}\sinh\tfrac{\theta}{2}\, g_{12}(\theta)g_8(\theta)g_2(\theta)\ , \end{aligned} \tag{2.81}$$

where

$$P_n(\theta) \;=\; \frac{\cos(\frac{n}{18}\pi) - \cosh\theta}{2\cos^2(\frac{n}{18}\frac{\pi}{2})} \tag{2.82}$$

$$g_n(\theta) \;=\; \exp\left[2\int_0^\infty \frac{\mathrm{d}x}{x}\frac{\cosh[(n/18-1/2)x]}{\cosh x/2\sinh x}\sin^2[(\mathrm{i}\pi-\theta)x/2\pi]\right]\ . \tag{2.83}$$

The $Q_{ii}^t(\theta)$ are polynomials in $\cosh(\theta)$. An upper bound on the degree d_P of these polynomials can be obtained from the following general formula for the asymptotic behaviour of form factors [36]:

$$\lim_{|\theta_i|\to\infty} F^\varphi_{a_1,\ldots,a_n}(\theta_1,\ldots,\theta_n) \sim \mathrm{e}^{y_\varphi|\theta_i|}\,, \qquad y_\varphi \le \Delta_\varphi\,. \tag{2.84}$$

This relationship fixes $d_P = 1$ for both $Q_{11}^t(\theta)$ and $Q_{22}^t(\theta)$:

$$Q_{ii}^t(\theta) \;=\; a_{ii}^t + b_{ii}^t\cosh(\theta)\,, \qquad i=1,2\ . \tag{2.85}$$

These coefficients a_{ii}^t and b_{ii}^t can be expressed in terms of the three-particle coupling constants Γ_{11}^2, Γ_{11}^4, Γ_{22}^2, Γ_{22}^4 and the one-particle form factors F_2^t, F_4^t by means of the residue equations

$$-\,\mathrm{i}\lim_{\theta\to\mathrm{i}u_{ab}^c}(\theta-\mathrm{i}u_{ab}^c)F_{ab}^\varphi(\theta) = \Gamma_{ab}^c F_c^\varphi \tag{2.86}$$

for the fusions

$$A_1 \times A_1 \to A_2, \qquad u_{11}^2 = \frac{10}{18}\pi, \tag{2.87}$$

$$A_1 \times A_1 \to A_4, \qquad u_{11}^4 = \frac{2}{18}\pi, \tag{2.88}$$

$$A_2 \times A_2 \to A_2, \qquad u_{22}^2 = \frac{12}{18}\pi, \tag{2.89}$$

$$A_2 \times A_2 \to A_4, \qquad u_{22}^4 = \frac{8}{18}\pi, \tag{2.90}$$

where u_{ab}^c denotes the fusion angle. The expressions we found are the following:

$$a_{11}^t = 1.14107 \cdot \Gamma_{11}^2 F_2^t - 1.77654 \cdot \Gamma_{11}^4 F_4^t \tag{2.91}$$
$$b_{11}^t = -1.21431 \cdot \Gamma_{11}^2 F_2^t - 10.2307 \cdot \Gamma_{11}^4 F_4^t \tag{2.92}$$
$$a_{22}^t = 0.306459 \cdot \Gamma_{22}^2 F_2^t - 1.37383 \cdot \Gamma_{22}^4 F_4^t \tag{2.93}$$
$$b_{22}^t = -1.76483 \cdot \Gamma_{22}^2 F_2^t - 2.74766 \cdot \Gamma_{22}^4 F_4^t \,. \tag{2.94}$$

In terms of these coefficients

$$F_{ii}^t(\mathrm{i}\pi) = a_{ii}^t - b_{ii}^t \,, \qquad i = 1, 2 \,. \tag{2.95}$$

The squares of three-particle coupling constants can be obtained from the S-matrix elements

$$S_{11}(\theta) = -f_{10}(\theta) f_2(\theta) \tag{2.96}$$
$$S_{22}(\theta) = f_{12}(\theta) f_8(\theta) f_2(\theta) \,, \tag{2.97}$$

where

$$f_n(\theta) = \frac{\tanh \frac{1}{2}(\theta + \mathrm{i}\pi \frac{n}{18})}{\tanh \frac{1}{2}(\theta - \mathrm{i}\pi \frac{n}{18})}, \tag{2.98}$$

by using the residue equation

$$-\,\mathrm{i} \lim_{\theta \to \mathrm{i}u_{ab}^c} (\theta - \mathrm{i}u_{ab}^c) S_{ab}(\theta) = (\Gamma_{ab}^c)^2 \tag{2.99}$$

for the fusions (2.87)-(2.90). We obtained

$$(\Gamma_{11}^2)^2 = 4.838705173^2 \qquad (\Gamma_{11}^4)^2 = 1.225805260^2 \tag{2.100}$$
$$(\Gamma_{22}^2)^2 = 11.15518618^2 \qquad (\Gamma_{22}^4)^2 = 19.10015279^2 . \tag{2.101}$$

Assuming $\Gamma_{ii}^2 > 0$, $\Gamma_{ii}^4 > 0$, these results can be substituted into (2.91)-(2.94), and then (2.95) takes the form of (2.55) and (2.56).

2.4.2 Appendix 2: Calculation of form factors by TCSA

A one-particle form factor of a field φ of conformal weights (Δ, Δ) at infinite R can be obtained as the limit of the finite R form factor:

$$F_A^\varphi = \langle 0|\varphi(0)|A\rangle = \lim_{R\to\infty} R^{-2\Delta}\sqrt{Rm}\langle 0|\varphi(0)|A\rangle_R \ , \tag{2.102}$$

where the subscript R on the right hand side indicates that the matrix element should be calculated in the theory defined at size R and m is the mass of the particle $|A\rangle$. In this formula $|A\rangle$ is a zero-momentum state and it is assumed that $\langle 0|0\rangle_R = \langle A|A\rangle_R = 1$. In the framework of the TCSA the absolute value of the matrix elements $\langle 0|\varphi(0)|A\rangle_R$ can be calculated. For a general matrix element the formula

$$\frac{\langle A|\varphi(0)|B\rangle}{\sqrt{\langle A|A\rangle}\sqrt{\langle B|B\rangle}} = \frac{\sum_{a,b} A_a^* B_b \langle a|\varphi(0)|b\rangle}{\sqrt{\sum_{a,b} G_{ab} A_a^* A_b}\sqrt{\sum_{a,b} G_{ab} B_a^* B_b}} \tag{2.103}$$

holds, where the subscript R is suppressed, it is not assumed that the eigenvectors $|A\rangle$ and $|B\rangle$ are normalized to unity, A_a and B_b are expansion coefficients with respect to the conformal basis used in the TCSA: $|A\rangle = \sum_a A_a|a\rangle$, $|B\rangle = \sum_b B_b|b\rangle$, and $G_{ab} = \langle a|b\rangle$ is the inner product matrix of the conformal basis vectors. The expansion coefficients A_a and B_b are calculated numerically up to overall constant factors; they are provided by the routine that one uses for the diagonalization of the Hamiltonian operator.

A two-particle form factor $F_{AA}^\varphi(\theta)$ at $\theta = \mathrm{i}\pi$ at infinite R can be obtained as the following limit of finite volume matrix elements:

$$\begin{aligned} F_{AA}^\varphi(\mathrm{i}\pi) &= \langle A(0)|\varphi(0)|A(0)\rangle \\ &= \lim_{R\to\infty} R^{-2\Delta} Rm(\langle A|\varphi(0)|A\rangle_R - \langle 0|\varphi(0)|0\rangle_R)\,. \end{aligned} \tag{2.104}$$

It is assumed that A is a self-conjugate particle, and normalization conditions similar to those for (2.102) apply. In the framework of the TCSA the matrix elements $\langle A|\varphi(0)|A\rangle_R$ and $\langle 0|\varphi(0)|0\rangle_R$ can be calculated in a similar way as the matrix element in (2.102), i.e. by the formula (2.103).

2.4.3 Appendix 3: Calculation of corrections to vacuum energy densities

The first order correction (2.59) to the vacuum energy density $\epsilon_{vac} = \lim_{R\to\infty} E_{vac}(R)/R$ at $g_2 = 1$, $g_4 = 0$ on the E_7-related axis was calculated by the following formula:

$$\delta\epsilon_{vac} = g_4 \frac{\mathrm{d}\epsilon_{vac}}{\mathrm{d}g_4}(g_4 = 0) = \lim_{R\to\infty} 2\pi g_4 \lambda_4 R^{-2\Delta_4}\langle 0|t(0)|0\rangle_R \ . \tag{2.105}$$

The numerical calculation of the first order corrections to the energy densities of the $|+\rangle$, $|-\rangle$, $|0\rangle$ vacua existing at the first order phase transition point is slightly more complicated, since these vacua are degenerate in infinite volume ($R = \infty$). Because of this degeneracy, one has to use, in general, degenerate perturbation theory, i.e. one obtains the first-order corrections by calculating the eigenvalues of the 3 by 3 matrix constituted by the 9 matrix elements $\langle +,-,0|H_p|+,-,0\rangle$ of the perturbing operator H_p between the three vacua. Those combinations of the vacua which evolve into the split vacua existing at nonzero perturbation are given by the eigenvectors of this matrix.

More precisely, in our case the first order corrections to the energy densities of the vacua are given by the eigenvalues of the matrix

$$M_{ij} = \lim_{R\to\infty} 2\pi g_2 \lambda_2 R^{-2\Delta_2} \langle U_i|\varepsilon(0)|U_j\rangle_R \,, \tag{2.106}$$

where $i,j = 1,2,3$, g_4 has the value -1, and $|U_1\rangle_R$, $|U_2\rangle_R$, $|U_3\rangle_R$ are the three vacua at cylinder circumference R, normalized to 1. The numbers $\langle U_i|\varepsilon(0)|U_j\rangle_R$ can be calculated as described above (see equation (2.103)). It is important, in general, that $|U_1\rangle_R$, $|U_2\rangle_R$, $|U_3\rangle_R$ should be orthogonal, otherwise the inverse of their inner product matrix has to be included in (2.106). In our case the vacua are split at finite R by tunneling effects, so $|U_1\rangle_R$, $|U_2\rangle_R$, $|U_3\rangle_R$ belong to different eigenvalues, therefore they can be identified uniquely and they are orthogonal.

The problem of the diagonalization of $\langle U_i|\varepsilon(0)|U_j\rangle_R$ can be simplified by symmetry considerations in our case: two of the three vacua $|U_1\rangle_R$, $|U_2\rangle_R$, $|U_3\rangle_R$ lie in the spin reversal even subspace, the third one lies in the odd subspace. We choose $|U_1\rangle_R$ and $|U_2\rangle_R$ to be the even vacua and $|U_3\rangle_R$ to be the odd one. Due to the spin reversal symmetry of the ε perturbation, the matrix elements $\langle U_{1,2}|\varepsilon(0)|U_3\rangle_R$ are all 0, therefore the diagonalization problem can be treated separately in the even and odd sectors. The odd vacuum (which becomes $\frac{|+\rangle-|-\rangle}{\sqrt{2}}$ in infinite volume) thus evolves into the odd (possibly metastable) vacuum of the perturbed theory, and the first-order correction to its energy density is given by

$$\delta\epsilon_{U_3} = \lim_{R\to\infty} 2\pi g_2 \lambda_2 R^{-2\Delta_2} \langle U_3|\varepsilon(0)|U_3\rangle_R \,. \tag{2.107}$$

In the even sector, one has to consider the 2 by 2 matrix $\langle U_{1,2}|\varepsilon(0)|U_{1,2}\rangle_R$. Since the duality D maps the even sector into itself and commutes with the unperturbed Hamiltonian operator in this sector, and $|U_1\rangle_R$ and $|U_2\rangle_R$ have different energies, $|U_1\rangle_R$ and $|U_2\rangle_R$ have to be eigenstates of D. The eigenvalues can be $+1$ or -1, because $D^2 = 1$. We also know that ε changes sign under duality, therefore $\langle U_1|\varepsilon(0)|U_1\rangle_R = \langle U_2|\varepsilon(0)|U_2\rangle_R = 0$. ε is also self-adjoint, so $\langle U_1|\varepsilon(0)|U_2\rangle_R = \langle U_2|\varepsilon(0)|U_1\rangle_R^*$. This number can be nonzero if the eigenvalues of $|U_1\rangle_R$ and $|U_2\rangle_R$ with respect to D have opposite sign. We denote the eigenvectors of the matrix $\langle U_{1,2}|\varepsilon(0)|U_{1,2}\rangle_R$ by $|V_+\rangle_R$ and $|V_-\rangle_R$. The eigenvalues of the matrix $\langle U_{1,2}|\varepsilon(0)|U_{1,2}\rangle_R$ are $\pm|\langle U_1|\varepsilon(0)|U_2\rangle_R|$, so the correction to the energy densities of the two vacua $|V_+\rangle_\infty$ and $|V_-\rangle_\infty$ are

$$\delta\epsilon_{V_+} = \lim_{R\to\infty} 2\pi g_2 \lambda_2 R^{-2\Delta_2} |\langle U_1|\varepsilon(0)|U_2\rangle_R| \,, \tag{2.108}$$

and

$$\delta\epsilon_{V_-} = \lim_{R\to\infty} -2\pi g_2 \lambda_2 R^{-2\Delta_2} |\langle U_1|\varepsilon(0)|U_2\rangle_R| \,. \tag{2.109}$$

Here we have chosen $|V_+\rangle_R$ to have the positive eigenvalue and $|V_-\rangle_R$ to have the negative one. Note that these formulas would not be meaningful without taking absolute values on the right hand side, since $|U_1\rangle_R$ and $|U_2\rangle_R$ are defined up to arbitrary phase factors.

The analytic result (2.113) described below, the Landau-Ginzburg picture and our numerical calculations of energy spectra all show that one vacuum gets a negative correction and two vacua get the same positive correction as we move into the high temperature phase. It follows then that

$$\delta\epsilon_{U_3} = \delta\epsilon_{V_+} = -\delta\epsilon_{V_-} \,, \tag{2.110}$$

and $\Delta E = 2\delta\epsilon_{U_3}$. The direct TCSA calculation of $\delta\epsilon_{U_3}$ and $\delta\epsilon_{V_+}$ confirms the equality $\delta\epsilon_{U_3} = \delta\epsilon_{V_+}$ and yields the result (2.40) for ΔE.

Having discussed the calculation of the energy density corrections, we turn to the description of the relation between the vacua $|U_1\rangle_\infty$, $|U_2\rangle_\infty$, $|U_3\rangle_\infty$; $|V_+\rangle_\infty$, $|V_-\rangle_\infty$ and $|+\rangle$, $|-\rangle$, $|0\rangle$. Equation (2.110) implies that

$$\langle U_3|\varepsilon|U_3\rangle_\infty = |\langle U_1|\varepsilon|U_2\rangle_\infty|\,, \tag{2.111}$$

and as we mentioned above, we also have

$$\langle U_1|\varepsilon|U_2\rangle_\infty = \langle U_2|\varepsilon|U_1\rangle^*_\infty\,, \tag{2.112}$$

and all other matrix elements of ε between $|U_1\rangle_\infty$, $|U_2\rangle_\infty$, $|U_3\rangle_\infty$ are zero. $\langle U_1|\varepsilon|U_2\rangle_\infty$ can be made real and positive by a phase redefinition of $|U_1\rangle_\infty$ or $|U_2\rangle_\infty$.

The matrix elements of ε between the $R = \infty$ eigenvectors $|+\rangle$, $|-\rangle$, $|0\rangle$ were calculated exactly in [51, 52]:

$$\langle +|\varepsilon|+\rangle = \langle -|\varepsilon|-\rangle = -\langle 0|\varepsilon|0\rangle = \Lambda_2 > 0\,, \tag{2.113}$$

and the not diagonal matrix elements are 0 (the numerical value of Λ_2 is given by (2.39), but it is irrelevant here). This result, together with the spin reversal properties, (2.111) and (2.112), allows us to identify $|U_1\rangle_\infty$, $|U_2\rangle_\infty$, $|U_3\rangle_\infty$ in terms of $|+\rangle$, $|-\rangle$, $|0\rangle$ as follows:

$$|U_1\rangle_\infty = \alpha\,\frac{|+\rangle + |-\rangle}{2} + \beta\,\frac{|0\rangle}{\sqrt{2}} \tag{2.114}$$

$$|U_2\rangle_\infty = \alpha\,\frac{|+\rangle + |-\rangle}{2} - \beta\,\frac{|0\rangle}{\sqrt{2}} \tag{2.115}$$

$$|U_3\rangle_\infty = \gamma\,\frac{|+\rangle - |-\rangle}{\sqrt{2}}\,, \tag{2.116}$$

where it is also assumed that the phases of $|U_1\rangle_\infty$ and $|U_2\rangle_\infty$ are chosen so that $\langle U_1|\varepsilon|U_2\rangle_\infty$ is real and positive. α, β and γ are unknown phase factors which are not determined by the information we have described so far, and they can be set to 1 by the following redefinition of the phases of $|+\rangle$, $|-\rangle$, $|0\rangle$ and $|U_3\rangle_R$: $|+\rangle \to \frac{1}{\alpha}|+\rangle$, $|-\rangle \to \frac{1}{\alpha}|-\rangle$, $|0\rangle \to \frac{1}{\beta}|0\rangle$, $|U_3\rangle_R \to \frac{\gamma}{\alpha}|U_3\rangle_R$. These redefinitions leave the previously stated relations involving these vectors unchanged. $|V_+\rangle_\infty$ and $|V_-\rangle_\infty$ can now be expressed as

$$|V_+\rangle_\infty = \tfrac{|U_1\rangle_\infty + |U_2\rangle_\infty}{\sqrt{2}} = \frac{|+\rangle + |-\rangle}{\sqrt{2}} \tag{2.117}$$

$$|V_-\rangle_\infty = \tfrac{|U_1\rangle_\infty - |U_2\rangle_\infty}{\sqrt{2}} = |0\rangle\,. \tag{2.118}$$

We note finally that since $|U_1\rangle_\infty$ and $|U_2\rangle_\infty$ are duality eigenstates with eigenvalues of opposite sign, equations (2.114) and (2.115) imply that the duality maps $|0\rangle$ and $\frac{|+\rangle+|-\rangle}{\sqrt{2}}$ into each other.

2.4.4 Appendix 4: Kink form factors

Along the first-order phase transition line ($g_2 = 0$, $g_4 < 0$), when the TIM has three degenerate vacua and an exact supersymmetry, in the infinite volume ($R = \infty$) the two-kink form factors

$$\begin{aligned}
\langle 0|\varepsilon(0)|K_{0-}(\theta_1)K_{-0}(\theta_2)\rangle &\equiv F^{\varepsilon}_{0-}(\theta_1-\theta_2)\ ,\\
\langle 0|\varepsilon(0)|K_{0+}(\theta_1)K_{+0}(\theta_2)\rangle &\equiv F^{\varepsilon}_{0+}(\theta_1-\theta_2)\ ,\\
\langle -|\varepsilon(0)|K_{-0}(\theta_1)K_{0-}(\theta_2)\rangle &\equiv F^{\varepsilon}_{-0}(\theta_1-\theta_2)\ ,\\
\langle +|\varepsilon(0)|K_{+0}(\theta_1)K_{0+}(\theta_2)\rangle &\equiv F^{\varepsilon}_{+0}(\theta_1-\theta_2)
\end{aligned}$$

are the following [49]:

$$F^{\varepsilon}_{0-}(\theta) = F^{\varepsilon}_{0+}(\theta)\ , \qquad F^{\varepsilon}_{-0}(\theta) = F^{\varepsilon}_{+0}(\theta)\ ,$$

$$F^{\varepsilon}_{0-}(\theta) = -\mathrm{i}(U_- - U_0)\frac{\mathrm{e}^{-\frac{\gamma}{2}(\pi+\mathrm{i}\theta)}}{p\sinh\frac{1}{p}(\theta-\mathrm{i}\pi)}F_0(\theta)\ , \tag{2.119}$$

$$F^{\varepsilon}_{-0}(\theta) = \mathrm{i}(U_- - U_0)\frac{\mathrm{e}^{\frac{\gamma}{2}(\pi+\mathrm{i}\theta)}}{p\sinh\frac{1}{p}(\theta-\mathrm{i}\pi)}F_0(\theta)\ , \tag{2.120}$$

where

$$U_0 = \langle 0|\varepsilon|0\rangle\ , \qquad U_- = \langle -|\varepsilon|-\rangle = \langle +|\varepsilon|+\rangle\ ,$$

$$F_0(\theta) = -\mathrm{i}\sinh\frac{\theta}{2}\,\exp\left[\int_0^\infty \frac{\mathrm{d}x}{x}\,\frac{\sinh(1-p)\frac{x}{2}}{\sinh\frac{px}{2}\cosh\frac{x}{2}}\,\frac{\sin^2(\mathrm{i}\pi-\theta)\frac{x}{2\pi}}{\sinh x}\right],$$

$$\gamma = \frac{1}{2\pi}\ln 2\ , \qquad p = 4\ .$$

These form factors have a pole at $\mathrm{i}\pi$, as can be explicitly seen from (2.119), (2.120).

2.4.5 Appendix 5: Semiclassical approach

In this Appendix we try to obtain some useful information about the evolution of mass spectrum by using a semiclassical treatment [58] [59]. This approach allows in particular to describe neutral bound states of kinks, in the (semiclassical) limit of big masses (and small rapidities rapidities $\theta \simeq 0$) for them. However we remark that the results presented must be taken with care and considered to be correct only qualitatively, since they rely on the properties of the Landau-Ginzburg potential and not on the real free energy of the considered critical model.
Bound states of kinks are obtain from the poles of two particles form factors

$$F^{\phi}_{ab}(\theta) = \langle a|\phi(0)|K_{ab}(\theta_1)K_{ba}(\theta_2)\rangle\,, \tag{2.121}$$

where a and b label two adjacent vacua at the border of two kinks and $\theta = (\theta_1 - \theta_2)$.
Formula above can be obtained by analytical continuation $\theta \to (i\pi - \theta)$ of

$$f^{\phi}_{ab} = \langle K_{ab}(\theta_1)|\phi(0)|K_a b(\theta_2)\rangle \;\simeq \int_{\infty}^{\infty} dx\, e^{iM_{ab}\theta x}\phi_{ab}(x)\,, \tag{2.122}$$

where M_{ab} is the "classical mass" of the kink:

$$M_{ab} = \int_{\infty}^{\infty} \epsilon_{ab}(x)dx \qquad \epsilon_{ab}(x) = \frac{1}{2}\left(\frac{d\phi_{ab}(x)}{dx}\right)^2 + U(\phi_{ab}(x))\,. \tag{2.123}$$

By using formula (2.121) we can study part of the low-temperature semiplane. In view of the pattern evolution for the masses described in the paper, we expect that semiclassical approach will work near the semiaxis $\eta_- \to -\infty$ and in a certain region in third square; conversely, we cannot say anything about the validity in second square. Because of this we specialize our discussion on the third square, and we choose the Landau-Ginzburg potential (pictured in figure 2.12) in the form

$$U(x) = (\phi(x)^2 + c)(\phi(x)^2 - \lambda^2)^2. \tag{2.124}$$

Obviously λ controls the distance between the real vacua, while c controls the height of the false vacuum. Given this potential, the solution of static equation of motion for the kinks reads:

$$\phi_{ab}(x) = \pm\lambda\ \ \mathrm{Tanh}(\lambda\sqrt{2(\lambda^2 + c)}x)\,, \tag{2.125}$$

from which:

$$F^{\phi}_{ab}(\theta) = \frac{i}{2\sqrt{\lambda^2 + c}}\,\frac{1}{\mathrm{Sinh}\left(\frac{(i\pi-\theta)}{\xi}\right)}\,, \qquad \xi = \frac{15\pi(\lambda^2 + c)}{2\lambda^4(5c + 3\lambda^2)} \tag{2.126}$$

and

$$M_{ab} = \frac{4\sqrt{2}\lambda^3(5c + 3\lambda^2)}{15\sqrt{c + \lambda^2}}\,. \tag{2.127}$$

The poles in (2.126) are located in

$$\theta_n = i\pi(1 - \xi n) \qquad , \qquad n = \pm1, \pm2, \pm3...., \tag{2.128}$$

so, if

$$\xi \geq 1\,, \tag{2.129}$$

there are no poles in physical strip $0 \leq Im\,\theta \leq \pi$. If vice versa $\xi < 1$ there are $[\frac{1}{\xi}]$ bound states with masses given by the formula:

$$m_n = 2M_{ab} \sin\left(n\,\frac{\pi\xi}{2}\right). \tag{2.130}$$

Only bound states for which $m_n > 2m_1$ are stable, the other ones are resonances. Every bound state has positive Z_2 parity, because the action of this symmetry simply interchanges kinks and antikinks, without adding any sign -1.
The quantities M_{ab} and $\frac{1}{\xi}$, seen as functions of c and λ, are monotonically increasing in both of variables, as one can see from graphs in figure below. This behavior is not necessarily contradicting our prediction about the number of particles and about their mass in the third square of the plane: spanning the third square towards the semiaxis $g_2 < 0, g_4 = 0$, one can justifiably expect a decrease of λ in addition to the increase of c. In this way we can obtain a behavior in agreement with our forecasts (note moreover that the dependence of M_{ab} and $\frac{1}{\xi}$ on λ is stronger than the dependence on c). At the end this semiclassical study seems to predict also a change (decrease) of the distance between the vacua.

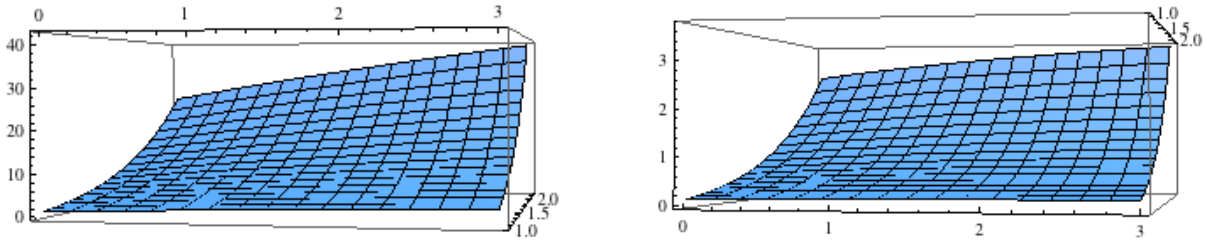

Figure 2.27: M_{ab} and $\frac{1}{\epsilon}$ as functions of c (horizontal axis) and λ (axis orthogonal to the plane).

2.4.6 Appendix 6: D_4 structure constants

The structure constants for the D-series unitary minimal models were studied e.g. in [73, 74]. They can be written as

$$C_{ijk} = M_{ijk}\sqrt{D_{\Delta_i\Delta_j\Delta_k} D_{\bar{\Delta}_i\bar{\Delta}_j\bar{\Delta}_k}}\,, \tag{2.131}$$

where Δ_i, $\bar{\Delta}_i$ are the left and right conformal weights of ϕ_i, $D_{\Delta_i\Delta_j\Delta_k}$ and $D_{\bar{\Delta}_i\bar{\Delta}_j\bar{\Delta}_k}$ are structure constants of the corresponding A-series minimal model (for the D_4 model this is the A_5 model), and M_{ijk} are called relative structure constants. The constants $D_{\Delta_i\Delta_j\Delta_k}$ and $D_{\bar{\Delta}_i\bar{\Delta}_j\bar{\Delta}_k}$ can be

calculated using the formulae given in [72]. For the D_4 case the relative structure constants M_{ijk} are real numbers on which the S_3 symmetry and

$$\sigma_1^\dagger = \sigma_2, \qquad \Omega_1^\dagger = \Omega_2 \tag{2.132}$$

impose some restrictions. The absolute values of these constants were found to be either 0 or 1 or $\sqrt{2}$. The latter value occurs in the following cases:

$$\begin{aligned} |M_{\sigma_2\sigma_1\sigma_1}| = |M_{\sigma_1\sigma_2\sigma_2}| = \\ |M_{\Omega_2\sigma_1\sigma_1}| = |M_{\Omega_1\sigma_2\sigma_2}| = |M_{\sigma_2\sigma_1\Omega_1}| = |M_{\sigma_1\sigma_2\Omega_2}| = \sqrt{2}\,. \end{aligned} \tag{2.133}$$

The signs of the relative structure constants were not completely fixed in [73, 74].

It is useful to introduce the combinations

$$\sigma_\pm = \frac{\sigma_1 \pm \sigma_2}{\sqrt{2}}\,, \tag{2.134}$$

$$\Omega_\pm = \frac{\Omega_1 \pm \Omega_2}{\sqrt{2}} \tag{2.135}$$

which are even and odd, respectively, under $\mathbb{Z}_2$ transformations. The model has an even part consisting of the modules I, ϵ, X, Y, σ_+, Ω_+, and an odd part consisting of the modules σ_-, Ω_-, J, $\bar{J}$, W, $\bar{W}$. The fields in the even part form a closed subalgebra, which is also contained by the A_5 model. This means that the even part of the D_4 model coincides with a sector of the A_5 model. The $\sqrt{2}$ mentioned above is eliminated from the relative structure constants by using the even and odd combinations introduced above.

Since in this paper we study the D_4 model with the ϵ and σ_+ perturbations, the relative structure constants that we actually need to know are $M_{i\epsilon j}$ and $M_{i\sigma_+ j}$. C_{ijk} with $j = \epsilon$ or σ_+ is nonzero if both $D_{\Delta_i\Delta_j\Delta_k}$ and $D_{\bar{\Delta}_i\bar{\Delta}_j\bar{\Delta}_k}$ are nonzero and the S_3 symmetry and (2.132) also allow a nonzero value. Then, the nonzero $M_{i\epsilon j}$ are

$$M_{I\epsilon\epsilon}, M_{\epsilon\epsilon I}, M_{X\epsilon\epsilon}, M_{\epsilon\epsilon X}, M_{X\epsilon Y}, M_{Y\epsilon X}, M_{\sigma_+\epsilon\sigma_+}, M_{\sigma_+\epsilon\Omega_+}, M_{\Omega_+\epsilon\sigma_+}, \tag{2.136}$$

for i and j in the even sector, and

$$M_{\sigma_-\epsilon\sigma_-}, M_{\sigma_-\epsilon\Omega_-}, M_{\Omega_-\epsilon\sigma_-}, M_{J\epsilon\bar{J}}, M_{\bar{J}\epsilon J}, M_{J\epsilon W}, M_{W\epsilon J}, M_{\bar{J}\epsilon\bar{W}}, M_{\bar{W}\epsilon\bar{J}}, \tag{2.137}$$

for i and j in the odd sector. The nonzero $M_{i\sigma_+ j}$ are

$$\begin{aligned} M_{I\sigma_+\sigma_+}, M_{\epsilon\sigma_+\sigma_+}, M_{\epsilon\sigma_+\Omega_+}, M_{X\sigma_+\sigma_+}, M_{X\sigma_+\Omega_+}, \\ M_{Y\sigma_+\sigma_+}, M_{\sigma_+\sigma_+ I}, M_{\sigma_+\sigma_+\epsilon}, M_{\Omega_+\sigma_+\epsilon}, M_{\sigma_+\sigma_+ X}, \\ M_{\Omega_+\sigma_+ X}, M_{\sigma_+\sigma_+ Y}, M_{\sigma_+\sigma_+\sigma_+}, M_{\Omega_+\sigma_+\sigma_+}, M_{\sigma_+\sigma_+\Omega_+}, \end{aligned} \tag{2.138}$$

for i and j in the even sector, and

$$\begin{aligned} M_{\bar{J}\sigma_+\sigma_-}, M_{\bar{J}\sigma_+\Omega_-}, M_{J\sigma_+\sigma_-}, M_{J\sigma_+\Omega_-}, \\ M_{W\sigma_+\sigma_-}, M_{\bar{W}\sigma_+\sigma_-}, M_{\sigma_-\sigma_+\bar{J}}, M_{\Omega_-\sigma_+\bar{J}}, M_{\sigma_-\sigma_+ J}, \\ M_{\Omega_-\sigma_+ J}, M_{\sigma_-\sigma_+ W}, M_{\sigma_-\sigma_+\bar{W}}, M_{\sigma_-\sigma_+\Omega_-}, M_{\Omega_-\sigma_+\sigma_-}, \end{aligned} \tag{2.139}$$

for i and j in the odd sector.

The signs of the constants listed in (2.136), (2.137), (2.138) and (2.139) are partially determined by the S_3 symmetry and by (2.132). The constants (2.136) and (2.138) are equal to 1 because the even sector coincides with a sector of the A_5 model.

In order to find the signs of the constants (2.137) and (2.139) for the odd sector we used the empirical criterion that physically meaningful spectra should be obtained if the D_4 conformal theory is perturbed by the ϵ and σ_+ fields. The TCSA calculations allow one to fix the signs of all constants (2.137) and (2.139) up to a trivial freedom that corresponds to sign changes of the basis vectors. Within one of these equivalent choices the result we obtained is that the constants (2.137) are equal to 1; the constants (2.139) are equal to -1, with the following exceptions:

$$M_{\Omega_-\sigma_+\bar{J}} = M_{\Omega_-\sigma_+ J} = M_{\bar{J}\sigma_+\Omega_-} = M_{J\sigma_+\Omega_-} = 1\,. \tag{2.140}$$

Chapter 3

QFT SIMULATION WITH ULTRACOLD ATOMS

In this Chapter we discuss how to simulate relativistic systems by ultracold atoms in optical lattices. We present in Section 1 a short review of the basic features of graphene, we then move in Section 2 to our proposal for the simulation of (3+1) interacting Dirac fermions. The Chapter ends with an overview on the possible developments, presently subject of investigation.

3.1 The 2D cornerstone: graphene

The energy spectrum of graphene was studied long ago in [84] where the low-energy excitations were shown to obey to a Dirac equation. This idea of simulating field theories by condensed matter systems and in particular graphene was put forward again after some decades in [85] and it is one of the reasons for the huge interest of this material. Indeed a lot of peculiar properties, like transport or proximity effects [95], can be explained as a result of the dynamics of its Dirac-like infrared excitations.
In the following we will give a short introduction to the physics of graphene, discussing some basic facts that will be generalized in section (3.2). The material exposed in this section is elaborated from [95].

3.1.1 Tight-binding approach

Graphene is made out of carbon atoms arranged in hexagonal structure as shown in Fig. 3.1. The structure is not a Bravais lattice but can be seen as a triangular lattice with a basis of two atoms per unit cell. The lattice vectors can be written as:

$$\mathbf{a_1} = \frac{a}{2}(3, \sqrt{3})\,, \qquad \mathbf{a_2} = \frac{a}{2}(3, -\sqrt{3})\,, \tag{3.1}$$

where $a \approx 1.42$ Å is the carbon-carbon distance. The reciprocal lattice vectors are given by:

$$\mathbf{b_1} = \frac{2\pi}{3a}(1, \sqrt{3})\,, \qquad \mathbf{b_2} = \frac{2\pi}{3a}(1, -\sqrt{3})\,. \tag{3.2}$$

Of particular importance for the physics of graphene are the two points K and K' at the corners of the graphene Brillouin zone (BZ). These are named Dirac points for reasons that will become clear later. Their positions in momentum space are given by:

$$\mathbf{K} = \left(\frac{2\pi}{3a}, \frac{2\pi}{3\sqrt{3}a}\right), \qquad \mathbf{K}' = \left(\frac{2\pi}{3a}, -\frac{2\pi}{3\sqrt{3}a}\right). \tag{3.3}$$

The three nearest neighbors vectors in real space are given by:

$$\delta_{\mathbf{1}} = \frac{a}{2}(1, \sqrt{3}) \qquad \delta_{\mathbf{2}} = \frac{a}{2}(1, -\sqrt{3}) \qquad \delta_{\mathbf{3}} = -a(1, 0) \tag{3.4}$$

while the six second-nearest neighbors are located at: $\delta_1' = \pm\mathbf{a}_1, \delta_2' = \pm\mathbf{a}_2, \delta_3' = \pm(\mathbf{a}_2 - \mathbf{a}_1)$. The tight-binding Hamiltonian for electrons in graphene considering that electrons can hop both to nearest and next nearest neighbor atoms has the form (we use units such that $\hbar = 1$):

$$\begin{aligned} H = & - t \sum_{\langle i,j\rangle,\sigma} \left(a^\dagger_{\sigma,i} b_{\sigma,j} + \text{h.c.}\right) \\ & - t' \sum_{\langle\langle i,j\rangle\rangle,\sigma} \left(a^\dagger_{\sigma,i} a_{\sigma,j} + b^\dagger_{\sigma,i} b_{\sigma,j} + \text{h.c.}\right), \end{aligned} \tag{3.5}$$

where $a_{i,\sigma}$ ($a^\dagger_{i,\sigma}$) annihilates (creates) an electron with spin σ ($\sigma = \uparrow, \downarrow$) on site $\mathbf{R}_i$ on sublattice A (an equivalent definition is used for sublattice B), t (≈ 2.8 eV) is the nearest neighbor hopping energy (hopping between different sublattices), t' [1]is the next nearest neighbor hopping energy (hopping in the same sublattice). The energy bands derived from this Hamiltonian have the form [84] [85]:

$$\begin{aligned} E_\pm(\mathbf{k}) &= \pm t\sqrt{3 + f(\mathbf{k})} - t' f(\mathbf{k}), \\ f(\mathbf{k}) &= 2\cos\left(\sqrt{3}k_y a\right) + 4\cos\left(\frac{\sqrt{3}}{2}k_y a\right)\cos\left(\frac{3}{2}k_x a\right), \end{aligned} \tag{3.6}$$

where the plus sign applies to the upper (π) and the minus sign the lower (π^*) band. It is clear from (3.6) that the spectrum is symmetric around zero energy if $t' = 0$. For finite values of t' the electron-hole symmetry is broken and the π and π^* bands become asymmetric. In Fig. 3.2 we show the full band structure of graphene with both t and t'. In the same figure we also show a zoom in of the band structure close to one of the Dirac points (at the K or K' point in the BZ). This dispersion can be obtained by expanding the full band structure, eq.(3.6), close to the $\mathbf{K}$ (or $\mathbf{K}'$) vector, eq.(3.3), as: $\mathbf{k} = \mathbf{K} + \mathbf{q}$, with $|\mathbf{q}| \ll |\mathbf{K}|$ [84]:

$$E_\pm(\mathbf{q}) \approx \pm v_F |\mathbf{q}| + \mathcal{O}((q/K)^2), \tag{3.7}$$

where $\mathbf{q}$ is the momentum measured relatively to the Dirac points and v_F represents the Fermi velocity, given by $v_F = 3ta/2$, with a value $v_F \simeq 1 \times 10^6$ m/s. This result was first obtained by Wallace [84].

[1]The value of t' is not well known but *ab initio* calculations [86] find $0.02t \lesssim t' \lesssim 0.2t$ depending on the tight-binding parameterization. These calculations also include the effect of a third nearest neighbors hopping, which has a value of around 0.07 eV. A tight binding fit to cyclotron resonance experiments [87] finds $t' \approx 0.1$ eV.

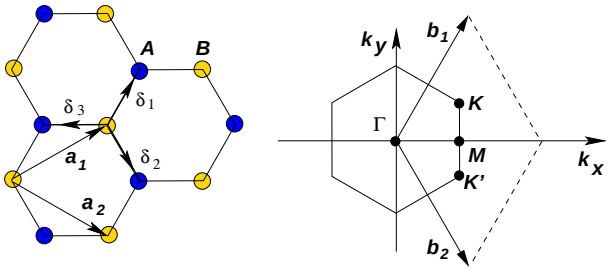

Figure 3.1: Left: Lattice structure of graphene, made out of two interpenetrating triangular lattices ($\mathbf{a}_1$ and $\mathbf{a}_2$ are the lattice unit vectors, and δ_i, $i = 1, 2, 3$ are the nearest neighbor vectors); Right: corresponding Brillouin zone. The Dirac cones are located at the K and K' points. Taken from [95] .

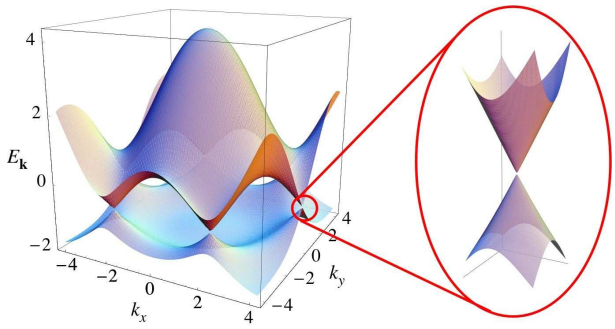

Figure 3.2: Left: Energy spectrum (in units of t) for finite values of t and t', with t =2.7 eV and $t' = 0.2t$. Right: zoom-in of the energy bands close to one of the Dirac points. Taken from [95].

The most striking difference between this result and the usual case, $\epsilon(\mathbf{q}) = q^2/(2m)$ where m is the electron mass, is that the Fermi velocity in (3.7) does not depend on the energy or momentum: in the usual case we have $v = k/m = \sqrt{2E/m}$ and hence the velocity changes substantially with energy. The expansion of the spectrum around the Dirac point including t' up to second order in q/K is given by:

$$E_{\pm}(\mathbf{q}) \simeq 3t' \pm v_F|\mathbf{q}| - \left(\frac{9t'a^2}{4} \pm \frac{3ta^2}{8}\sin(3\theta_{\mathbf{q}})\right)|\mathbf{q}|^2\,, \tag{3.8}$$

where

$$\theta_{\mathbf{q}} = \arctan\left(\frac{q_x}{q_y}\right)\,, \tag{3.9}$$

is the angle in momentum space. Hence, the presence of t' shifts in energy the position of the Dirac point and breaks electron-hole symmetry. Notice that up to order $(q/K)^2$ the dispersion does not depend on the direction in momentum space and has a three fold symmetry.

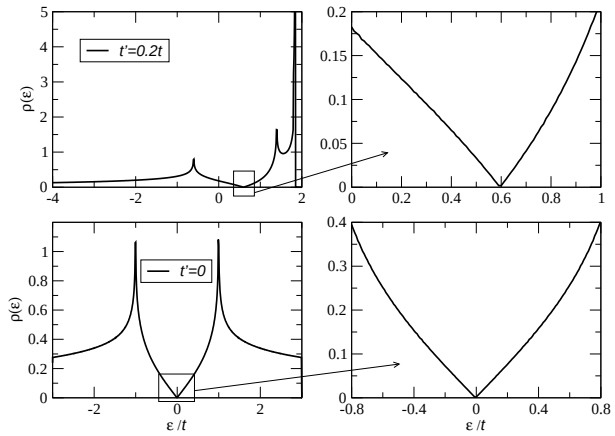

Figure 3.3: Density of states per unit cell as a function of energy (in units of t) computed from the energy dispersion (3.6), $t' = 0.2t$ (top) and for $t' = 0$ (bottom). Also shown is a zoom in of the density of states close to the neutrality point of one electron per site. For the case $t' = 0$ the density of states close to the neutrality point can be approximated by $\rho(\epsilon) \propto |\epsilon|$. Taken from [95].

3.1.2 Density of states

The density of states per unit cell, derived from (3.6), is given in Fig. 3.3 for both $t' = 0$ and $t' \neq 0$, showing in both cases a semi-metallic behavior [84],[88]. For $t' = 0$ it is possible to derive an analytical expression for the density of states per unit cell as a function of the energy [89]. Close to the Dirac point the dispersion is approximated by (3.7) and the expression for the density of states per unit cell is given by (with a degeneracy of 4 included):

$$\rho(E) = \frac{2A_c}{\pi}\frac{|E|}{v_F^2} \tag{3.10}$$

where A_c is the unit cell area given by $A_c = 3\sqrt{3}a^2/2$.

3.1.3 Dirac fermions

Let us consider Hamiltonian (3.5) with $t' = 0$ and consider the Fourier transform of the electron operators:

$$a_n = \frac{1}{\sqrt{N_c}}\sum_{\mathbf{k}} e^{-i\mathbf{k}\cdot\mathbf{R}_n} a(\mathbf{k}), \tag{3.11}$$

where N_c is the number of unit cells. Using this transformation, let us write the field a_n as a sum of two terms, coming from expanding the Fourier sum around $\mathbf{K'}$ and $\mathbf{K}$. This produces an approximation for the representation of the field a_n as a sum of two new fields, written as

$$\begin{aligned} a_n &\simeq e^{-i\mathbf{K}\cdot\mathbf{R}_n} a_{1,n} + e^{-i\mathbf{K'}\cdot\mathbf{R}_n} a_{2,n}\,, \\ b_n &\simeq e^{-i\mathbf{K}\cdot\mathbf{R}_n} b_{1,n} + e^{-i\mathbf{K'}\cdot\mathbf{R}_n} b_{2,n}\,, \end{aligned} \tag{3.12}$$

where the index $i = 1$ ($i = 2$) refers to the K (K') point. These new fields, $a_{i,n}$ and $b_{i,n}$ are assumed to vary slowly over the unit cell. The procedure for deriving a theory that is valid close to the Dirac point consists in using this representation in the tight-binding Hamiltonian and expanding the operators up to a linear order in δ. In the derivation one uses the fact that $\sum_\delta e^{\pm i\mathbf{K}\cdot\delta} = \sum_\delta e^{\pm i\mathbf{K}'\cdot\delta} = 0$. After some straightforward algebra we arrive at [85]:

$$H = -iv_F \int dxdy \left(\hat{\Psi}_1^\dagger(\mathbf{r})\sigma \cdot \nabla \hat{\Psi}_1(\mathbf{r}) + \hat{\Psi}_2^\dagger(\mathbf{r})\sigma^* \cdot \nabla \hat{\Psi}_2(\mathbf{r}) \right) , \tag{3.13}$$

with Pauli matrices $\sigma = (\sigma_x, \sigma_y)$, $\sigma^* = (\sigma_x, -\sigma_y)$, and $\hat{\Psi}_i^\dagger = (a_i^\dagger, b_i^\dagger)$ ($i = 1, 2$). It is clear that the effective Hamiltonian (3.13) is made of two copies of the massless Dirac-like Hamiltonian, one holding for $\mathbf{p}$ around $\mathbf{K}$ and other for $\mathbf{p}$ around $\mathbf{K}'$. Notice that, in first quantized language, the two-component electron wavefunction, $\psi(\mathbf{r})$, close to the K point, obeys the 2D Dirac equation:

$$-iv_F\sigma \cdot \nabla\psi(\mathbf{r}) = E\psi(\mathbf{r}) . \tag{3.14}$$

In momentum space, the wavefunction for the momentum around $\mathbf{K}$ has the form:

$$\psi_{\pm,\mathbf{K}}(\mathbf{k}) = \frac{1}{\sqrt{2}} \begin{pmatrix} e^{-i\theta_\mathbf{k}/2} \\ \pm e^{i\theta_\mathbf{k}/2} \end{pmatrix} , \tag{3.15}$$

for $H_K = v_F\sigma \cdot \mathbf{k}$, where the $\pm$ signs correspond to the eigenenergies $E = \pm v_F k$, that is, for the π and π^* band, respectively, and $\theta_\mathbf{k}$ is given by (3.9). The wavefunction for the momentum around $\mathbf{K}'$ has the form:

$$\psi_{\pm,\mathbf{K}'}(\mathbf{k}) = \frac{1}{\sqrt{2}} \begin{pmatrix} e^{i\theta_\mathbf{k}/2} \\ \pm e^{-i\theta_\mathbf{k}/2} \end{pmatrix} , \tag{3.16}$$

for $H_{K'} = v_F\sigma^* \cdot \mathbf{k}$. Notice that the wavefunctions at $\mathbf{K}$ and $\mathbf{K}'$ are related by time reversal symmetry: if we set the origin of coordinates in momentum space in the M-point of the BZ (see Fig.3.1), time reversal becomes equivalent to a reflection along the k_x axis, that is, $(k_x, k_y) \to (k_x, -k_y)$. Also note that if the phase θ is rotated by 2π the wavefunction changes sign indicating a phase of π (in the literature this is commonly called a Berry phase). This change of phase by π under rotation is characteristic of spinors. In fact, the wavefunction is a two component spinor.

A relevant quantity used to characterize the eigenfunctions is their helicity defined as the projection of the momentum operator along the (pseudo)spin direction. The quantum mechanical operator for the helicity has the form:

$$\hat{h} = \frac{1}{2}\sigma \cdot \frac{\mathbf{p}}{|\mathbf{p}|} . \tag{3.17}$$

It is clear from the definition of $\hat{h}$ that the states $\psi_\mathbf{K}(\mathbf{r})$ and $\psi_{\mathbf{K}'}(\mathbf{r})$ are also eigenstates of $\hat{h}$:

$$\hat{h}\,\psi_\mathbf{K}(\mathbf{r}) = \pm\frac{1}{2}\psi_\mathbf{K}(\mathbf{r}), \tag{3.18}$$

and an equivalent equation for $\psi_{\mathbf{K}'}(\mathbf{r})$ with inverted sign. Therefore electrons (holes) have a positive (negative) helicity. Equation (3.18) implies that σ has its two eigenvalues either in the direction of

($\Uparrow$) or against ($\Downarrow$) the momentum $\mathbf{p}$. This property says that the states of the system close to the Dirac point have well defined *chirality* or helicity. Notice that chirality is not defined in regards to the real spin of the electron (that has not yet appeared in the problem) but to a pseudo-spin variable associated with the two components of the wavefunction. The helicity values are good quantum numbers as long as the Hamiltonian (3.13) is valid. Therefore the existence of helicity quantum numbers holds only as an asymptotic property, which is well defined close to the Dirac points $\mathbf{K}$ and $\mathbf{K}'$. Either at larger energies or due to the presence of a finite t' the helicity stops being a good quantum number.

3.2 (3 + 1) Massive Dirac Fermions by Ultracold Atoms

Based on the paper:
L. Lepori, G. Mussardo and A. Trombettoni,
"(3+1) Massive Dirac Fermions by Ultracold Atoms in Optical Lattices",
arXiv:1004.4744 [hep-th].

3.2.1 Introduction

For their high level of control, trapped ultracold atoms are ideal systems for simulating in a tunable way strongly interacting models [90]. A well-known example is the experimental realization of interacting lattice Hamiltonians: for bosonic gases, the Mott-superfluid transitions has been both detected [91] and investigated in a variety of interesting situations, including low dimensional and disordered set-ups [90]; for fermionic gases, the recent studies [92, 93] of metallic and insulating phases of a two-species mixture in a $3D$ optical lattice have opened the way to experimentally investigating the rich phase diagram of the Fermi-Hubbard model.

The examples mentioned above refer to the ability of cold atom systems to simulate non-relativistic Hamiltonians but a fascinating new challenge is the tunable experimental realization of relativistic systems which are relevant to high energy physics and quantum gauge theories [94]. It is worth mentioning, for instance, the simulation of the properties of graphene [95], i.e. $(2 + 1)$ relativistic Dirac fermions, obtained by using ultracold fermions in honeycomb lattices [96, 97, 98, 99]. Other recent proposals to realize massless $(2 + 1)$ Dirac fermions consist of ultracold fermions on a square lattice coupled with properly chosen Rabi fields [100], interacting bosons in a two-dimensional lattice in a bichromatic light-shift potential which produces an effective staggered magnetic field [101] and bosons with internal energy levels in a tripod configuration [102].

It is then highly interesting to see whether it is possible to go beyond the (2+1) case and simulate relativistic $(3 + 1)$ Dirac fermions. We are concerned, in particular, with the possibility to make them massive and also interacting, possibly in a Lorentz invariant way. Mixtures of two ultracold fermionic species (and recently of three species [103, 104]) may also be useful for the experimental realization of Dirac fermions with internal degrees of freedom. New developments in this direction could open the way to simulate, by cold atom systems, Kogut-Susskind staggered lattice fermions [105, 106] or more general elementary particle theories. In perspective, this development could permit to study in a controllable experimental set-up part of the phase diagram of QCD [107].

A method of simulating the Dirac equation in $(3 + 1)$ dimensions for a free spin-1/2 particle in a single trapped ion was presented in [108], where the transition from massless to massive fermions was also studied. This method has been recently experimentally implemented in [109] where the $(1 + 1)$ Dirac equation has been simulated: the Zitterbewegung for different initial superpositions of positive- and negative- energy spinor states, as well as the crossover from relativistic to non-relativistic dynamics, have been studied [109].

The aim of this Chapter is to discuss an experimental scheme to realize $(3 + 1)$ massive Dirac fermions (with a mass eventually time-dependent) using ultracold atomic fermions, a set-up which makes possible to control interactions through Feshbach resonances [90] and to realize mixtures of different internal states: this would allow for the simulation of relativistic *interacting* field theories.

Here we propose to use non-relativistic polarized ultracold fermions in a rotating cubic optical lattice with tight-binding Hamiltonian

$$H = -t \sum_{\langle i,j \rangle} \left(c_i^\dagger e^{-iA_{ij}} c_j + h.c. \right) , \tag{3.19}$$

where $c_i^\dagger$ creates an atom in the i-th well of the lattice, t is the tunneling parameter (assumed for the moment equal along the three axes x, y and z) and the sum is on nearest-neighbours wells. The lattice (created with three counter-propagating laser beams) is assumed to be rotating with angular velocity $\vec{\omega}$ so that the electrically neutral atoms feel an effective magnetic field: with the minimal substitution $-i\hbar\vec{\nabla} \to -i\hbar\vec{\nabla} - m\vec{A}$ (where m is the mass of the atoms and $\vec{A} = \vec{\omega} \times \vec{r}$ is the analog of the magnetic vector potential) we have the Hamiltonian (3.19), with $A_{ij} = (m/\hbar) \int_i^j \vec{A} \cdot d\vec{l}$. We will discuss in detail the origin of the fictitious magnetic fiend in the next paragraph.

Rotating lattices have been efficiently realized quite recently employing four intersecting laser beams manipulated with acousto-optical deflectors [111]). Alternatively, one could also end up in the Hamiltonian (3.19) using, on a cubic lattice, fermions subjected to a synthetic magnetic field obtained by spatially dependent optical coupling between internal states of the atoms [112].

Before studying the spectrum of the Hamiltonian (3.19), let's briefly comment on the reason of its choice: one may wonder, in fact, if a simpler Hamiltonian – without a magnetic field – of the form $H = -t \sum_{i,j} c_i^\dagger B_{ij} c_j$ ($B_{ij} = 1$ if i and j are nearest-neighbours and 0 otherwise) is able to simulate $(3+1)$ Dirac fermions. This is equivalent to ask whether it is possible to realize, with a suitable choice of B_{ij}, a semi-metal such that the bands touch at *isolated* points. In [115] the symmetries groups which lead to a spectrum without Fermi surface and energy gap were classified: although this result can be used to exclude certain classes of B's matrices, it does not help however to identify the tight-binding Hamiltonians which could have the desired spectral properties. By direct inspection, we checked that the $3D$ Bravais lattices with a single atom per cell and only nearest-neighbour hoppings does not give band touching in isolated points at zero energy. It is for this reason that we focus our attention on the realization of Dirac fermions using an artificial uniform magnetic field.

3.2.2 Experimental set-up

Since the atoms of the lattice are electrically neutral, a magnetic field cannot be imposed directly on the system but its effect must be simulated artificially. This can be accomplished either by spatially dependent optical coupling between internal states (see for instance [112, 113, 114]) or by giving a rotation to the lattice, in presence of a parabolic trapping [110, 111]. The first technique has the advantage to be less sensitive to the imperfection of the trapping potential and thus easier to implement; moreover, relying on assisted hoppings, it allows to avoid secondary effects from not nearest-neighbour transitions. Anyway, it has the drawback to require many lasers and to exploit couplings with the hyperfine levels structure. Since for our purposes we would desire to keep the internal states free (as they can be used as "colours"), we will focalize below on the second technique.

We suppose to have a rotating optical lattice with angular velocity $\vec{\omega}$ and we call S the inertial system in which the lattice rotates and S' the accelerated one referring to a certain rotating point

P. A particle in P with mass m and velocity $\vec{v}$ in S' undergoes an apparent force

$$\vec{F}_{\rm TOT} = -2m\,(\vec{\omega}\times\vec{v}) - m\,(\vec{\omega}\times\vec{\omega}\times\vec{r})\,, \tag{3.20}$$

where $\vec{r}$ is distance between P and the center of the rotation.
If we cancel the second term by imposing a confining parabolic potential $\frac{1}{2}m|\vec{\Omega}|^2|\vec{r}|^2$, with $\vec{\Omega}=\vec{\omega}$, we obtain a fictitious "Lorentz force"

$$\vec{F}_{\rm TOT} = 2m\,(\vec{v}\times\vec{\omega}) \tag{3.21}$$

experienced by an atom in P and due to a fictitious magnetic field $\vec{B} = \frac{2m\vec{\omega}}{q}$ (q is an effective charge of the atoms). The vector potential turns out to be $\vec{A} = \frac{1}{2}\,\vec{B}\times\vec{r}$, then this force can be put in relation with the hamiltonian (in S')

$$H = \frac{1}{2m}(\vec{p} - m\,\vec{\omega}\times\vec{r})^2\,. \tag{3.22}$$

This scheme continues to hold at the quantum level, then (3.22) can be taken as the quantum hamiltonian describing in S' the rotating lattice (with the parabolic trapping).
In order to obtain a dispersion law (3.28), it's required on each plaquette a flux $\frac{\Phi_0}{2}$, where $\Phi_0 = \frac{h}{q}$ is the elementary flux. This condition is fulfilled for

$$\vec{\omega} = \frac{h}{4ma^2}(1,1,1)\,, \tag{3.23}$$

where a is the lattice spacing. For a realistic lattice size $a \approx 2\,\mu m$ and K atoms we obtain a rotation frequency $\nu \equiv |\vec{\omega}|/2\pi \sim 200Hz$. From now on we set $\Phi_0 = 1$ and $a = 1$.

3.2.3 Energy spectrum and Dirac points

The magnetic field $\vec{B} = \pi(1,1,1)$ induces a π-flux on every square face (see the schematic plot in fig. 3.4). In oder to diagonalize the Hamiltonian (3.19) is mostly convenient to use the gauge

$$\vec{A} = \pi(0, x-y, y-x)\,, \tag{3.24}$$

similarly to [116]. The quasimomenta $\vec{k}$ take the values in the magnetic Brillouin zone [118], given by [1] $-\pi/2 < k_{x,y} < \pi/2$, $-\pi < k_z < \pi$. The other two choices with interchanged (k_x, k_y, k_z) are equivalent, giving the same energy levels [118].
Notice that two sides of the zone have half of the length of the normal Brillouin zone. This because, in presence of a magnetic flux

$$\Phi = 2\,\pi\frac{p}{n}\,\Phi_0 \tag{3.25}$$

(Φ_0 is the elementary flux) per elementary plaquette, the translations $\tilde{T}_i$ sin different directions do not commute any longer [118]:

$$\tilde{T}_i\tilde{T}_j = e^{i2\pi\frac{p}{n}}\,\tilde{T}_i\tilde{T}_j\,. \tag{3.26}$$

[1] $k_{a=(x,y,z)}$ refers to the eigenvalues of the generalized *magnetic momentum* $\hat{P} = \hat{p} - q\vec{A}(\vec{x})$. The translation operators $\tilde{T}_a$ are related to $\hat{P}_a$ as $\tilde{T}_a = e^{i\theta_a\hat{P}_a}$.

In our case $p = 1$, $n = 2$ and a complete set of commuting translations is obtained by doubling two translations, for instance $\tilde{T'}_x = 2\tilde{T}_x$ and $\tilde{T'}_y = 2\tilde{T}_y$. Correspondingly, the side of the reciprocal lattice is divided by two in each direction.
Since the choice (3.24) divides the lattice sites in two inequivalent sets [2], say A and B (see fig. 3.4), we can write the Fourier transforms as $c_\Gamma(\vec{k}) = \sum_{j\in\Gamma} c_j e^{i\vec{k}\cdot\vec{j}}$ (where $\Gamma = A, B$); plugging in eq. (3.19), we get a two by two hamiltonian matrix:

$$-\begin{pmatrix} 2t\, cosk_z & 2t\, e^{-i\frac{\pi}{2}} cosk_y + 2t\, cosk_x \\ 2t\, e^{i\frac{\pi}{2}} cosk_y + 2t\, cosk_x & 2t\, cos(k_z + \pi) \end{pmatrix} . \tag{3.27}$$

In obtaining this matrix we neglected the contribute of the excited levels in any single valley (excited Wannier functions): this is true with low filling (like half filling here), at low temperature and with valley depth V_0, such deep that in each valley the distance between the ground state level and the excited ones is large in comparison with the thermal fluctuations.
Diagonalizing (3.27) we obtain the following spectrum [116, 119]:

$$E(\vec{k}) = \pm 2\, t \sqrt{cos^2 k_x + cos^2 k_y + cos^2 k_z}\, . \tag{3.28}$$

An energy spectrum like eq.(3.28) was obtained for $PbTe$-type narrow-gap semiconductors with antiphase boundaries [120]; a model having this spectrum has been recently used in [121], where it was shown that a suitable distortion of tunneling couplings in fermionic lattices can introduce a scalar and a Yang-Mills field.

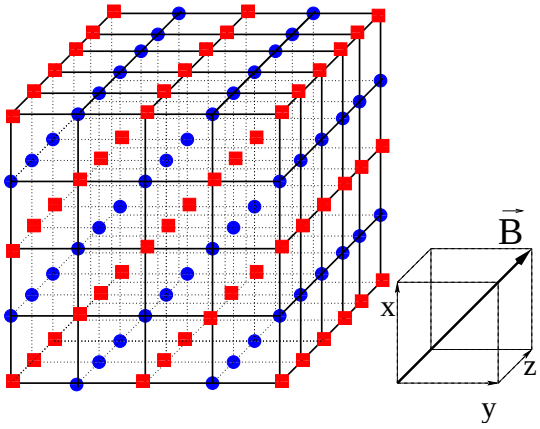

Figure 3.4: Sets A (red squares) and B (blue circles) on the cubic lattice (right: artificial magnetic field $\vec{B}$).

For half-filling the Fermi energy is zero and there is a vanishing gap between valence ($E < 0$) and conducting bands ($E > 0$) at the *isolated* Dirac points $\vec{k} = \pm\frac{\pi}{2}(\pm 1, \pm 1, \pm 1)$. A pair of inequivalent Dirac points is given by $\vec{k}_R = \frac{\pi}{2}(1, 1, 1)$ and $\vec{k}_L = -\frac{\pi}{2}(1, 1, 1)$. Expanding the energy around these Dirac points we have $E(\vec{k}_{L/R} + \vec{q})/\hbar \approx v_F|\vec{q}|$, where the Fermi velocity is given by $v_F = 2ta/\hbar$.

[2] Every site of a subset has particular hoppings on the links starting from it.

Close to these zero-gap points, the quasiparticles behave as massless $(3+1)$ Dirac fermions of both the chiralities and the linearized form of the Hamiltonian (3.19) becomes, in the continuum limit, the $3D$ Dirac Hamiltonian

$$H = \int d^3\vec{k} \left(\psi(\vec{k})^\dagger_R \, \vec{\sigma} \cdot \vec{k} \, \psi(\vec{k})_R - \psi(\vec{k})^\dagger_L \, \vec{\sigma} \cdot \vec{k} \, \psi(\vec{k})_L \right), \tag{3.29}$$

where $\vec{\sigma} = (\sigma_x, \sigma_y, \sigma_z)$ are the Pauli matrices and the two-components spinors $\psi_L(\vec{k})$, $\psi_R(\vec{k})$ are respectively

$$\psi_R(\vec{k}) = \begin{pmatrix} c_A(\vec{k} + \vec{k}_R) \\ c_B(\vec{k} + \vec{k}_R) \end{pmatrix}; \; \psi_L(\vec{k}) = \begin{pmatrix} c_A(\vec{k} + \vec{k}_L) \\ c_B(\vec{k} + \vec{k}_L) \end{pmatrix}. \tag{3.30}$$

In ordinary space the expression (3.30) becomes:

$$H = -2it \int d\vec{r} \left(\psi^\dagger_R \vec{\sigma} \cdot \vec{\nabla} \psi_R - \psi^\dagger_L \vec{\sigma} \cdot \vec{\nabla} \psi_L \right), \tag{3.31}$$

the usual Dirac hamiltonian in the chiral basis.
The appearance of fermions of having both the chiralities is expected, according to the well known no-go theorem [122] which states the impossibility to simulate chiral local theories on a lattice.
In experimental realizations, the magnetic field $\vec{B} = \pi(1,1,1)$ may be subjected to some fluctuations which change the magnetic flux per placquette, $2\pi\Phi$, around the value $\Phi = 1/2$. In the thermodynamical limit $L \to \infty$, where $N = L^3$ is the number of sites of the cubic lattice, these fluctuations are expected to influence the Dirac cones because, when the flux on a placquette is different from a rational number p/q, the usual Bloch functions are no longer a faithful representation of the translation group and therefore the energy spectrum assumes a fractal structure [123, 124, 125]. Note, however, that for finite L, the spectrum is not sensibly affected by fluctuations of Φ which are much smaller than $1/L$ [3]. To clarify this point, consider two close rational values of the flux, say $\frac{1}{2}$ and $\frac{51}{100}$: in the second case one has $q = 100$ sub-bands, while there are only $q = 2$ in the first case. However, if $L \ll 1/\delta\Phi$, the q sub-bands are gathered in two groups, each of them almost degenerate and the two cases are practically indistinguishable. This conclusion can be explicitly checked by numerically diagonalizing the Hamiltonian (3.19): e.g., even for a rather small size ($L = 16$) with open boundary conditions and a fairly large value of $\delta\Phi$ ($\sim 5\%$ of $\Phi = 1/2$), the spectral density is not sensibly affected and it is in reasonable agreement with the one computed from eq. (3.28). This situation is described in figure (3.5).

Many species In the discussion above one can consider two (or eventually more) fermionic species: they can be either different hyperfine levels of the same fermionic species or different species of a mixture (e.g., a Li-K mixture). Experiments with collisionally stable mixtures of two [90] and also three [103, 104]) fermionic species has been recently reported. The low-energy Hamiltonian will be then simply the sum of free Hamiltonians of the type (3.31).

[3] It's easy to show that for $(\Phi \cdot L) \to 0$ with a certain power k, the eigenvalues of the perturbed (by a magnetic fluctuations around π) tight-binding hamiltonian tend to the eigenvalues of the unperturbed hamiltonian *at least* as fast as $(\Phi \cdot L)^k$.

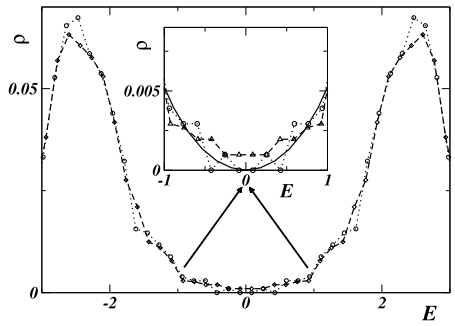

Figure 3.5: Density of states (normalized to unity) vs. E (in units of t) for $L = 16$ and open boundary conditions computed in 40 intervals for $\Phi = \frac{1}{2}$ (circles) and $\Phi + \delta\Phi$, with $\delta\Phi/\Phi = 0.06$ (triangles). Dotted (dashed) lines among circles (triangles) are just a guide for eyes. The inset shows a zoom of the main figure, with the solid line obtained from (3.28).

Asymmetric and secondary hoppings So far we have considered equal hopping parameters along the x, y and $z-$axes but, since the tunneling rates depend on the power of the lasers, one can easily generalize further the model by realizing different hopping parameters t_x, t_y, t_z. The energy spectrum in this case is

$$E(\vec{k}) = \pm 2\sqrt{t_x^2\, cos^2 k_x + t_y^2\, cos^2 k_y + t_z^2\, cos^2 k_z}\ : \tag{3.32}$$

the isolated Dirac points are therefore unaffected by the anisotropy of the hopping parameters.

The energy spectrum can be also derived including next-nearest-neighbour hopping rates; in this case it turns out to be [117]:

$$\begin{aligned} E(\vec{k}) = \pm 2[(2t_x cosk_x - 2t'_{yz} sink_y sink_z)^2 + \\ (2t_y cosk_y - 2t'_{zx} sink_z sink_x)^2 + (2t_z cosk_z - 2t'_{xy} sink_x sink_y)^2]^{\frac{1}{2}}\ . \end{aligned} \tag{3.33}$$

We assumed for simplicity the realistic case of isotropy of the hoppings. A rapid analysis of (3.33) shows that for every values of $c = \frac{t'}{t}$ two zero-energy points are present with varying positions ($|k^{R/L}_{x,y,z}| \to 0$ as c goes from 0 to ∞); of course in the real experiments we will have $0 < c < 1$. However, the terms in $(\sin k_i \sin k_j)$ suggest a quadratic contribution to the dispersion close to the Fermi points

$$E(\vec{p}) = a(t)|\vec{p}| + b(t')|\vec{p}|^2 + O(|\vec{p}|^2) \tag{3.34}$$

and then a spoiling of the fermion spectrum. Because of this reason, in order that the low-energy dynamics to be still well described by Dirac fermions, we need to require the condition $c << 1$, so that $b(t') << a(t)$. These unwanted effects from minor hoppings are known to occur also in graphene [95], we indeed expect them onto every geometry. Anyway, as stressed in [**?**], the can be highly limited by using assisted hopping techniques [114, 130]

3.2.4 Spinor field operators

The spinors operators can be written *in terms of free energy-positive solutions* (indices $i = 1, 2$) *and negative energy solutions* (indices $i = 3, 4$) of the Dirac equation, reading [140]:

$$\begin{aligned}\psi(x) = \int \tfrac{\mathrm{d}^3\vec{p}}{(2\pi)^3}\tfrac{1}{\sqrt{2E_{\vec{p}}}}\left(\textstyle\sum_{s=1,2} b^{(s)}_{\vec{p}}u^{(s)}(\vec{p})\,\mathrm{Exp}(-i(|E|t-\vec{p}\cdot\vec{x}))\right)+\\ +\int \tfrac{\mathrm{d}^3\vec{p}}{(2\pi)^3}\tfrac{1}{\sqrt{2E_{\vec{p}}}}\left(\textstyle\sum_{s=3,4} b^{(s)}_{\vec{p}}u^{(s)}(\vec{p})\,\mathrm{Exp}(i(|E|t-\vec{p}\cdot\vec{x}))\right),\end{aligned} \tag{3.35}$$

where the index s labels the different solutions (corresponding to different physical polarizations) of the Dirac equation. The version of the fields used nowadays in quantum field theory is recovered by posing [140]:

$$b^{(s)}_{-\vec{p}} = d^{(s)\,\dagger}_{\vec{p}} \qquad u^{(s)}_{-\vec{p}} = v^{(s)\,\dagger}_{\vec{p}} \qquad (s = 3, 4)\,. \tag{3.36}$$

Written as above, the field $\psi(x)$ creates every possible excitations, while $\psi^\dagger(x)$ annihilates them. In the *chiral* case we have:

$$\begin{aligned}\psi_L(x) = \int \tfrac{\mathrm{d}^3\vec{p}}{(2\pi)^3}\tfrac{1}{\sqrt{2E_{\vec{p}}}}\left(b^{(L)}_{\vec{p}}u^{(L)}(\vec{p})\,\mathrm{Exp}(-i(|E|t-\vec{p}\cdot\vec{x}))\right)+\\ +\int \tfrac{\mathrm{d}^3\vec{p}}{(2\pi)^3}\tfrac{1}{\sqrt{2E_{\vec{p}}}}\left(d^{(R)}_{\vec{p}}\tilde{u}^{(R)}(\vec{p})\,\mathrm{Exp}(i(|E|t-\vec{p}\cdot\vec{x}))\right),\end{aligned} \tag{3.37}$$

where $d^{(R)}_{\vec{p}}$ and $\tilde{u}^{(R)}(\vec{p})$ refer to negative-energy solutions. The expression for $\psi_R(x)$ has inverted chiralities.

This way to quantize the fermion fields is obviously preferable for the treatments of condensed matter phenomena involving particles and holes; moreover, having in mind interacting theories and/or superconductive states, it directly suggests to adopt a different form for the bilinears, not involving $\psi^\dagger(x)$. These bilinears are [142]

$$i\,\psi^t(x)\gamma_1\gamma_3 M\,\psi(x)\,, \tag{3.38}$$

where M denotes the usual set $(\mathbf{1}, \gamma_5, \gamma_\mu, \gamma_\mu\gamma_5, \sigma_{\mu\nu})$.

3.2.5 Obtaining a mass term and a disorder through a Bragg pulse

Let now expose the ultracold atomic gas to a Bragg pulse (see for example [126, 127]). For deep optical lattices, the Hamiltonian (3.19) acquires a new term of the form

$$H_B = V_0\left(\sum_j c^\dagger_j c_j\, e^{i\vec{k}_{Bragg}\cdot\vec{j}}e^{-i\omega t} + h.c.\right) \tag{3.39}$$

where the sum runs on the lattice sites while $\vec{k}_{Bragg}$ and ω are the differences between the wave-vectors and the frequencies of the used lasers. The Bragg term (3.39) gives rise to a mass of the Dirac fermions: choosing $\vec{k}_{Bragg} = \vec{k}_L - \vec{k}_R = (\pi, \pi, \pi)$, the quasiparticles around the Dirac point

$\vec{k}_L$ ($\vec{k}_R$) are transferred close to the Dirac point $\vec{k}_R$ ($\vec{k}_L$) inverting the chirality. This is possible because

$$\vec{k}_L + \vec{k}_{Bragg} = \vec{k}_R$$

(by definition) and also $\vec{k}_R + \vec{k}_{Bragg}$ is a wave-vector equivalent to $\vec{k}_L$, as illustrated in fig. 3.6: indeed $\vec{k}_R + \vec{k}_{Bragg} = \vec{k}_L + 2(\pi/2)(1,0,0) + 2(\pi/2)(0,1,0) + \pi(0,0,1)$. Notice that here one is exploiting the peculiar symmetry of the Brillouin zone: indeed, for instance, for the two inequivalent Dirac points $\vec{k}_1^{hon.}$ and $\vec{k}_2^{hon.}$ of an honeycomb lattice (used for the simulation of $(2+1)$ Dirac fermions [96]), a Bragg term with $\vec{k}_{Bragg} = \vec{k}_1^{hon.} - \vec{k}_2^{hon.}$ would not give a mass, since $\vec{k}_1^{hon.} + \vec{k}_{Bragg} = \vec{k}_2^{hon.}$ (by definition), but $\vec{k}_2^{hon.} + \vec{k}_{Bragg}$ is not equivalent to $\vec{k}_1^{hon.}$.

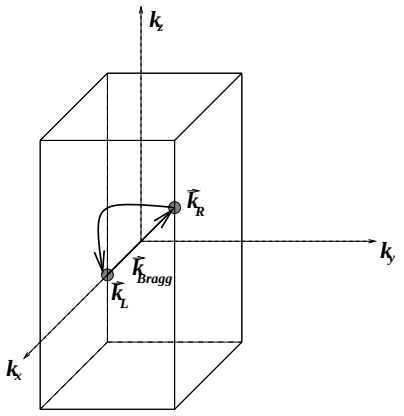

Figure 3.6: Dirac points $\vec{k}_R$ and $\vec{k}_L$ and magnetic Brillouin zone: the Bragg wave-vector $\vec{k}_{Bragg}$ is chosen to be $\vec{k}_{Bragg} = \vec{k}_L - \vec{k}_R$.

The Bragg pulse then results in adding a mass term to the Dirac Hamiltonian (3.31)

$$\frac{V_0}{2}\, cos(\omega t)(\psi_L^\dagger \psi_R \,+\, \psi_R^\dagger \psi_L) = \frac{V_0}{2}\, cos(\omega t)\, \bar{\psi}\psi\,, \tag{3.40}$$

where $\psi = \begin{pmatrix} \psi_R \\ \psi_L \end{pmatrix}$ and $\bar{\psi} = \psi^\dagger \begin{pmatrix} \mathbf{0} & \mathbf{1} \\ \mathbf{1} & \mathbf{0} \end{pmatrix}$ ($\mathbf{0}$ and $\mathbf{1}$ are the 2×2 zero and identity matrices) [4] Notice that above we exploited the periodicity of the magnetic dual lattice. When the frequency difference vanishes, $\omega = 0$, one has a time-independent Dirac mass while, keeping $\vec{k}_{Bragg}$ fixed, but changing randomly the intensity of the two lasers, one has also the interesting possibility to realize a Dirac fermion with random mass.

In presence of many species of hopping atoms on the lattice, the mass of different Dirac fermions obtained by Bragg pulses can be in principle different.

[4] The explicit time dependence does not spoil the Lorentz covariance: indeed a change of sign of the mass can always be reabsorbed in the definition of the fermion, by the transformations $\psi_R(\vec{r}) \to \psi_R(\vec{r})$, $\psi_L(\vec{r}) \to -\psi_L(\vec{r})$.

In this system one can also think to study the effect of randomness: for example one can let the coefficient V_0 to randomly varying whit time, yielding in this way a random mass. One could also in principle study the effect of a random noise $\vec{\eta}$ to the momentum $\vec{\Delta}$: $\vec{k}_{Bragg} = \vec{\Delta} + \vec{\eta}$.. Obviously $|\vec{\eta}|$ must be small enough not to push the quasiparticles out of the Dirac wells. These ingredients make the system suitable to study diffusion and possibly localization in the relativistic Dirac equation.

Electromagnetic coupling

The term (3.39) is actually a particular case of a more general situation: starting from the Hamiltonian $H = -t\sum_{\langle i,j\rangle} c_j^\dagger\, e^{-i(A_{ij}+\mathcal{A}_{ij})}c_i + \sum_j A_0(j)\, c_j^\dagger c_j$ and repeating almost unchanged the calculation that led to eq. (3.31), one gets (for simplicity with $t_x = t_y = t_z = t$) in the continuum limit the Dirac Hamiltonian in an e.m. field

$$H = \int d\vec{r}\, A_0 \left(\psi_R^\dagger(\vec{r})\psi_R(\vec{r}) + \psi_L^\dagger(\vec{r})\psi_L(\vec{r})\right) +$$

$$- 2it \int d\vec{r} \left(\psi_R^\dagger(\vec{r})\, \vec{\sigma}\cdot\vec{D}\,\psi_R(\vec{r}) - \psi_L^\dagger(\vec{r})\, \vec{\sigma}\cdot\vec{D}\,\psi_L(\vec{r})\right) , \tag{3.41}$$

where the perturbations $\mathcal{A}_{ij}$ and A_0 are intended to be slowly varying in space and time and $\vec{D} = \vec{\nabla} + \vec{\mathcal{A}}$.

3.2.6 The Berry phase in the relativistic regime

Since for $\omega \neq 0$ the mass in (3.40) varies cyclically, it's natural to wonder about the Berry phase obtained in a period by its wave function. In this Section we study some general aspects of the Berry phase in the relativistic regime.
We analyze in the following the evolution of the levels for the time depending hamiltonian given by the sum of the kinetic term (3.31) and of the mass term (3.40). First of all we note that even with this hamiltonian the momentum is a conserved quantity and because of this, during the evolution, both the mass and the energy of a particle will change, in oder to fulfill the mass shell condition. We consider therefore the set of free particle states with fixed momentum $\vec{p}$ and varying (m, E) spanned during the evolution.
If we consider the Berry phase as an holonomy on a $U(1)$ gauge bundle having the space of parameters as the base space [138], this additional requirement must be posed "at hand", as a condition in the connection.
Following [137], we define the Berry phase as:

$$\eta_B = i\int_+ \mathrm{d}m(t)\, \langle \bar{u}(r,\vec{p},m(t))|\tfrac{\partial}{\partial m(t)}|u(r,\vec{p},m(t))\rangle\, , \tag{3.42}$$

where u are the energy positive spinors functions, varying the mass and the energy, and $\int_+$ denote the integrals on them [5]; the explicit expression of these states is available in every classical book of relativistic quantum mechanics. The total integral is onto a period of $m(t)$. Note that, by inserting

[5] Indeed a change of sign of the mass along the cycle can always be reabsorbed in the definition of the fermion, by the transformations $\psi_R(\vec{r}) \to \psi_R(\vec{r})$, $\psi_L(\vec{r}) \to -\psi_L(\vec{r})$

$\bar{u}$ in the expression for the connection, we have explicitly imposed Lorentz invariance.
The matrix elements are easily computed to be

$$\langle \bar{u}(r,\vec{p},m(t))|\tfrac{\partial}{\partial m(t)}|u(r,\vec{p},m(t))\rangle = -\tfrac{1}{2}V_0\,\omega\, sin\omega t\,. \tag{3.43}$$

The integral in (3.42) is zero, then the Berry phase turns out to be vanishing; we explicitly checked that this was not the result if we didn't impose the Lorentz covariance. The same outcomes are valid for negative energy spinors.
In the case described here there's only a cyclically varying parameter; we stress that this fact generally doesn't assure that Berry phase is 0, since a closed form on a not contractible manifold can be globally not exact [139].
It would be interesting to repeat the calculation in the case of many cyclically varying parameters, we plan to do it in a future work.

3.2.7 3D - 2D crossover

Using anisotropic hopping parameters, we can easily realize the crossover from $(3+1)$ to $(2+1)$ Dirac fermions: to this aim, it is sufficient to lowering an hopping parameter to zero (say t_z, amounting to increase the power of the laser along z) while keeping fixed the effective magnetic field $\vec{B}$. In order to perform the $2D$ limit ($t_z \to 0$), we set

$$\begin{aligned}\psi_R(\vec{k}+\vec{k_R}) &\equiv \sigma_x\psi_1(\vec{k}+\vec{k}'_R)\\ \psi_L(\vec{k}+\vec{k_L}) &\equiv \sigma_x\sigma_z\psi_2(\vec{k}+\vec{k}'_L)\end{aligned} \tag{3.44}$$

with $\vec{k}'_R = (\frac{\pi}{2},-\frac{\pi}{2},-\frac{\pi}{2})$ and $\vec{k}'_L = (-\frac{\pi}{2},\frac{\pi}{2},-\frac{\pi}{2})$, clearly equivalent to $\vec{q}_R$ and $\vec{q}_L$. This transformation allows to express Hamiltonian (3.31) in the form

$$H = 2\int d\vec{k}\,\left(\psi_1^\dagger(\vec{k})\,\vec{\sigma}\cdot\vec{\mathcal{K}}\,\psi_1(\vec{k}) + \psi_2^\dagger(\vec{k})\,\vec{\sigma}\cdot\vec{\mathcal{K}}\,\psi_2(\vec{k})\right)\,, \tag{3.45}$$

where we introduced the (vector) notation $\vec{\mathcal{K}} \equiv (t_xk_x, t_yk_y, t_zk_z)$. In the $2D$ limit ($t_z \to 0$), this expression becomes

$$\begin{aligned}H^{2D} = 2\int d\vec{p}\,\big(&\bar{\psi}_1^{2D}(\vec{p})\,\vec{\alpha}\cdot\vec{p}\,\psi_1^{2D}(\vec{p}) \;+\\ &+\;\bar{\psi}_2^{2D}(\vec{p})\,\vec{\alpha}\cdot\vec{p}\,\psi_2^{2D}(\vec{p})\big)\,,\end{aligned}$$

where $\vec{p} = (t_xk_x, t_yk_y)$, $\vec{\alpha} = i(\sigma_x,\sigma_y)$, $\gamma_0 = \sigma_z$ and

$$\psi_{1,2}^{2D}(\vec{p}) = \lim_{k_z\to 0} e^{i\frac{\pi}{4}\sigma_z}\,\psi_{1,2}\left(\vec{k}\pm\left(\frac{\pi}{2},\pm\frac{\pi}{2},\frac{\pi}{2}\right)\right)\,. \tag{3.46}$$

This is nothing else that the Hamiltonian for $(2+1)$ Dirac fermions obtained in [85]. Hence, in the $2D$ limit, we obtain directly a pair of $(2+1)$ massless fermions, as expected [129].

Furthermore, in the limit $t_z \to 0$, the Bragg term (3.39) gives mass also to the $(2+1)$ Dirac fermions: indeed, the mixing matrix σ_x between ψ_1^{2D} and ψ_b^{2D} can be diagonalized yielding a term proportional to

$$\bar{\psi}_a^{2D}\psi_a^{2D} - \bar{\psi}_b^{2D}\psi_b^{2D}\,, \tag{3.47}$$

where $\psi_a^{2D} = \frac{1}{\sqrt{2}}(\psi_1^{2D} + \psi_2^{2D})$ and $\psi_b^{2D} = \frac{1}{\sqrt{2}}(\psi_1^{2D} - \psi_2^{2D})$. This basis transformation is analogous to the change of basis from Dirac to Pauli basis in $3D$. The minus sign in the second term of (3.47) can be always reabsorbed by multiplying ψ_b by a matrix M anticommuting with σ_z and such that $M^\dagger M = 1$ (as σ_x or σ_y): then (3.47) turns out to be a mass term for the $2D$ Dirac fermions.
The same conclusion can be obtained by noticing that in the 2D limit the mass term (3.40) becomes a Lorentz (SO(2,1)) invariant coupling between the species of 2D fermions:

$$m(\psi_1^{2D}(\vec{p})^\dagger\sigma_3\psi_2^{2D}(\vec{p}) \,+\, \psi_2^{2D}(\vec{p})^\dagger\sigma_3\psi_1^{2D}(\vec{p}))\,. \tag{3.48}$$

This interaction between the fermions gives to them a mass m at perturbative level, as can be easily shown by computing the (Fourier transform of) dressed propagator for the fermions:

$$\tfrac{1}{p-m}\,\tfrac{p}{p+m}|_{p=m} \;=\; \tfrac{1}{p-m}\,\tfrac{1}{2} \quad , \quad p = \gamma^\mu p_\mu\,. \tag{3.49}$$

This argument takes us to infer again that a Bragg term (3.39) gives mass also to 2D fermions on square lattice.
The mechanism for mass generating described above is very general: any bilinear term giving a transition between different species of Dirac fermions renormalizes the dressed propagators such to make appear a mass for all the species involved. This mechanism can be exploited in any dimension of the space-time and whatever is the set of quantum numbers discriminating the species (in the present case hyperfine levels, atomic numbers or polarizations of the atoms on the lattice). An explicit example is shown in [130].

3.2.8 Effects of interatomic interactions

Let' s consider two-body interactions among ultracold fermions of the form

$$\sum_{i,j} U_{i,j}\, c_i^\dagger c_i c_j^\dagger c_j \;: \tag{3.50}$$

eq. (3.50) describes general non-local interactions among atoms of the same species, as it may be realized in p-wave channels [131]. We assume for simplicity that U_{ij} is a function only of $\vec{r} = \vec{i} - \vec{j}$.

In order to derive the interaction between fermions that (3.50) produces, we go in the quasi-momentum space as before, we divide the pairs (i,j) in the four combinations (A/B, A/B) and we replace $\sum_{i,j}$ with $\sum_i \sum_{\vec{r}}$ $(\vec{r} = \vec{j} - \vec{i})$. We arrive to the expression:

$$\begin{aligned} &\textstyle\sum_{(\alpha,\beta)=(A/B,A/B)} \Big[\int \prod_{t=1}^4 d^3\vec{k_t}\, \tilde{U}_{\alpha,\beta}(|\vec{q}|)\cdot \\ &\cdot c_\alpha(\vec{k_1})^\dagger c_\alpha(\vec{k_2}) c_\beta(\vec{k_3})^\dagger c_\beta(\vec{k_4}) \,\cdot\, (2\pi)^3\delta^3(\vec{k_2}+\vec{k_4}-\vec{k_1}-\vec{k_3}) \,+\, \text{h.c.}\Big]\,, \end{aligned} \tag{3.51}$$

where $\vec{q} = \vec{k}_3 - \vec{k}_4$ is the transferred momentum. We remark for future importance that, in presence of unklapp processes, the delta of (quasi-)momentum conservation must be intended up a sum of Brillouin zone vectors.
We would like to show that the four lattice Fourier transforms can be taken to be equal once we consider the low energy limit of the present model; this allow to rewrite (3.51) as

$$\begin{aligned} &\int \prod_{k=1}^{4} \mathrm{d}^3\vec{k_t}\, \tilde{U}(|\vec{q}|)\, \psi(\vec{k_1})^\dagger \psi(\vec{k_2}) \psi(\vec{k_3})^\dagger \psi(\vec{k_4}) \cdot \\ &\cdot (2\pi)^3 \delta^3(\vec{k}_2 + \vec{k}_4 - \vec{k}_1 - \vec{k}_3) \; + \; \text{h.c.}\,. \end{aligned} \tag{3.52}$$

Our argument is clearer if we adopt the (*symmetric*) gauge $\pi(z, x, y)$ as in [128]; in this gauge we have 8 inequivalent vertices ($\alpha, \beta = 1, ..., 8$) but the calculation develops in the same manner as above. The sublattices formed by the 8 different vertices differ by relative shifts ($\vec{\delta}_{\alpha,\beta}$) of the order of the lattice space. The Fourier transforms $\tilde{U}_{\alpha,\alpha}(|\vec{q}|)$ are clearly all equivalent, then it remains to show that $\tilde{U}_{\alpha,\alpha}(|\vec{q}|) = \tilde{U}_{\alpha,\beta}(|\vec{q}|)$ if $\alpha \neq \beta$. We pose:

$$\vec{r}_{\alpha,\beta} = \vec{r}_{\alpha,\alpha} + \vec{\delta}_{\alpha,\beta}\,, \tag{3.53}$$

$$\tilde{U}_{\alpha,\alpha}(|\vec{q}|) = \sum_{\alpha,\alpha} U(\vec{r}_{\alpha,\alpha}) \mathrm{Exp}(-i\vec{q}\cdot\vec{r}_{\alpha,\alpha}) \tag{3.54}$$

and

$$\begin{aligned} &\tilde{U}_{\alpha,\beta}(|\vec{q}|) = \textstyle\sum_{\alpha,\beta} U(\vec{r}_{\alpha,\beta}) \mathrm{Exp}(-i\vec{q}\cdot\vec{r}_{\alpha,\beta})) \; = \\ &= \textstyle\sum_{\alpha,\alpha} U(\vec{r}_{\alpha,\beta}) \mathrm{Exp}(-i\vec{q}\cdot\vec{r}_{\alpha,\alpha}) \mathrm{Exp}(-i\vec{q}\cdot\vec{\delta}_{\alpha,\beta})\,. \end{aligned} \tag{3.55}$$

The expansion

$$\begin{aligned} &U(\vec{r}_{\alpha,\beta}) \mathrm{Exp}(-i\vec{q}\cdot\vec{\delta}_{\alpha,\beta}) \approx \\ &\approx \; (1 - i\vec{q}\cdot\vec{\delta}_{\alpha,\beta})(U(\vec{r}_{\alpha,\alpha}) + \vec{\nabla} U(\vec{r}_{\alpha,\alpha})\cdot\vec{\delta}_{\alpha,\beta}) \end{aligned} \tag{3.56}$$

and the property of the Fourier transform

$$F\left(\frac{\mathrm{d}f(x)}{\mathrm{d}x}\right) = ikF(f(x)) \tag{3.57}$$

yield the thesis, at first order in $\vec{\delta}_{\alpha,\beta}$. We obtain at the end the equation (3.52).
We focus now on the low energy degrees of freedom:

$$\begin{aligned} &\int \prod_{t=1}^{4} \mathrm{d}^3\vec{p_t}'\, \tilde{U}(|\vec{q}|)\, \psi(\vec{p_1})^\dagger_\mu\, \psi(\vec{p_2})_\nu\, \psi(\vec{p_3})^\dagger_\rho\, \psi(\vec{p_4})_\sigma \cdot \\ &\cdot (2\pi)^3 \delta^3(\vec{p}_2 + \vec{p}_4 - \vec{p}_1 - \vec{p}_3) \; + \; \text{h.c.}\,, \end{aligned} \tag{3.58}$$

where $\vec{k_i} \equiv \vec{p_i} + \vec{q}_{R/L}$ and the greeks index run on (R, L).
We stress that the formula (3.58) is expected, at least in the case that the Fermi liquid is not spoiled by the interactions and the interacting fermions are "adiabatically close" to the free fermions. We

will return later on this important point.

Covariant interactions It is well known that the interatomic term (3.50) does not generally give rise to a Lorentz invariant interaction among the Dirac spinors. Indeed (3.58) is in general a non Lorentz-covariant interaction term; in order to obtain a covariant interaction we must have an inversion of the chirality in every bilinear entering in the four-fields term (3.58). As can easy seen from field quantization in subsection (3.2.4), this requirement is equivalent in our case to have a dynamics involving only the processes with $|\vec{q}| \approx |\vec{\Delta}|$ (and not the ones with $|\vec{q}| \approx 0$). This translates in imposing on the potential:

$$\tilde{U}(0) = 0\,, \tag{3.59}$$

where $\tilde{U}(\vec{k})$ denotes the Fourier transform of $U(\vec{r})$. The condition (3.59) could be obtained with potentials typical of the p-wave scattering.
The interaction from $\vec{q} \approx 0$ scattering processes would read as

$$\tilde{U}(0) \int d^4x\, \psi^\dagger(x)\psi(x)\psi^\dagger(x)\psi(x) \tag{3.60}$$

and it breaks explicitly Lorentz covariance. Obviously, if $|\tilde{U}(0)| \ll |\tilde{U}(|\tilde{\Delta}|)|$ and $|\tilde{U}(0)| \ll ta^3$, its effect is negligibly small.
Once (3.59) is imposed, for the low-energy dynamics considered here the two-body interaction reduces approximately to $\tilde{U}(|\vec{k}|) \approx \tilde{U}(|\vec{\Delta}|)$ [where $\Delta = \vec{k}_L - \vec{k}_R = \pi(1,1,1)$]. The discarded derivative terms are expected to be negligible for the dynamics of IR excitations.
This procedure results in the locality of the bilinears in the quartic interaction terms: using the expressions (3.30) in the interacting non-relativistic Hamiltonian, one gets

$$\tilde{U}(|\vec{\Delta}|) \int d^4x\, (\bar{\psi}(x)\psi(x))(\bar{\psi}(x)\psi(x))\,. \tag{3.61}$$

Although not strictly renormalizable, the term (3.61) induces an effective interaction term [6] with coupling parameter having dimensions $[\text{mass}]^{-2}$, similarly to the interacting term in the Nambu-Jona-Lasinio model [133]). Indeed, as pointed out in [135], the irrelevance in IR of a general four-fermion interaction is at the basis of the Fermi liquid behaviour; this feature is lost for instance in presence of pairings driving the system towards a superconducting state.
The term (3.61) is present both it the massless case and when Bragg pulses are used to make massive the Dirac fermions. Notice however that (3.61) is likely to yield a mass term at loop level (as well as renormalization contributions for the Fermi velocity and dispersion rule), see more details at the end of the subsection.

Stability of the Fermi liquid The interatomic term (3.50) could even spoil the picture in terms of Dirac spinors (low-energy quasiparticles). Indeed this holds as far as the Fermi liquid is

[6] As pointed out in [134, 135] a QFT description of the IR limit of a many body system is generally ill defined in D greater than 1, due to extended Fermi surface. In our case the last one has a null measure surface and the separated wells correspond to different chiralities (3D)/species (2D), then the theory is well defined. In particular the IR QFT has transferred momentum close to 0.

not spoiled, that is the lifetime τ of the quasi-particle excitations is finite and $\Gamma = h/\tau$ is smaller than their energy. However, with a weak two-body potential ($U(\vec{r}) \ll t$), the same condition (3.59) guarantees the validity of the Fermi liquid and of relativistic description.
In the following we present a simple estimate of the quasiparticle lifetime carried on the following lines, as in [132]. The leading process that affects the lifetime of a quasiparticle above the Fermi energy (and generally can cause the spoiling of the Fermi liquid) is the creation of a pair hole-particle by an exchange of energy-momentum with the quasiparticle such it remains over the Fermi surface. Let's calculate the width (inverse of the lifetime) associated to this process. This can can be written as

$$\frac{1}{\tau} = \frac{2\pi}{L^D} \int |\tilde{U}(\vec{q})|^2 \rho(\vec{k}_2)\, \rho(\vec{k}_3)\, \rho(\vec{k}_4) \delta^4(\vec{k}_3^{\mu} + \vec{k}_4^{\mu} - \vec{k}_1^{\mu} - \vec{k}_2^{\mu}) \prod_{i=2}^{4} \mathrm{d}^3 \vec{k}_i \,, \tag{3.62}$$

where $\vec{k}_1$ is the initial momentum, D is the dimensionality, $\vec{k}_2$ is the second incoming momentum and $\vec{k}_3, \vec{k}_4$ are the final ones. We stress that, since we do not have additional quantum number further that the momentum, we do not have exchange terms in (3.62).
The quantity $\rho(\{\vec{k}_i\})$ is the density in the phase space, it can approximated with the space phase density in the non interacting case [7] and it can be rewritten as:

$$\rho(\{\vec{k}_i\}) = \rho(\{|\vec{k}_i|\}, \{\Omega_i\}) = \tilde{\rho}(\{E_i\}, \{\Omega_i\}) \,, \tag{3.63}$$

where Ω_i is the solid angle of the momentum $\vec{k}_i$. We also took into account that the energy must depend directly on the modulus of the momentum. The energy are measured form the Dirac points and the quantity $|V(\vec{q})|^2$ is supposed to depend only on the modulus of $\vec{q}$.
Since $|V(\vec{q})|^2$ and the density $\tilde{\rho}$ are positive, we can write:

$$\begin{aligned} \tfrac{1}{\tau} = \tfrac{2\pi}{L^D} \textstyle\int |\tilde{U}(\vec{q})|^2 \prod_{i=2}^{4} \tilde{\rho}(\{E_i\}, \{\Omega_i\})\, \delta^4(\vec{k}_3^{\mu} + \vec{k}_4^{\mu} - \vec{k}_1^{\mu} - \vec{k}_2^{\mu}) \cdot \\ \cdot \mathrm{d}E_i\, \mathrm{d}\Omega_i < \tfrac{2\pi}{L^D} \textstyle\int |\tilde{U}(\vec{q})|^2 \prod_{i=2}^{4} \tilde{\rho}(\{E_i\}, \{\Omega_i\}) \mathrm{d}E_i\, \mathrm{d}\Omega_i \,. \end{aligned} \tag{3.64}$$

Writing $\tilde{\rho}(\{E_i\}, \{\Omega_i\})$ in its factorized form and integrating on $\mathrm{d}\Omega_i$ we obtain:

$$\frac{1}{\tau} < \frac{2\pi}{L^D} \int_0^{\Lambda} |\tilde{U}(\vec{q})|^2 \prod_{i=2}^{4} \bar{\rho}(E_i)\, \mathrm{d}E_i \tag{3.65}$$

The quantities $\bar{\rho}(E_i)$ are nothing but the non interacting energy densities of the states. In the formula (3.65) we explicitly inserted an energy cut-off in the integration for future convenience; in the low energy limit it tends to zero.
The lifetime surely is finite if the quantity on the right in (3.65) is finite; since the integral is on a finite interval, a *sufficient* condition is that

$$lim_{\{E, \vec{\eta} \to 0\}} \left(|\tilde{U}(\vec{0} + \vec{\eta})|^2 + |\tilde{U}(\vec{\Delta} + \vec{\eta})|^2\right) \cdot \bar{\rho}(E)^3 \; < \infty \,. \tag{3.66}$$

[7] The interaction makes the spectrum and the energy density change, anyway, if the coupling is weak (as assumed in our case), this approximation is expected to work.

We used the fact that only the excitations close to the Dirac point contributes in the I.R. and we approximated $\bar{\rho}(E_i)$ to be equal; this approximation does not change our qualitative argument.
Since E and η are not completely independent variable, the limit (3.66) must be dealt with great care. The density $\bar{\rho}(E)$ tends to zero near the Dirac points as a power of E, then one case when (3.66) is valid is when $|\tilde{U}(\vec{0}+\vec{\eta})|$ and $\tilde{U}(\vec{\Delta}+\vec{\eta})|$ are finite; this is true with our precedent choice (3.59). Therefore we can conclude that, with our choice 3.59 for the potential, the lifetime does not diverge.
Although a behaviors as non-Fermi liquid is signaled by a divergence of the inverse lifetime (for instance in the case of the Luttinger liquids), the discussion up to this point does not state rigorously that our interaction preserves the Fermi liquid. Indeed, for such a system the sufficient condition reads:

$$\frac{\Gamma}{E} << 1\,, \tag{3.67}$$

where $\Gamma = \frac{h}{\tau}$ is the width of the quasiparticle and E its energy from the Dirac point, as above. This condition explains for instance the marginality of the graphene with Coulomb interaction [134], where $\Gamma \sim E$ (while in normal 3D metals $\Gamma \sim E^2$). In order to deal with our case and in view of (3.65), it' s useful to study when

$$\frac{h}{E}\,\frac{2\pi}{L^D}\int_0^{\Lambda} |\tilde{U}(\vec{q})|^2 \prod_{i=2}^{4} \bar{\rho}(E_i)\,\mathrm{d}E_i \;<<\; 1\,, \tag{3.68}$$

since this clearly guarantees the condition (3.67).
We define for brevity $\int_0^{\Lambda} |\tilde{U}(\vec{q})|^2 \prod_{i=2}^{4} \bar{\rho}(E_i)\,\mathrm{d}E_i \equiv \Theta$.
Since

$$(|\tilde{U}(\vec{0}+\vec{\eta})|^2 + |\tilde{U}(\vec{\Delta}+\vec{\eta})|^2) \to c < \infty \quad \text{if} \quad \vec{\eta} \to 0 \tag{3.69}$$

we have approximately

$$\Theta \sim \frac{2\pi}{L^D}\,(|\tilde{U}(\vec{0}+\vec{\eta})|^2 + |\tilde{U}(\vec{\Delta}+\vec{\eta})|^2)\,\left(\int_0^{\Lambda} \bar{\rho}(E)\,\mathrm{d}E\right)^3 \tag{3.70}$$

and the behaviour near $E = 0$ is basically determined by the integral on the energy.
Defining as $F(E)$ the primitive function of $\bar{\rho}(E)$ we obtain the condition:

$$\frac{2\pi h}{L^D}\,(|\tilde{U}(\vec{0}+\vec{\eta})|^2 + |\tilde{U}(\vec{\Delta}+\vec{\eta})|^2)\cdot F(\Lambda)^3 \;<<\; E\,. \tag{3.71}$$

The behaviour of the energy density, generally vanishing for $E \to 0$ like a positive power of E, implies that (3.71) is fulfilled in our case. Moreover, the rapid vanishing of $\bar{\rho}(E)$ justifies a' posteriori the approximation (3.70).
Summing up, our discussion shows that the condition (3.59) is sufficient to guarantee the stability of the Fermi liquid description, then confirmating the validity of the description of QFT in terms of relativistic fermions (single particle low-energy excitations) interacting [8].
We also stress that an effect of the interactions is to renormalize the Fermi velocity and the mass.

[8] Indeed a naive power counting as in [134] suggest power low decay $\frac{1}{r^\alpha}$, $\alpha \leq 1$ for the Fermi liquid breaking.

In particular, even starting with massless excitations (without a Bragg pulse), the interaction (3.61) gives a mass term (indeed (3.61) has not chiral symmetry, as in the case of Nambu Jona-Lasinio model [133], protecting from mass generation).
These effects can be estimated by calculating the interacting Green function of the fermions (quasiparticles). We compute in particular the self-energy $\Sigma(p)$, with $p = (\omega, \vec{p})$; it's know that $\mathrm{Re}\,\Sigma(\omega, \vec{p})$ is the correction to the energy, while $\mathrm{Im}\Sigma(\omega, \vec{p})$ is the decay width of the quasiparticle due to the interaction (see above).
The calculation must be accomplished starting from the interaction (3.52)

$$\begin{aligned} &\int \textstyle\prod_{k=1}^{4} \mathrm{d}^3\vec{k_t}\, \tilde{U}(|\vec{q}|)\, \psi(\vec{k_1})^\dagger \psi(\vec{k_2}) \psi(\vec{k_3})^\dagger \psi(\vec{k_4}) \cdot \\ &\qquad \cdot (2\pi)^3 \delta^3(\vec{k}_2 + \vec{k}_4 - \vec{k}_1 - \vec{k}_3) \;+\; \text{h.c.} \end{aligned} \tag{3.72}$$

involving *all* the spectrum of the quasiparticles. Notice that in this expression enter excitations having, for a given quasimomentum $\vec{k}$, two different energies (positive and negative, measured from the Fermi point); this is the main difference with the usual computations in condensed matter theory.
We consider only the one-loop contribution $G^1(p)$, equivalent to the Hartree-Fock correction [135, 136]. The relevant diagrams are [135, 136]:

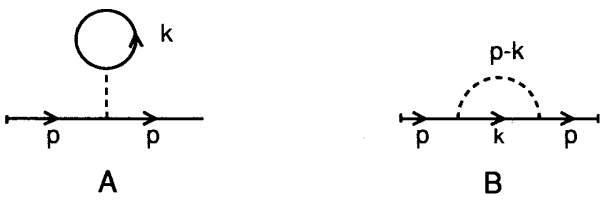

Figure 3.7: One-loop diagrams contributing to the self-energy

and correspond to the expressions

$$\begin{aligned} G_A(p) &= -i\,(G^{(0)}(p))^2\, U(0) \int \tfrac{\mathrm{d}^4k}{(2\pi)^4}\, G^{(0)}(k) \quad \text{Hartree contrib.} \\ G_B(p) &= -(G^{(0)}(p))^2 \int \tfrac{\mathrm{d}^4k}{(2\pi)^4}\, G^{(0)}(k)\, \tilde{U}(p-k) \quad \text{Fock contrib.}\,, \end{aligned} \tag{3.73}$$

where $\tilde{U}(p) = \tilde{U}(\vec{p})$ and $G^{(0)}(p)$ is the bare Green function:

$$G^{(0)}(p) = \frac{1}{\omega - \xi(\vec{p}) + i\delta\,\mathrm{sign}(\xi(\vec{p}))} \quad , \quad \xi(\vec{p}) = \epsilon(\vec{p}) - \mu\,. \tag{3.74}$$

We have $G^{(1)}(p) = G_A(p) + G_B(p)$ and $\Sigma^{(1)}(\omega, \vec{p}) = \frac{G^{(1)}(p)}{(G^{(0)}(p))^2}$.
The first term $G_A(p)$ is zero, since for hypothesis $\tilde{U}(0) = 0$. The second term can be written as [136]

$$G_B(p) = -(G^{(0)}(p))^2 \int\int \frac{\mathrm{d}\omega}{(2\pi)} \frac{\mathrm{d}^3\vec{k}}{(2\pi)^3}\, \tilde{U}(\vec{p} - \vec{k})\, G^{(0)}(\vec{k})\,. \tag{3.75}$$

The integral on ω can be evaluated by the residue theorem and it goes through by closing the path:

- on the lower semiplane for [136] for $\xi(\vec{p}) > 0$, this selects the poles with negative energy;
- on the upper semiplane for [136] for $\xi(\vec{p}) < 0$, this selects the poles with positive energy. This point is not present in the standard computation in condensed matter theory.

Since for every quasi-momentum in the Brillouin zone we have both a positive energy and a negative energy solution, the procedure above yields:

$$\begin{aligned} \Sigma_{+}^{(1)}(p) &= \int \tfrac{\mathrm{d}^3\vec{k}}{(2\pi)^3}\, \tilde{U}(\vec{p}-\vec{k}) \quad \text{for} \quad \xi(\vec{p}) > 0\,, \\ \Sigma_{-}^{(1)}(p) &= -\int \tfrac{\mathrm{d}^3\vec{k}}{(2\pi)^3}\, \tilde{U}(\vec{p}-\vec{k}) \quad \text{for} \quad \xi(\vec{p}) < 0\,. \end{aligned} \tag{3.76}$$

The corrections to the "free" energies have different sign, as expected. Since we supposed $U(\vec{r}) = U(|\vec{r}|)$, we have that $\tilde{U}(\vec{k}) = \tilde{U}(|\vec{k}|)$ is real and $\Gamma = \mathrm{Im}\Sigma(p) = 0$, then at this order we have no decay width of the quasiparticles (in agreement with the Hartree-Fock theory). Depending on the particular form of the potential $U(r)$, the terms (3.76) give a gap between the two sub-bands (positive and negative), a mass correction and a correction to the Fermi velocity; this can be seen by expanding $\Sigma_{\pm}^{(1)}(p)$, close to the Fermi points, as a Laurent series in $|\vec{p}|$: the gap turns out to be twice the constant term in the expansion, the correction to the Fermi velocity is the (modulus of the) coefficient of the linear term, while the mass is given by the coefficient of the $\frac{1}{|\vec{p}|}$ term.

Many species We observe that when $\mathcal{N}$ different fermionic species are considered the interaction term (3.50) reads $\sum_{i,j}\sum_{\alpha,\beta=1}^{\mathcal{N}} U_{i,j}^{\alpha,\beta}\, c_{i;\alpha}^{\dagger} c_{i;\alpha} c_{j;\beta}^{\dagger} c_{j;\beta}$. In general, the interaction intra-(α=β) and inter-(α≠β) species are different: however, the condition (3.59), necessary to have Lorentz invariant interaction terms, simply reads $\tilde{U}^{\alpha,\beta}(0) = 0$. It would be very interesting to study the appearance of superconductive states or bound states in presence of an asymmetry on the interaction between different colours.
If instead the interaction is independent on the internal degrees of freedom α, β, then eq. (3.61) becomes $\tilde{U}(|\vec{\Delta}|) \int d^4x\, (\bar{\psi}_\alpha \psi^\alpha)(\bar{\psi}_\beta \psi^\beta)$. The condition of colour independence is required in order to obtain colour symmetry, relevant for simulation of high energy theories.

Interactions in 2D The $2D$ limit can be obtained from the mapping (3.44). Although in 2D there is no chirality, the condition (3.59) is still required; this can be seen easily by remembering that $\bar{\psi} = \psi^\dagger \sigma_z$. We end up in a coupling having different $(2+1)$ Dirac spinors ψ_1^{2D} and ψ_2^{2D} in each bilinear.
The discussion for the stability of the 2D interacting fermions can be carried on similarly as above; anyway the problem was already tackled in literature (see for instance ([134]) and citing papers): interactions vanishing at infinity faster than $\frac{1}{|\vec{r}|}$ do not spoil the Fermi liquid.

3.2.9 Gap equations with attractive interactions

The first natural development of work presented in this Chapter is the study of the possible superconducting phases, once an attractive interaction (here supposed Lorentz covariant) is added.
In this light, following [144], we derive the relativistic gap equation with a certain number of colours

(labelled by greeks indices). For simplicity, we insert only a single flavour (mass); the extension to an arbitrary number is straightforward. The calculation is carried on for the case of a (Lorentz) scalar interaction and it extends the results in Ohsaku's work [143] in the case of one colour.
at this level there are no problems to repeat it for interactions involving different pairs of bilinears $\bar{\psi}(x)\, M\, \psi(x)$.
The Hamiltonian is:

$$\begin{array}{c} H_0 = \sum_k \int \mathrm{d}^3 w\, \bar{\psi}_\mu(-i\vec{\gamma}\cdot\nabla + m + g\gamma_\mu A^\mu - \gamma_0\mu)\,\psi_\mu \\ + \\ H_i = \frac{1}{2}\sum_{\epsilon,\gamma}\int \mathrm{d}^3 y\, \mathrm{d}^3 z\, V_{\epsilon,\gamma}(z-y)\,\bar{\psi}_\epsilon(z)\bar{\psi}_\gamma(y)\psi_\gamma(y)\psi_\epsilon(z)\,. \end{array} \tag{3.77}$$

Lorentz covariance forces the interaction to be local, that means depending only on a single variable; nevertheless in the derivation we will keep y and z.

In the Heisenberg representation one has for an operator O:

$$\frac{\mathrm{d}O}{\mathrm{d}t} = i[H, O],. \tag{3.78}$$

The one has:

$$[H_0, \psi_\alpha(x)] = -H_0\,\psi_\alpha(x) \tag{3.79}$$

$$[H_0, \bar{\psi}_\alpha(x)] = \bar{\psi}_\alpha(x) H_0^{\leftarrow} \tag{3.80}$$

$$[\bar{\psi}_\epsilon(z)\bar{\psi}_\gamma(y)\psi_\gamma(y)\psi_\epsilon(z), \psi_\alpha(x)] = -2\gamma_0\psi_\alpha(x)\bar{\psi}_\epsilon(z)\psi_\epsilon(z) \tag{3.81}$$

$$[\bar{\psi}_\epsilon(z)\bar{\psi}_\gamma(y)\psi_\gamma(y)\psi_\epsilon(z), \bar{\psi}_\alpha(x)] = 2\gamma_0\bar{\psi}_\alpha(x)\bar{\psi}_\gamma(z)\bar{\psi}_\gamma(z)\,. \tag{3.82}$$

Above and in the following, the left arrow on a certain operator means that the operator is left acting.
The correlation functions are defined as in [143]:

$$\begin{array}{cc} G_{\alpha\beta}(x,x') = -i\langle\psi_\alpha(x)\bar{\psi}_\beta(x')\rangle\,, & \bar{G}_{\beta\alpha}(x,x') = i\langle\bar{\psi}_\alpha(x')\psi_\beta(x)\rangle\,, \\ F_{\alpha\beta}(x,x') = \langle\psi_\alpha(x)\psi_\beta(x')\rangle\,, & \bar{F}_{\alpha\beta}(x,x') = \langle\bar{\psi}_\alpha(x)\bar{\psi}_\beta(x')\rangle\,. \end{array} \tag{3.83}$$

One has four equation; the first equation is:

$$\begin{array}{c} i\gamma_0\left(\frac{\mathrm{d}}{\mathrm{d}t} - H_0\right) G_{\alpha\beta}(x,x') + \\ +i\sum_\epsilon \int \mathrm{d}^3 z V_{\alpha\epsilon}(x-z)[G_{\alpha\epsilon}(x,z)G_{\epsilon\beta}(z,x') + F_{\alpha\epsilon}(x,z)\bar{F}_{\epsilon\beta}(z,x') + \\ +G_{\alpha\beta}(x,x')G_{\epsilon\epsilon}(z,z)] = \delta_{\alpha\beta}\delta(x-x')\,. \end{array} \tag{3.84}$$

We easily recover Ohsaku's formula by posing $V(x-y) = -g\,\delta^3(x-y)$, $\alpha = \beta$ and by discarding Hartree terms (first and third) in (3.84).

The second equation reads:

$$\begin{array}{c} i\gamma_0\left(\frac{\mathrm{d}}{\mathrm{d}t} + H_0\right)(-i)F_{\alpha\beta}(x,x') - \\ -\sum_\gamma \int \mathrm{d}^3 y V_{\alpha\gamma}(x-y)[-\bar{G}_{\gamma\gamma}(y,y)F_{\alpha\beta}(x,x') + \bar{G}_{\alpha\gamma}(x,y)F_{\beta\gamma}(y,x') - \\ -\bar{G}_{\beta\gamma}(x',y)F_{\alpha\gamma}(y,x)] = 0\,. \end{array} \tag{3.85}$$

We easily recover Ohsaku's formula by posing $V(x-y) = -g\,\delta^3(x-y)$, $\alpha = \beta$ and by discarding Hartree terms (first and second)in (3.85) .

The third equation is:

$$i\gamma_0 \left(\tfrac{\mathrm{d}}{\mathrm{d}t} + H_0^{\leftarrow}\right)(-i)\bar{F}_{\alpha\beta}(x,x') +$$

$$+i\textstyle\sum_\gamma \int \mathrm{d}^3y V_{\alpha\gamma}(x-y)[i\,\bar{F}_{\alpha\gamma}(x,y)G_{\gamma\beta}(y,x') + i\,\bar{G}_{\gamma\alpha}(y,x)\bar{F}_{\gamma\beta}(y,x') - \tag{3.86}$$

$$-i\,\bar{F}_{\alpha\beta}(x,x')\bar{G}_{\gamma\gamma}(y,y)] = 0\,.$$

We easily recover Ohsaku's formula by posing $V(x-y) = -g\,\delta^3(x-y)$, $\alpha = \beta$ and by discarding Hartree terms (second and third) in (3.86).

For the fourth equation one has:

$$i\gamma_0 \left(\tfrac{\mathrm{d}}{\mathrm{d}t} + H_0^{\leftarrow}\right)(-\bar{G}_{\alpha\beta}(x',x)) +$$

$$+\textstyle\sum_\epsilon \int \mathrm{d}^3z V_{\alpha\epsilon}(x-z)[i\,\bar{F}_{\epsilon\alpha}(z,x)F_{\epsilon\beta}(z,x') + i\,\bar{G}_{\epsilon\epsilon}(z,z)\bar{G}_{\beta\alpha}(x',x) - \tag{3.87}$$

$$-i\,\bar{G}_{\beta\epsilon}(x',z)\bar{G}_{\epsilon\alpha}(z,x)] = \delta_{\alpha\beta}\delta(x-x')\,.$$

We easily recover Ohsaku's formula by posing $V(x-y) = -g\,\delta^3(x-y)$, $\alpha = \beta$ and by discarding Hartree terms (second and third) in (3.87).

We finally mention that it's possible to extend this computation to interactions involving different pairs of bilinears $\bar{\psi}(x)\,M\,\psi(x)$.

3.2.10 Conclusions

We have shown that ultracold atoms in a rotating optical lattice are able to simulate $(3+1)$ Dirac fermions, with their mass generated by a Bragg pulse which transfers particles from a Dirac point to the other. When the two lasers of the Bragg pulse have the same frequencies, the Dirac mass is time-independent, otherwise one has a sinusoidal time-dependence of the mass. This property could be used to study adiabatic or quenched dynamics in the Dirac equation; with random Bragg pulses, it can be used to investigate instead diffusion and disorder in relativistic quantum mechanics.

We have also analyzed the crossover from $(3+1)$ to $(2+1)$ Dirac fermions which can be induced by anisotropic lattices. Finally, we have also given a criterion for the interatomic interactions in order to get relativistically invariant effective interaction terms. Interesting perspectives along this line include the possibilities: (i) to study the relativistic Hamiltonian for several species with general interactions (in particular with no intra-species interactions);
(ii) to simulate the Nambu-Jona-Lasinio model [133] in the case that the umklapp processes $\{RR\} \Leftrightarrow \{LL\}$ can be neglected;
(iii) to manipulate the ultracold atomic lattice for realizing Majorana fermions [141];
(iv) to study the (eventually attractive) relativistic interacting theory obtained, also in the $3D-2D$ crossover. With this idea in mind, we presented in 3.2.9 preliminary results on the Gork'ov equations in the case of a Lorentz scalar interaction and many species.

3.2.11 Appendix 1: eigenvalues of cubic lattice

We report below the C program that we used to check some results described in this Chapter. The program simulates the hopping of atoms on a cubic lattice (and on the square lattice obtained in the strongly anisotropic limit) in the magnetic field $\vec{B} = \pi(1, 1, 1)$ and it allows to calculate the spectrum and the energy density of the eigenstates. In the (initial) part, where the variables are defined:
a) L is the lattice size;
b) Di (i= 1, 2, 3), assumed to be positive and much less than 0, measure the deviations from the π flux. The part of the code involving these variables was inserted to check the stability of the systems against small flux fluctuations (no Hofstadter butterfly);
c) H3 is 1 for the cubic lattice and 0 for the square one;
d) P is set equal to 1 to fix periodic boundary conditions, to 0 if no boundary conditions are inserted. Obviously all the calculations were done in the last case;
e) V is the coupling of the Bragg pulse, it must be much less the 1.

```
/*
 *  cubopert4massa.cpp
 *
 *
 *  Created by Luca Lepori on 01/11/09.
 *  Copyright 2009 SISSA. All rights reserved.
 *
 */

// To be compiled with
//g++ -I‘gsl-config --cflags‘ -o <nome eseguibile>
//<nomefile.cc> ‘gsl-config --libs‘

// I use the gauge  A = Pi*((1/2)+z-x,-(1/2)+x-z,0)
/*

In the periodic case I obtain analytical values by the formula:
 For[a = 0, a < L/2, a++,
 For[b = 0, b < L/2, b++,
 For[c = 0, c < L, c++,
 Print[N[2*
 Sqrt[(Cos[(2*Pi*a/L)]^2) + (Cos[2*Pi*b/L]^2) + (Sin[2*Pi*c/L]^2)]]]]]];

*/
#include <iostream>
#include <fstream>
#include <gsl/gsl_math.h>
```

```
#include <gsl/gsl_complex.h>
#include <gsl/gsl_vector_complex_double.h>
#include <gsl/gsl_matrix_complex_double.h>
#include <gsl/gsl_complex_math.h>
#include <gsl/gsl_eigen.h>
#include <cmath>
#include <complex>
using namespace std;

int main (void)
{
int L;
float D1;
float D2;
float D3;
float H3;
int P;
float V;
printf("Insert L: ");
scanf("%d",&L);
printf("Insert D1: ");
scanf("%f",&D1);
printf("Insert D2: ");
scanf("%f",&D2);
printf("Insert D3: ");
scanf("%f",&D3);
printf("Insert H3: ");
scanf("%f",&H3);
// H3 real, generally not integer, if it's 0 we have the 2D case.
printf("Insert P: ");
scanf("%d",&P);
// P=0 no boundary conditions,  P=1 with boundary conditions.
printf("Insert V: ");
scanf("%f",&V);
// V is Bragg coupling, it must be small in comparison to  1.
ofstream outfile;
outfile.open("cmag.dat", ios::out);


Sites labelled as  j,i,h
```

```
if (P == 1 && L%2 == 0 ) {
const int N = L*L*L;
// Having periodic boundary conditions, I need a vector L^3,
since I have L sites from 0 to L-1.
gsl_vector_complex* data = gsl_vector_complex_alloc(N*N);
gsl_complex num;
gsl_complex conj;
gsl_complex add1p;
gsl_complex add2p;
gsl_complex add1;
gsl_complex add2;
gsl_complex bragg;

for (int h = 0; h < L; h++) {
for (int i = 0; i < L; i++) {
for (int j = 0; j < L; j++){

add1p = gsl_complex_polar (1, (M_PI)*(i+j+h));
add2p = gsl_complex_polar (1, -(M_PI)*(i+j+h));
add1 = gsl_complex_mul_real (add1p, V);
add2 = gsl_complex_mul_real (add2p, V);
bragg = gsl_complex_add (add1, add2);

gsl_vector_complex_set(data, (j+i*L+h*L*L)*N+(j+i*L+h*L*L), bragg);

if (h+1 < L) {
GSL_SET_COMPLEX(&num, H3, 0);
gsl_vector_complex_set(data, (j+i*L+h*L*L)*N+(j+i*L+(h+1)*L*L), num);
gsl_vector_complex_set(data, (j+i*L+(h+1)*L*L)*N+(j+i*L+h*L*L), num);
}
else {
GSL_SET_COMPLEX(&num, H3, 0);
gsl_vector_complex_set(data, (j+i*L+h*L*L)*N+(j+i*L+0*L*L), num);
gsl_vector_complex_set(data, (j+i*L+0*L*L)*N+(j+i*L+h*L*L), num);
};

if (j+1 < L) {
num = gsl_complex_polar (1, (M_PI)*(-1+2*(1+D3)*i-2*(1+D1)*h)/2);
gsl_vector_complex_set(data, (j+i*L+h*L*L)*N+(j+1+i*L+h*L*L), num);
conj = gsl_complex_polar (1, -(M_PI)*(-1+2*(1+D3)*i-2*(1+D1)*h)/2);
gsl_vector_complex_set(data, (j+1+i*L+h*L*L)*N+(j+i*L+h*L*L), conj);
}
else {
```

```
num = gsl_complex_polar (1,(M_PI)*(-1+2*(1+D3)*i-2*(1+D1)*h)/2);
gsl_vector_complex_set(data, (j+i*L+h*L*L)*N+(0+i*L+h*L*L), num);
conj = gsl_complex_polar (1, -(M_PI)*(-1+2*(1+D3)*i-2*(1+D1)*h)/2);
gsl_vector_complex_set(data, (0+i*L+h*L*L)*N+(j+i*L+h*L*L), conj);
};

if (i+1 < L) {
num = gsl_complex_polar (1, (M_PI)*(1+2*(1+D2)*(h-i))/2);
gsl_vector_complex_set(data, (j+i*L+h*L*L)*N+(j+(i+1)*L+h*L*L), num);
conj = gsl_complex_polar (1, -(M_PI)*(1+2*(1+D2)*(h-i))/2);
gsl_vector_complex_set(data, (j+(i+1)*L+h*L*L)*N+(j+i*L+h*L*L), conj);
}
else {
num = gsl_complex_polar (1, (M_PI)*(1+2*(1+D2)*(h-i))/2);
gsl_vector_complex_set(data, (j+i*L+h*L*L)*N+(j+0*L+h*L*L), num);
conj = gsl_complex_polar (1, -(M_PI)*(1+2*(1+D2)*(h-i))/2);
gsl_vector_complex_set(data, (j+0*L+h*L*L)*N+(j+i*L+h*L*L), conj);
}

}
}
}


gsl_vector_view partereale = gsl_vector_complex_real(data);
gsl_vector_view parteimmaginaria = gsl_vector_complex_imag(data);

// check whether the matrix is hermitian
int p =0;
for (int i = 0; i < N; i++) {
for (int j = 0; j < N; j++) {
double x1 = gsl_vector_get(&partereale.vector,i*N+j);
double x2 = gsl_vector_get(&partereale.vector,j*N+i);
double y1 = gsl_vector_get(&parteimmaginaria.vector,i*N+j);
double y2 = gsl_vector_get(&parteimmaginaria.vector,j*N+i);
if ((x1 != x2) && (y1 != -y2)) { p = p+1; }
} }

if(p == 0)

{

/*
```

```
 ofstream outf("entrate.dat", ios::out);
for (int i = 0; i < N; i++) {
for (int j = 0; j < N; j++) {
//      double x = GSL_REAL(gsl_complex_vector_get(data,i*N+j));
//double y = GSL_IMAG(gsl_complex_vector_get(data,i*N+j));
double x = gsl_vector_get(&partereale.vector,i*N+j);
double y = gsl_vector_get(&parteimmaginaria.vector,i*N+j);
outf << "Entry (" << i << "," << j << ") = " << x << "+i" << y << endl;
}
}

outf.close();
*/


cout << "Initialized data" << endl;

gsl_matrix_complex_view m = gsl_matrix_complex_view_vector (data, N, N);
gsl_vector *eval = gsl_vector_alloc (N);
gsl_matrix_complex *evec = gsl_matrix_complex_alloc (N, N);
gsl_eigen_hermv_workspace * w = gsl_eigen_hermv_alloc (N);
gsl_eigen_hermv (&m.matrix, eval, evec, w);
gsl_eigen_hermv_free (w);
//  gsl_eigen_hermv_sort (eval, evec,
// GSL_EIGEN_SORT_ABS_ASC);

outfile << N << endl;
outfile << D1 << endl;
outfile << D2 << endl;
outfile << D3 << endl;
outfile << H3 << endl;
outfile << P << endl;
outfile << V << endl;
outfile << "autovalori" << endl;

for (int t = 0; t < N; t++) {
double eval_t = gsl_vector_get (eval, t);
outfile << eval_t << endl;

// In case one wants to see also the eigenvectors...
//gsl_vector_view evec_i = gsl_matrix_column (evec, i);
//outfile << "eigenvector = \n";
//for (int j = 0; j < N; j++)
```

```
// outfile << gsl_vector_get(&evec_i.vector,j) << endl;

}
outfile.close();
gsl_vector_free (eval);
gsl_matrix_complex_free (evec);
return 1;

}

else{
cout << "Initialized data" << endl;
printf("error\n");
outfile.close();
}
return 0;
}

else if((P == 1) && L%2 == 1) {
cout << "Initialized data" << endl;
printf("error\n");
outfile.close();
}

  else{

const int Lprime = L+1;
const int N = Lprime*Lprime*Lprime;
// Now no periodic boundary conditions, I nedd a vector
// (L+1)^3 since I have L+1 sites from 0 to L.
gsl_vector_complex* data = gsl_vector_complex_alloc(N*N);
gsl_complex num;
gsl_complex conj;
gsl_complex add1p;
gsl_complex add2p;
gsl_complex add1;
gsl_complex add2;
gsl_complex bragg;

for (int h = 0; h < L+1; h++) {
for (int i = 0; i < L+1; i++) {
for (int j = 0; j < L+1; j++) {
```

```
add1p = gsl_complex_polar (1, (M_PI)*(i+j+h));
add2p = gsl_complex_polar (1, -(M_PI)*(i+j+h));
add1 = gsl_complex_mul_real (add1p, V);
add2 = gsl_complex_mul_real (add2p, V);
bragg = gsl_complex_add (add1, add2);
gsl_vector_complex_set(data, (j+i*Lprime+h*Lprime*Lprime)*N+
(j+i*Lprime+h*Lprime*Lprime), bragg);


if (h+1 < L+1) {
GSL_SET_COMPLEX(&num, H3, 0);
         gsl_vector_complex_set(data, (j+i*Lprime+h*Lprime*Lprime)*N+(j+i*Lprime+
         (h+1)*Lprime*Lprime), num);
gsl_vector_complex_set(data, (j+i*Lprime+(h+1)*Lprime*Lprime)*N+
(j+i*Lprime+h*Lprime*Lprime), num);
};

if (j+1 < L+1) {
num = gsl_complex_polar (1, (M_PI)*(-1+2*(1+D3)*i-2*(1+D1)*h)/2);
gsl_vector_complex_set(data, (j+i*Lprime+h*Lprime*Lprime)*N+
(j+1+i*Lprime+h*Lprime*Lprime), num);
conj = gsl_complex_polar (1, -(M_PI)*(-1+2*(1+D3)*i-2*(1+D1)*h)/2);
gsl_vector_complex_set(data, (j+1+i*Lprime+h*Lprime*Lprime)*N+
(j+i*Lprime+h*Lprime*Lprime), conj);
};

if (i+1 < L+1) {
num = gsl_complex_polar (1, (M_PI)*(1+2*(1+D2)*(h-i))/2);
gsl_vector_complex_set(data, (j+i*Lprime+h*Lprime*Lprime)*N+
(j+(i+1)*Lprime+h*Lprime*Lprime), num);
conj = gsl_complex_polar (1, -(M_PI)*(1+2*(1+D2)*(h-i))/2);
gsl_vector_complex_set(data, (j+(i+1)*Lprime+h*Lprime*Lprime)*N+
(j+i*Lprime+h*Lprime*Lprime), conj);
};
}
}
}

gsl_vector_view partereale = gsl_vector_complex_real(data);
gsl_vector_view parteimmaginaria = gsl_vector_complex_imag(data);

// check whether the matrix is hermitian
int p =0;
```

```
for (int i = 0; i < N; i++) {
for (int j = 0; j < N; j++) {
double x1 = gsl_vector_get(&partereale.vector,i*N+j);
double x2 = gsl_vector_get(&partereale.vector,j*N+i);
double y1 = gsl_vector_get(&parteimmaginaria.vector,i*N+j);
double y2 = gsl_vector_get(&parteimmaginaria.vector,j*N+i);
if ((x1 != x2) && (y1 != -y2)) { p = p+1; }
} }

if(p == 0)

{
/*
ofstream outf("entrate.dat", ios::out);
for (int i = 0; i < N; i++) {
for (int j = 0; j < N; j++) {
//      double x = GSL_REAL(gsl_complex_vector_get(data,i*N+j));
//double y = GSL_IMAG(gsl_complex_vector_get(data,i*N+j));
double x = gsl_vector_get(&partereale.vector,i*N+j);
double y = gsl_vector_get(&parteimmaginaria.vector,i*N+j);
outf << "Entry (" << i << "," << j << ") = " << x << "+i" << y << endl;
}
}

outf.close();
*/


cout << "Initialized data" << endl;

gsl_matrix_complex_view m = gsl_matrix_complex_view_vector (data, N, N);
gsl_vector *eval = gsl_vector_alloc (N);
gsl_matrix_complex *evec = gsl_matrix_complex_alloc (N, N);
gsl_eigen_hermv_workspace * w = gsl_eigen_hermv_alloc (N);
gsl_eigen_hermv (&m.matrix, eval, evec, w);
gsl_eigen_hermv_free (w);
//  gsl_eigen_hermv_sort (eval, evec,
// GSL_EIGEN_SORT_ABS_ASC);

outfile << N << endl;
outfile << D1 << endl;
outfile << D2 << endl;
outfile << D3 << endl;
```

```
outfile << H3 << endl;
outfile << P << endl;
outfile << V << endl;
outfile << "autovalori" << endl;

for (int t = 0; t < N; t++) {
double eval_t = gsl_vector_get (eval, t);
outfile << eval_t << endl;

// In case one wants to see also the eigenvectors...
//gsl_vector_view evec_i = gsl_matrix_column (evec, i);
//outfile << "eigenvector = \n";
//for (int j = 0; j < N; j++)
// outfile << gsl_vector_get(&evec_i.vector,j) << endl;

}
outfile.close();
gsl_vector_free (eval);
gsl_matrix_complex_free (evec);
return 1;

}

else{
cout << "Initialized data" << endl;
printf("error\n");
outfile.close();
}



return 0;

}
}
}
```

Chapter 4

Conclusions and Outlook

In this thesis we have investigated and exploited some links between QFT and Condensed Matter / Statistical Physics systems. The study develops in two opposite directions: on one hand we describe how QFT methods can be usefully used to describe condensed matter systems with diverging correlation length (second order phase transition) or anyway with a dynamic dominated by long range excitations (in the IR limit). On the other hand we tackle the problem how QFT can be efficiently simulated by using condensed matter devices.

In the first part of the thesis (Chapter 2) we described the scaling limit of classical 2D Tricritical Ising model and 3-states Potts model under respectively energy density and vacancy density perturbations and energy density and magnetic field perturbations. The study was carried on by Truncated Conformal Space Approach and by Form Factors perturbations theory approach. We also took some advantages from the Landau-Ginzburg description.
The natural future developments of the arguments exposed are:

- the extension to massless integrable models (and relative perturbations), like the one describing flow from TIM to Ising or the $O(3)$ with π topological term. The main difficulties are the presence of IR divergences in form factors (FF) and the slow convergence of the Lehman expansion; for these reasons high particle-FF and new re-summation techniques are required. The problem is partially approached in [145] and citing papers.

- the extension to low dimensional theories having finite volume, temperature (especially when high-temperature expansions are not reliable) and density; after a long period without significative achievements, some notable works [146, 147, 148, 149, 150, 151] in last years opened new possibilities.

The construction of an analytical formalism for the investigation of non integrable field theories, different from perturbation theory close to integrable trajectories, seems instead an hard task, due to the impossibility to identify the exact scattering matrix. We mention however that, even for non integrable theories, the numerical methods exploited in Chapter 2 are able to give good estimations on the low-particle form factors. This allows for in turn, thanks to the fast convergence of the Lehman series in the massive case, to reproduce effectively the correlation functions for the

various operators. The method was widely exploited in the recent papers [146, 147].
Another hint, mainly useful for a qualitative understanding, could come just from the ideas that inspired the second part of the thesis, namely from the simulations of low-dimensional statistical model and field theories on 1D ultracold atoms devices, realized by strongly anisotropic traps and/or optical lattices.

In the second part of this thesis (Chapter 3) we dealt with the simulation of relativistic model by ultracold atoms. We discussed in particular a cold-atoms set-up able to simulate (3+1) Dirac fermions and some applications, relevant both in elementary particle and in condensed matter physics. We also showed the possibility to add a tunable mass by using Bragg pulses, an effective external electromagnetic coupling and an internal interaction, also covariant. Finally we considered the 2D limit, describing the emergence of (2+1) Dirac fermions in presence of a strongly anisotropic lattice.
The rich physics of the described system deserves investigation in various directions:

- the study of the effects of an attractive interaction, in particular the possibility of superconductive phases and their nature. The system that we have proposed notably allows to span various regimes, i.e. massive, quasi-chiral, chiral, with absence or presence of coupling particle-antiparticle.
- the physics of this system in presence of interaction can be made even richer by adding different species of particles. In this case the systems could form, in some region of the space of parameters, phases different from conventional superconductivity (see [153] and citing papers). A central issue is here the role played by the asymmetry on the interaction between different colours, as well as by the fact that the particles are generally distinguishable. A more ambitious aim is the realization of colour-flavour locked phases.
- the systems we are dealing with is suitable for the synthesis of fractional zero (Majorana) modes: since in normal phase it has quasiparticle excitations described by a Dirac equation, a BCS superconductive phase in presence of vortices is expected to host self-adjoint null excitations [141] with anyon statistics. These modes are object of great interest since they are shown to be use for topological quantum computation [152]. The mechanism works both in 2D and in 3D.
- the effect of varying parameters like the hopping and the mass, in particular the emergence of Berry phase when the former ones vary cyclically or the possibility of localization in presence of disorder. We also mention the possibility to simulate quenched dynamics in a QFT.
- the issues discussed above can be studied both in 3D and in 2D; it would the interesting to examine the effect of the dimensionality and the possible change of behaviour at the crossover.
- the system makes possible to simulate dynamics both Lorentz covariant and not, with the possibility to interpolate adiabatically between them. The natural questions is the what's the effect of of Lorentz covariance on the various aspects of the dynamics.
- the simulation of fermionic gauge theories, the major challenge being the simulation of *dynamical* gauge (possibly not abelian) fields.

Further research activity

During the period of the PHD, I also continued to work on the subject on my master degree thesis, the problem of colour confinement. All my research activity was done in collaboration with the Lattice Gauge Theory group of Pisa University, headed by Prof. Adriano di Giacomo. The topics tackled are:

Not perturbative QCD: colour confinement and deconfining transition. Checks and improvements of the dual superconductivity picture for confinement and comparison with other (topological) pictures. Study (also by lattice simulations) of the deconfining transition (order, parameters signaling it, thermodynamic quantities). Topological classification of the path-integral configurations relevant for confinement.

The results are published in the articles [4, 5].

Acknowledgements

I am pleased to thank warmly my advisor Prof. Giuseppe Mussardo (SISSA), my co-advisor Dr. Andrea Trombettoni (SISSA), Prof. Gesualdo Delfino (SISSA) and my master degree advisor Prof. Adriano di Giacomo (University of Pisa) for their deep efforts in educating me as a physicist during these amazing four years.

I thank Prof. German Sierra (Universidad Autonoma de Madrid), who acted as the external referee for this thesis, for the valuable comments and suggestions.

My gratitude for many fruitful discussions goes to Dr. Miguel Aguado (Max Planck Institute fur Quantenoptik, Garching), Prof. Francesca Biagini (Ludwig Maximilians Universitat, Munich), Giovanni Borghi (SISSA), Prof. Pasquale Calabrese (University of Pisa), Prof. Rocco Chirivi' (University of Lecce), Dr. Luca Dell'Anna (SISSA), Dr. Jarah Evslin (University of Pisa), Dr. Serena Fagnocchi (University of Nottingham), Dr. Fabio Ferrari Ruffino (Sao Paulo-Sao Carlos University), Dr. Luca Ferretti (Universidad Autonoma de Barcelona), Prof. Paolo Furlan (University of Trieste), Dr. Andrea Gambassi (SISSA), Dr. Paolo Grinza (Universidad de Santiago de Compostela), Prof. Enore Guadagnini (University of Pisa), Prof. Simon Hands (University of Swansea), Prof. Robert Konik (BNL, Brookhaven), Prof. Kenichi Konishi (University of Pisa), Prof. Fulvio Lazzeri (University of Pisa), Prof. Andre' Leclair (Cornell University), Dr. Stefano Liberati (SISSA), Dr. Luca Maccione (Desy), Prof. Christiane de Morais Smith (University of Utrecht), Prof. Alessandro Michelangeli (Ludwig Maximilians Universitat, Munich), Dr. Patrick Ohberg (University of Edinburgh), Prof. Valentina Petkova (INRNE, Sofia), Dr. Fabrizio Pucci (University of Bielefeld), Dr. Lorenzo Sindoni (Max-Planck-Institute fur Gravitationsphysik, Golm), Prof. Pasquale Sodano (University of Perugia), Prof. Gabor Tacaks (HAS, Budapest), Prof. George Thompson (ICTP, Trieste), Dr. Gabor Tszolt Toth (KFKI, Budapest), Dr. Walter Vinci (University of Minnesota), Prof. Jean-Bernard Zuber (LPTHE, Jussieu).

Bibliography

[1] L. Lepori, G. Mussardo and G. Z. Toth, J. Stat. Mech. **0809** (2008) P09004 [arXiv:0806.4715 [hep-th]].

[2] L. Lepori, G. Z. Toth and G. Delfino, J. Stat. Mech. **0911** (2009) P11007 [arXiv:0909.2192 [hep-th]].

[3] L. Lepori, G. Mussardo and A. Trombettoni, arXiv:1004.4744 [hep-th].

[4] A. Di Giacomo, L. Lepori and F. Pucci, JHEP **0810** (2008) 096 [arXiv:0810.4226 [hep-lat]].

[5] C. Bonati, A. Di Giacomo, L. Lepori and F. Pucci, Phys. Rev. D **81** (2010) 085022 [arXiv:1002.3874 [hep-lat]].

[6] G. Mussardo, "*Statistical Field Theory*, An Introduction to Exactly Solved Models in Statistical Physics ", Oxford University Press 2010.

[7] V. Riva., PHD Thesis, arXiv: hep-th/0411083.

[8] M. Z. Hasan, C. L. Mele, arXiv: 1002.3895.

[9] A.M. Polyakov, JETP Lett. 12 (1970) 381.

[10] Belavin A, Polyakov A and Zamolodchikov A, *Nucl. Phys. B* **241** (1984), 333; Friedan D, Qiu Z and Shenker S, *Phys. Rev. Lett* **52** (1984), 1575.

[11] P. Ginsparg, *"Applied Conformal Field Theory"*, in: *Fields, strings and critical phenomena*, Les Houches Lecture Notes 1988, eds. E. Brézin and J. Zinn-Justin.

[12] A.B. Zamolodchikov and Al.B. Zamolodchikov, Sov. Sci. Rev. A. Phys. 10 (1989) 269.

[13] P. Di Francesco, P. Mathieu and D. Sénéchal, *Conformal field theory*, Springer, New York (1997).

[14] *Finite–Size Scaling*, edited by J.L. Cardy, Amsterdam, North–Holland, 1988.

[15] H.W.J. Blote, J.L. Cardy and M.P. Nightingale, Phys. Rev. Lett. 56 (1986) 742;

J.L. Cardy, Nucl. Phys. B 240 (1984) 514; Nucl. Phys. B 270 (1986) 186; Nucl. Phys. B 275 (1986) 200; *Conformal invariance and statistical mechanics*, Les Houches 1988, North Holland, Amsterdam.

[16] I. Affleck, Phys. Rev. Lett. 56 (1986) 746.

[17] D. Friedan, Z. Qiu and S. Shenker, Phys. Rev. Lett. 52 (1984) 1575.

[18] A.B. Zamolodchikov, Adv. Studies in Pure Math. 19 (1989) 641.

[19] G. Mussardo, Phys. Rep. 218 (1992) 215, and references therein.

[20] A.B. Zamolodchikov and Al.B. Zamolodchikov, Ann. Phys. 120 (1979) 253.

[21] R.J. Eden, P.V. Landshoff, D.I. Olive and J.C. Polkinghorne, *The analytic S-matrix*, Cambridge University Press, 1966.

[22] M. Karowski, P. Weisz, Nucl. Phys. B 139 (1978) 445.

[23] V. P. Yurov and A. B. Zamolodchikov, Int. J. Mod. Phys. A **5** (1990) 3221-3246.
V.P. Yurov and Al.B. Zamolodchikov, Int. J. Mod. Phys. A 6 (1991) 3419.

[24] F.A. Smirnov, *Form Factors in Completely Integrable Models of Quantum Field Theory* (World Scientific) 1992.

[25] Al.B. Zamolodchikov, Nucl. Phys. B 358 (1991) 524;
J.L. Cardy and G. Mussardo, Nucl. Phys. B 410 (1993) 451;
G. Delfino and G. Mussardo, Phys. Lett. B 324 (1994) 40;
G. Delfino and G. Mussardo, Nucl. Phys. B 455 (1995) 724.

[26] A.B. Zamolodchikov, Sov. J. Nucl. Phys. 44 (1986) 529.

[27] A. Cappelli, Modular Invariant Partition Functions Of Superconformal Theories Phys. Lett. B 185 (1987), 82.

[28] Friedan D, Qiu Z, Shenker S, *Phys. Lett. B.* **151** (1985), 37.

[29] Z. Qiu, *Supersymmetry, two-dimensional critical phenomena and the tricritical Ising Model*, Nucl. Phys. B 270 [FS16] (1986), 205.

[30] M. Bershadsky, V. Knizhnik and M. Teitelman, Phys. Lett. B 151 (1985), 31.

[31] G. Mussardo, G. Sotkov, M. Stanishkov Nucl. Phys. **B** 305 (1988) pag. 69.

[32] Goddard P, Kent A and Olive D I, *Commun. Math. Phys.* **103** (1986) 105.

[33] Lukyanov S L and Fateev V A, *Sov. J. Nucl. Phys.* **49** (1989) 925 [*Yad. Phys.* **49** (1989) 1491].

[34] Lassig M, Mussardo G and Cardy J L, *Nucl. Phys. B* **348** (1991) 591–618.

[35] Delfino G, Mussardo G and Simonetti P, *Nucl. Phys. B* **473** (1996) 469.

[36] Delfino G and Mussardo G, *Nucl. Phys. B* **455** (1995) 724 [hep-th/9507010].

[37] Controzzi D and Mussardo G, *Phys. Lett. B* **617** (2005) 133-139 [hep-th/0503018].

[38] Mussardo G, *JHEP* **0708: 003** (2007) arXiv:0706.2546 [hep-th].

[39] Zamolodchikov A B, in "Fields, strings and quantum gravity", Proceedings of the Beijing Conference 1989, edited by Al.B. Zamolodchikov, p. 349. [*Nucl. Phys. B* **358** (1991) 497].

[40] Zamolodchikov Al B, *Nucl. Phys. B* **358** (1991) 524.

[41] Kastor D A, Martinec E J and Shenker S H, *Nucl. Phys. B* **316** (1989) 590.

[42] Christe P and Mussardo G, *Nucl. Phys. B* **330** (1990) 465

[43] Fateev V A and Zamolodchikov A B, *Int. J. Mod. Phys. A* **5** (1990) 1025.

[44] Zamolodchikov A B, *Sov. J. Nucl. Phys.* **44** (1986) 529.

[45] Klassen T R and Melzer E, *Nucl. Phys. B* **370** (1992) 511–550.

[46] Fateev V A, *Phys. Lett. B.* **324** (1994) 45.

[47] Delfino G, Mussardo G and Simonetti P, *Phys. Rev. D* **51** (1995) 6620.

[48] McCoy B M and Wu T T, *Phys. Rev. D* **18** (1978) 1259.

[49] Delfino G, *Nucl. Phys. B* **554** (1999) 537–551 [hep-th/9903082]

[50] Guida R and Magnoli N, *Phys. Lett. B* **411** (1997) 127-133.

[51] Fateev V, Lukyanov S, Zamolodchikov A and Zamolodchikov A, *Nucl. Phys. B* **516** (1998) 652-674.

[52] Fioravanti D, Mussardo G and Simon P, *Phys. Rev. E* **63** (2001) 016103 [cond-mat/0008216].

[53] Acerbi C, Mussardo G and Valleriani A, *Int. J. Mod. Phys. A* **11** (1996) 5327–5364 [hep-th/9601113].

[54] Pozsgay B and Takács G, *Nucl. Phys. B* **748** (2006) 485 [hep-th/0604022].

[55] Delfino G, Grinza P and Mussardo G, *Nucl. Phys. B* **737** (2006) 291 [hep-th/0507133].

[56] Tóth G Zs, *J. Phys. A* **37** (2004) 9631–9650 [hep-th/0406139].

[57] Tóth G Zs, "Investigations in two-dimensional quantum field theory by the bootstrap and TCSA methods", PhD thesis, Eötvös University, Budapest, 2006, arXiv:0707.0015[hep-th].

[58] G. Mussardo, V. Riva, G. Sotkov, *Nucl. Phys. B* **670** (2003) 464-478.

[59] G.Mussardo, *Nucl.Phys.B* **779** (2007) 101-154.

[60] G. Delfino and P. Grinza, Nucl. Phys. B **791** (2008) 265 [arXiv:0706.1020 [hep-th]].

[61] B. M. McCoy and T. T. Wu, Phys. Rev. D **18** (1978) 1259.

[62] G. Delfino, J. Phys. A **37** (2004) R45 [arXiv:hep-th/0312119].

[63] G. Delfino and G. Mussardo, Nucl. Phys. B **516** (1998) 675 [arXiv:hep-th/9709028].

[64] G. Mussardo, G. Takacs, J. Phys. A **42** (2009) 304022 [arXiv:0901.3537 [hep-th]].

[65] R. B. Potts, Proc. Cambridge Phil. Soc. 48 (1952) 106.

[66] F. Y. Wu, Rev. Mod. Phys. **54** (1982) 235.

[67] A. A. Belavin, A. M. Polyakov and A. B. Zamolodchikov, Nucl. Phys. B **241** (1984) 333.

[68] Vl. S. Dotsenko, Nucl. Phys. B 235 (1984) 54; Vl. S. Dotsenko and V. A. Fateev, Nucl. Phys. B **240** (1984) 312.

[69] J. L. Cardy, Nucl. Phys. B **270** (1986) 186.

[70] G. Feverati, F. Ravanini and G. Takacs, Phys. Lett. B **430** (1998) 264.

[71] P. Dorey, A. Pocklington, R. Tateo and G. Watts, Nucl. Phys. B **525** (1998) 641.

[72] V. S. Dotsenko and V. A. Fateev, Phys. Lett. B **154** (1985) 291.

[73] V. B. Petkova and J. B. Zuber, Nucl. Phys. B **438** (1995) 347 [arXiv:hep-th/9410209].

[74] V. B. Petkova and J. B. Zuber, Nucl. Phys. B **603** (2001) 449 [arXiv:hep-th/0101151].

[75] L. Chim, A. B. Zamolodchikov, Int. J. Mod. Phys. A **7** (1992) 5317.

[76] S. B. Rutkevich, arXiv:0907.3697 [cond-mat.stat-mech]

[77] G. Delfino, Nucl. Phys. B **818** (2009) 196 [arXiv:0902.3339 [hep-th]].

[78] Z. Bajnok, L. Palla, G. Takacs and F. Wagner, Nucl. Phys. B **601** (2001) 503 [arXiv:hep-th/0008066].

[79] R. Koberle, J. A. Swieca, Phys. Lett. B **86** (1979) 209.

[80] A. B. Zamolodchikov, Int. J. Mod. Phys. A **3** (1988) 743.

[81] G. Delfino and J. Cardy, Nucl. Phys. B **519** (1998) 551 [arXiv:hep-th/9712111].

[82] M. Caselle, G. Delfino, P. Grinza, O. Jahn and N. Magnoli, J. Stat. Mech. **0603** (2006) P008 [arXiv:hep-th/0511168].

[83] I. Runkel, Nucl. Phys. B **579** (2000) 561 [arXiv:hep-th/9908046].

[84] P. R. Wallace, Ph. Rev. **71** (1947), 622.

[85] G. W. Semenoff, Phys. Rev. Lett. **53** (1984), 2449.

[86] S. Reich et al., Phys. Rev. B **66** (2002) 035412.

[87] R. Deacon et al., Phys. Rev. B **76** (2007) 081406.

[88] C. Bena and S. A. Kivelson, Phys. Rev. B **72** (2005) 125432.

[89] J.P. Hobson and W. A. Nierenberg, Phys. Rev. 89 (1953) 662.

[90] I. Bloch, J. Dalibard, and W. Zwerger, Rev. Mod. Phys. **80** (2008) 885.

[91] M. Greiner, O. Mandel, T. Esslinger, T. E. Hansch, and I. Bloch, Nature **415** (2002) 39.

[92] U. Schneider, L. Hackermuller, S. Will, T. Best, I. Bloch, T. A. Costi, R. W. Helmes, D. Rasch, and A. Rosch, Science **322** (2008) 1520.

[93] R. Jordens, N. Strohmaier, K. Gunther, H. Moritz, and T. Esslinger, Nature **455** (2008) 204.

[94] See e.g. the website of a recent conference on the subject: http://www.fercook.com/gaugeatoms/index.html

[95] A. H. Castro Neto, F. Guinea, N. M. R. Peres, K. S. Novoselov, and A. K. Geim, Rev. Mod. Phys. **81** (2009) 109.

[96] S. L. Zhu, B. G. Wang, and L. M. Duan, Phys. Rev. Lett. **98** (2007) 260402.

[97] B. Wunsch, F. Guinea, and F. Sols, New J. Phys. **10** (2008) 1030027.

[98] C. Wu and S. Das Sarma, Phys. Rev. B **77** (2008) 235107.

[99] K. L. Lee, B. Grémaud, R. Han, B.-G. Englert, and C. Miniatura, Phys. Rev. A **80** (2009) 043411.

[100] J. M. Hou, W. X. Yang, and X. J. Liu, Phys. Rev. A **79** (2009) 043621.

[101] L.-K. Lim, C. Morais Smith, and A. Hemmerich, Phys. Rev. Lett. **100** (2008) 130402.

[102] G. Juzeliunas, J. Ruseckas, M. Lindberg, L. Santos, and P. Ohberg, Phys. Rev. A **77** (2008) 011802(R).

[103] E. Wille *et al.*, Phys. Rev. Lett. **100** (2008) 053201.

[104] T. B. Ottenstein, T. Lompe, M. Kohnen, A. N. Wenz, and S. Jochim, Phys. Rev. Lett. **101** (2008) 203202.

[105] J. Kogut and L. Susskind, Phys. Rev. D **11** (1975) 395.

[106] L. Susskind, Phys. Rev. D **16** (1977) 3031.

[107] M. G. Alford, A. Schmitt, K. Rajagopal, and T. Schäfer, Rev. Mod. Phys. **80** (2008) 1455.

[108] L. Lamata, J. Leon, T. Schatz and E. Solano, Phys. Rev. Lett. **98** (2007) 253005.

[109] Gerritsma R., Kirchmair G., Zahringer F., Solano E., Blatt R. Roos C. F., Nature 463 (2010) 68.

[110] S. Tung, V. Schweikhard, and E. A. Cornell, Phys. Rev. Lett. **97** (2006) 240402.

[111] R. A. Williams, S. Al-Assam, and C. J. Foot, Phys. Rev. Lett. **104** (2010) 050404.

[112] Y.J. Lin, R.L. Compton, K.Jimenez-Garcia, J.V. Porto, I.B. Spielman, Nature **462** (2009) 628.

[113] D. Jaksch, P. Zoeller, New Journ. Phys. **5** (2003) 56.1-56.11.

[114] F. Gerbier, J. Dalibard, New Journ. Phys. **12** (2010) 033007.

[115] A. A. Abrikosov and S. D. Beneslavskii, Sov. Phys. JETP **32**, 699 (1070).

[116] Y. Hasegawa, J. Phys. Soc. Jap. **59** (1990) 4384.

[117] Y. Hasegawa, Physica C, 185-189 (1991) 1541-1542.

[118] E.g., see chapter 6 of L. D. Landau, E. M. Lifshits, and L. P. Pitaevskii, *Statistical physics, part 2* (London, Pergamon, 1980).

[119] R. B. Laughlin and Z. Zou, Phys. Rev. B **41** (1990) 664.

[120] E. D. Fradkin, E. Dagotto, and D. Boyanovsky, Phys. Rev. Lett. **57** (1986) 2967.

[121] P. Maraner and J. K. Pachos, Phys. Lett. A **373** (2009) 2616.

[122] H.B. Nielsen, M. Ninomiya, Phys. Lett. **B 130** (1983) 389.

[123] D. R. Hofstadter, Phys. Rev. B **14** (1976) 2239.

[124] M. Koshino and H. Aoki, Phys. Rev. B **67** (2003) 195336.

[125] J. Bruning, V. V. Demidov, and V. A. Geyler, Phys. Rev. B **69** (2004) 033202.

[126] P. B. Blakie, R. J. Ballagh, and C. W. Gardiner, Phys. Rev. A **65** (2002) 033602.

[127] A. M. Rey, P. B. Blakie, G. Pupillo, C. J. Williams, and C. W. Clark, Phys. Rev. A **72** (2005) 023407.

[128] R. B. Laughlin and Z. Zou, Phys. Rev. B **41** (1990) 664.

[129] I. Affleck and J. Brad Marston, Phys. Rev. B **37** (1987) 3774.

[130] A. Bermudez, L. Mazza, M. Rizzi, N. Goldman, M. Lewenstein and M. A. Martin-Delgado, arXiv:1004.5101 [cond-mat.quant-gas]

[131] V. Gurarie and L. Radzihovsky, Ann. Phys. **322** (2007) 2.

[132] G. Giuliani and G. Vignale, *Quantum theory of the electron liquid* (Cambridge, University Press, 2005).

[133] Y. Nambu and G. Jona-Lasinio, Phys. Rev. **122** (1961) 345.

[134] J. Gonzalez, F. Guinea and M. A. H. Vozmediano, Nucl. Phys. B **424** (1994) 595 [arXiv:hep-th/9311105].

[135] J. Gonzalez, M.A. Martin-Delgado, G. Sierra, A. H. Vozmediano, "Quantum Electron Liquids and High Tc Superconductivity", Lectures Notes in Physics, Springer.

[136] X. G. Wen, "Quantum field theory of many body system", Oxford Graduate Texts.

[137] M. V. Berry, Proc. Roy. Soc. Lond. A **392** (1984) 45.

[138] B. Simon, Phys. Rev. Lett. **51** (1983) 2167.

[139] M. Nakahara, "Geometry, topology and physics", second edition, IoP.

[140] J. J. Sakurai, "Advanced quantum mechanics",

[141] R. Jackiw and P. Rossi, Nucl. Phys. B **190** (1981) 681.

[142] K. Capelle and E. K. U. Gross, Phys. Rev. B. **59** (1999) 7140.

[143] T.Ohsaku, Phys. Rev. B **65** (2001) 024512.

[144] A. A. Abrikosov, L. P. Gorkov and L.E. Dzyaloshinski, "Methods of quantum field theory in statistical physics", Pergamon Press.

[145] G. Delfino, G. Mussardo and P. Simonetti, Phys. Rev. D **51** (1995) 6620 [arXiv:hep-th/9410117].

[146] B. Pozsgay and G.Takacs, Nucl. Phys. B 788 (2008) 167 [arXiv:0706.1445 [hep-th]].

[147] B. Pozsgay and G.Takacs, Nucl. Phys. **B** 788 (2008) 209 [arXiv:0706.3605 [hep-th]].

[148] M. Kormos and G. Takacs, Nucl. Phys. **B** 803 (2008) 277 [arXiv:0712.1886 [hep-th]].

[149] R.M. Konik, Phys. Rev. **B** 68, 104435 (2003).

[150] F.H.L. Essler and R.M. Konik, J. Stat. Mech. 0909 (2009) P09018.

[151] G.Takacs, Nucl. Phys. **B** 825 (2010) 466 [arXiv:0907.2109 [hep-th]].

[152] C. Nayak, S. H. Simon, A. Stern, M. Freedman and S. Das Sarma, Rev. Mod. Phys. **80** (2008) 1083.

[153] P. Lecheminant et al., Phys. Rev. Lett. 95 (2005) 240402.